AD-A069 611 NAVAL RESEARCH LAB WASHINGTON D C F/G 11/2
HIGH PERFORMANCE COMPOSITES AND ADHESIVES FOR V/STOL AIRCRAFT.(U)
MAY 79 L B LOCKHART
UNCLASSIFIED NRL-MR-4005 NL

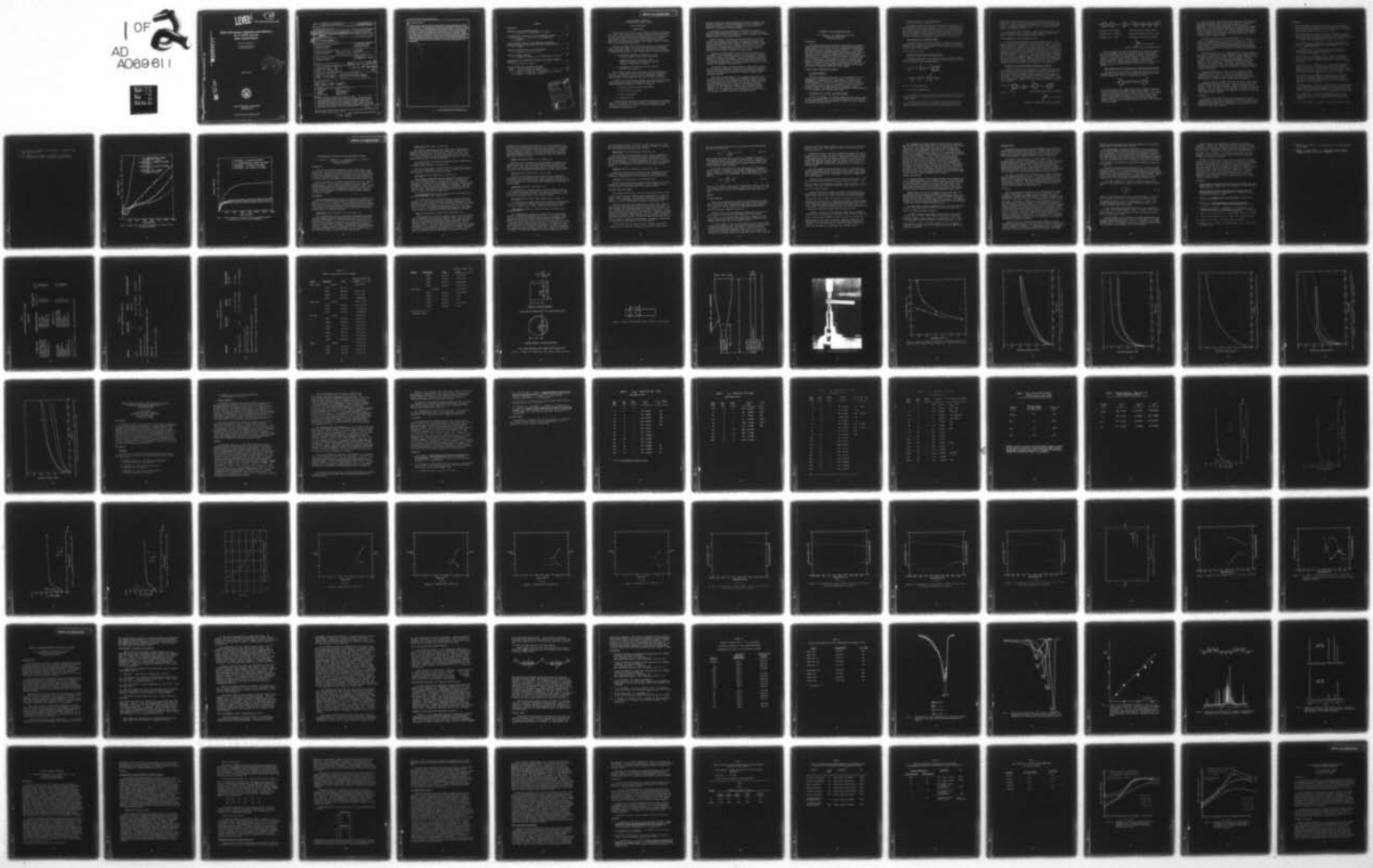


611

LEVEL II

(12) B.S.

NRL Memorandum Report 4005

High Performance Composites and Adhesives for V/STOL Aircraft Third Annual Report

LUTHER B. LOCKHART, JR.

Polymeric Materials Branch
Chemistry Division

May 23, 1979

NAVAL RESEARCH LABORATORY
Washington, D.C.

NRL Memorandum Report 4005

A055 926

SECURITY CLASSIFICATION OF THIS PAGE (When Data Entered)

REPORT DOCUMENTATION PAGE	READ INSTRUCTIONS BEFORE COMPLETING FORM
1. REPORT NUMBER NRL Memorandum Report 4005 ✓	2. GOVT ACCESSION NO. 3. RECIPIENT'S CATALOG NUMBER
4. TITLE (and Subtitle) (6) HIGH PERFORMANCE COMPOSITES AND ADHESIVES FOR V/STOL AIRCRAFT — ~~THIRD ANNUAL REPORT~~ AD54637	5. TYPE OF REPORT & PERIOD COVERED Progress Report for the Period 1 Sept 1977 — 30 Nov 1978 6. PERFORMING ORG. REPORT NUMBER
7. AUTHOR(s) (10) Luther B. Lockhart, Jr. ~~Editor~~	8. CONTRACT OR GRANT NUMBER(s)
9. PERFORMING ORGANIZATION NAME AND ADDRESS Naval Research Laboratory Washington, DC 20375	10. PROGRAM ELEMENT, PROJECT, TASK AREA & WORK UNIT NUMBERS NRL Problem C04-10.01 PE 62761N; F 54-502-001
11. CONTROLLING OFFICE NAME AND ADDRESS Naval Air Systems Command Washington, DC 20361 (12) 162 p.	12. REPORT DATE May 23, 1979 13. NUMBER OF PAGES 165
14. MONITORING AGENCY NAME & ADDRESS (if different from Controlling Office) Naval Air Development Center Warminster, PA 18974	15. SECURITY CLASS. (of this report) UNCLASSIFIED 15a. DECLASSIFICATION/DOWNGRADING SCHEDULE
16. DISTRIBUTION STATEMENT (of this Report) Approved for public release; distribution unlimited. (11) 23 May 79 (9) Annual Rept. no. 3, 1 Sep 77 - 30 Nov 78	
17. DISTRIBUTION STATEMENT (of the abstract entered in Block 20, if different from Report) (16) F54502 (17) SF54502004	
18. SUPPLEMENTARY NOTES (14) NRL-MR-4005	
19. KEY WORDS (Continue on reverse side if necessary and identify by block number) V/STOL aircraft — Fracture Composites — Polymer characterization Adhesives — Design optimization Polymer synthesis — Radiation curing	
20. ABSTRACT (Continue on reverse side if necessary and identify by block number) An interdisciplinary program has been undertaken to address the composite and adhesive materials requirements of V/STOL aircraft. The primary tasks are to develop and characterize high modulus, high toughness resins with use temperatures of 350°F to 450°F or higher, to develop fabrication technology for newly developed resin matrices for graphite-fiber reinforced composites, to develop composite failure criteria for design optimization and to establish appropriate quality control parameters. This report is the third annual review of the program, → over (Continues)	

DD FORM 1 JAN 73 1473 EDITION OF 1 NOV 65 IS OBSOLETE
S/N 0102-014-6601

SECURITY CLASSIFICATION OF THIS PAGE (When Data Entered)

251 950

20. Abstract (Continued)

covering the period 1 September 1977 to 30 November 1978. The reporting period was extended to permit completion of an important phase of the task on fracture behavior of composites. During the reporting period, two of the original tasks, Resin Synthesis and Radiation Curing, were terminated but related work is being continued under other in-house projects to follow up leads developed in this program. Among recent accomplishments are the demonstration that resin fracture energy can affect composite interlaminar toughness in fiber-reinforced composites, the development of quality control methodology for phthalocyanine precursor resins, the successful fabrication of phthalocyanine/graphite fiber composites from prepreg, and the completion of room temperature fracture tests of NARMCO 5208/T300 composite over four quadrants of load space and Hexcel F178/T300 composite in one quadrant and further verification of the ability to use this data to predict failure in a box-beam structure.

CONTENTS

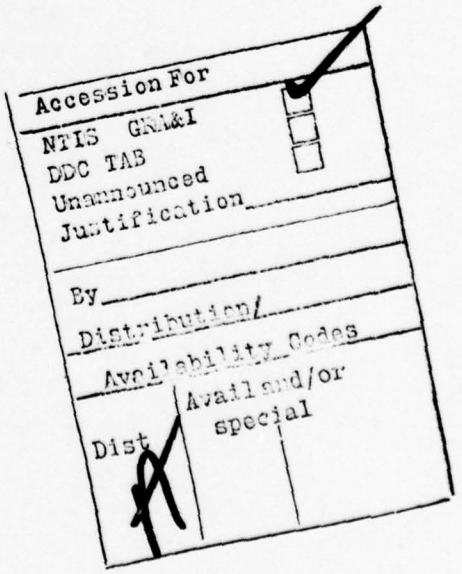

HIGH PERFORMANCE COMPOSITES AND ADHESIVES FOR V/STOL AIRCRAFT

Third Annual Report

INTRODUCTION

The principal driving force behind composite materials' development in the Navy is the requirement for lighter weight structural materials. The severe weight constraints on carrier-based aircraft in general and vertical/short take-off and landing (V/STOL) aircraft in particular have caused the Navy to look to new design concepts using easily fabricated, fiber-reinforced composites that combine superior stiffness with a high strength-to-weight ratio.

The need to maximize structural weight savings, necessitated by the heavy V/STOL power plant, has led to an in-depth study at the Naval Research Laboratory (NRL) of the variables that influence the behavior of composites and adhesives. NRL's V/STOL studies in this area include

- Pilot-plant synthesis and selection of resin systems designed to meet V/STOL requirements
- Composition analysis and quality control, adhesive formulation and testing, and graphite composite fabrication and testing
- Development of failure criteria for composite materials and structures

NRL's overall effort employs a blending of basic and applied research. It draws heavily from past and on-going basic research at NRL in polymer fracture testing, radiation technology, automated material failure characterization and structure failure prediction.

A number of promising polymer systems, including the NRL-developed phthalocyanines, are under consideration for the resin matrix of graphite-reinforced composites. Qualities sought are

- Long-term stability above 400°F (204°C)
- Insensitivity to moisture
- Ease of fabrication
- Reasonable cost

Thermomechanical properties of candidate thermosetting and thermoplastic resin systems are being evaluated. Key parameters include the effects of temperature and moisture on modulus (stiffness), glass

Note: Manuscript submitted March 20, 1979.

transition temperature (softening point) and fracture toughness. The projected outcome is a better understanding of the interrelationship between the molecular structure of polymers and their mechanical properties, particularly fracture toughness.

Fabrication variables involved in the assembly and curing of angle-ply laminates are being evaluated. The use of radiation-curable resins for the production of laminates and bonded structures with reduced residual strains is also being explored.

Quality assurance techniques are being developed for cured and uncured resin systems, and the effects of long-term storage on the uncured resin-impregnated fiber (prepreg) materials are being studied. Important factors in the final selection of the resin(s) will be the availability of adequate quality control procedures to monitor the batch-to-batch variability of production lots of resins, and the assessment of the storage lifetime of uncured systems.

Significant accomplishments expected from this program are the development of the technology to predict the resistance of composites and bonded joints to flaw propagation and the development of failure criteria for composite structures. Computer-controlled equipment and software have already been developed for obtaining fracture data from the simultaneous application of complex in-plane loads (tension, shear, rotation) to composites and bonded joints.

Information derived from these studies is being used to identify the critical bulk mechanical properties that contribute to improved fracture-resistant composites. Procedures are also being developed to evaluate the performance of composites in simple structures under multiaxial loadings.

Among recent accomplishments are the demonstration that resin fracture energy can affect composite interlaminar toughness in fiber-reinforced composites, the development of quality control methodology for phthalocyanine precursor resins, the successful fabrication of phthalocyanine/graphite fiber composites from prepreg, and the completion of room temperature fracture tests of NARMCO 5208/T300 composite over four quadrants of load space and Hexcel F178/T300 composite in one quadrant and further verification of the ability to use this data to predict failure in a box-beam structure.

SYNTHESIS OF HIGH TEMPERATURE RESINS

J. R. Griffith, J. G. O'Rear and T. M. Keller
Polymeric Materials Branch
Chemistry Division

INTRODUCTION

Past annual reports have elaborated on the synthesis of diamide-linked phthalonitrile monomers and their thermosetting polyphthalocyanine polymers (1,2), as well as on the synthesis of a fluoropolyol polyacrylate resin for ionizing radiation curing (2). One phase of this task during FY78 has been directed toward synthesizing additional quantities of known or modified phthalocyanine and fluoroacrylate monomers and their resulting polymers, procuring and characterizing the final shipments of commercial C_{10} diamide monomer, and shipping the latter to prepreggers. Additionally, syntheses accomplished under another in-house program during FY78 are relevant to this program. Several new classes of diether-linked phthalonitrile monomers and their respective diether-linked polyphthalocyanine polymers have been produced and are undergoing evaluation in this program.

DIAMIDE-LINKED PHTHALONITRILE MONOMERS

C_{22} Diamide Monomer

Additional quantities of C_{22}-acid, i.e., docosanedioc acid, were prepared via a multistep process. This acid is of interest as an intermediate for preparing both diamide-linked and diether-linked polyphthalocyanines. A portion of the C_{22}-acid has been converted to the C_{22}-diamide monomer, since this compound was previously shown to provide amide-linked polyphthalocyanines with superior toughness (fracture energy). This material has been undergoing further evaluation in the Thermomechanical Characterization Task.

Procurement of Commercial C_{10}-Diamide Monomer

A total of 96 pounds of C_{10}-diamide monomer has been procured under contract from Eastman Kodak Co. following technology transfer from NRL. The completed delivery has been examined in detail and found acceptable by our quality assurance tests.

Prepreg Shipments of C_{10}-Diamide Monomer

The commercial C_{10}-diamide monomer procurement has satisfied our in-house needs as well as our commitments to the Ferro Corporation and U. S. Polymeric for prepreg production. Evaluations of these prepregs, both tape and fabric, is providing information on processing differences between two commercial sources and will provide materials for fabrication into composites for evaluation in the in-plane loader and in the simulated box-beam tests described in later sections of this report.

Resin Monomers for Professor Gillham

Additional amounts of the Me-C_6-diamide, C_{10}-diamide, C_{13}-diamide and C_{22}-diamide monomers have been supplied to Professor John Gillham (Princeton) for torsion braid analysis. These results are presented in a later section of this report.

FLUOROPOLYACRYLATE RESINS

Cis-Trans Fluoropolyol Polyacrylate Resins

Additional quantities of the 100% esterified fluoropolyol acrylate resin have been prepared by esterifying the following polyol with excess acrylic anhydride in the customary manner:

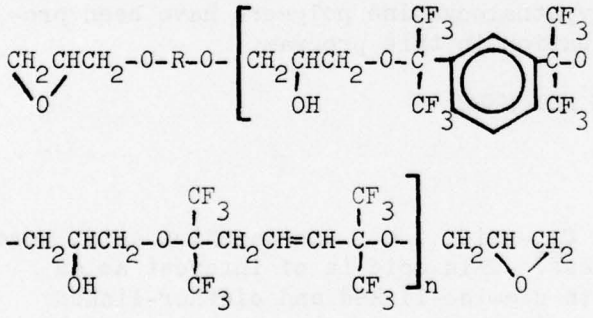

where R = $-C(CF_3)_2C_6H_4C(CF_3)_2-$

or $-C(CF_3)_2CH_2CH=CHC(CF_3)_2-$

This completely esterified resin may be polymerized by either free-radical catalysts or by ionizing radiation into a hard, clear, cross-linked polymer.

A fluoropolyol acrylate of 10% acrylate content has also been prepared. Since lower cross-link density usually provides resins of greater extensibility and toughness, it was hoped that this material

would lead to radiation-curable resins of improved peel strength. In the present case, however, ionizing radiation curing gave a soft, weak rubber. To optimize toughness and extensibility, a 50 to 80% acrylate content is indicated; meanwhile blends of the 10 and 100% acrylated polyols are undergoing evaluation.

The promising results obtained on these radiation-curable fluoropolyol polyacrylate resins justifies further study; to exploit this lead, a separate in-house program has been initiated.

SECOND-GENERATION POLYPHTHALOCYANINE RESINS

In our continuing investigation of phthalocyanines (3-9), a new class of phthalonitrile monomers in which either an alkoxy or a phenoxy linkage connects the aromatic bis-orthodinitriles has been synthesized. These monomers are prepared by the simple nucleophilic displacement of a nitro substituent, which is activated by cyano groups, from an aromatic ring by either an alkoxide or a phenoxide-containing unit. Nucleophilic aromatic displacement of activated nitro groups has been the subject of many investigations (10-12), but it has only recently become a valuable tool for synthesis. In general, a nitro group can be readily displaced when it is positioned ortho or para to another substituent capable of stabilizing a negative charge. Numerous examples of nitro displacement involving activation by sulfone, carboxamide, ketone, phenyl, ester, aldehyde and cyano substituents have appeared in the literature.

Synthesis of New Diether-linked Phthalonitrile Monomers

A mixture of either an α,ω-alkanediol or a bisphenol derivative, 4-nitrophthalonitrile and an excess amount of anhydrous potassium carbonate in dry dimethyl sulfoxide (DMSO) is stirred at 70-80°C for 4-6 hours under an inert atmosphere to afford phthalonitrile monomers in high yield. Nucleophilic displacement of the nitro substituent occurs more readily for the bisphenols than for the α,ω-alkanediols. No attack of the nucleophile at either of the cyano groups was observed in any of these systems.

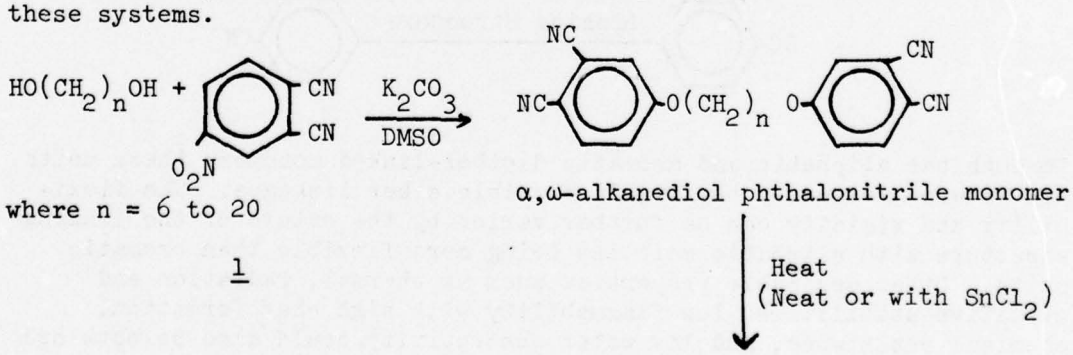

where n = 6 to 20

1

α,ω-alkanediol phthalonitrile monomer

Heat
(Neat or with $SnCl_2$)

Aliphatic Diether-Linked Polyphthalocyanine

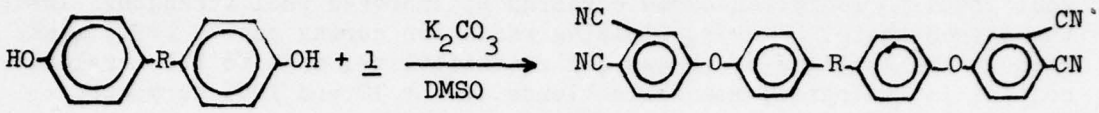

Bisphenol A, R = CH_3CCH_3 — Bisphenol-A phthalonitrile monomer

Bisphenol A6F, R = CF_3CCF_3 — Bisphenol-A6F phthalonitrile monomer

Bisphenol S, R = O=S=O — Bisphenol-S phthalonitrile monomer

↓ Heat (Neat or with $SnCl_2$)

Aromatic Diether-Linked Polyphthalocyanine

When the monomers are melted and heated in the absence or presence of suspended stannous chloride, a dark green or blue color develops which is characteristic of phthalocyanine formation. Polymerization occurs by a cyclic addition reaction without formation of volatile by-products to produce a solid, voidfree material. When heated neat, gelation occurs more readily for the aliphatic diether-linked monomers than for the more aromatized monomers. The cure time of both types of monomers is greatly reduced by the addition of stannous chloride.

Major Gains with the Second-Generation Polyphthalocyanine Resins

The limiting factor regarding the physical properties of a polyphthalocyanine is attributed to the linking structure between the two terminal dicyanophenyl units of a phthalonitrile monomer.

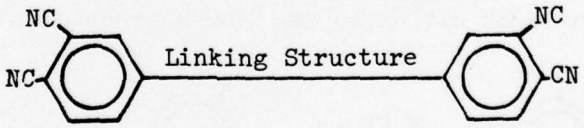

In both the aliphatic and aromatic diether-linked monomers these units are interconnected by the highly flexible ether linkages. The flexibility and rigidity can be further varied by the nature of the linking structure with aliphatic moieties being more flexible than aromatic units. Other desirable properties such as thermal, radiation and oxidative stabilities, low flammability with high char formation, chemical resistance, and low water absorptivity could also be obtained by such variations.

Both the aliphatic and aromatic diether-linked polyphthalocyanines show high thermal and oxidative stabilities (Figure 1). The former were able to withstand temperatures greater than 200°C without degradation, 230°C with slight degradation, but decomposed when heated above 250°C. The latter were stable for an extended period at 280°C before any weight loss occurred. The aromatic diether-linked phthalocyanine containing the sulfone moiety initially showed a small weight increase at 280°C and then gradually lost weight when held at this temperature for prolonged periods.

In previous studies, the alkanediamide-linked (i.e. the C_{10}-diamide) polyphthalocyanines were shown to lose about 2 wt. % during 1000 hours at 235°C and 7% during 1000 hours at 250°C (9). These results show the alkanediamide-linked polyphthalocyanines to be more stable thermally in air than the aliphatic diether-linked polyphthalocyanines but considerably less stable than the aromatic diether-linked polyphthalocyanines.

The water absorptivity of a polyphthalocyanine will also depend on the nature of the linking structure between the phthalocyanine nuclei. Polar groups located on the linking structure would be expected to show a stronger attraction for water than non-polar groups. Both the aliphatic and the aromatic diether-linked polyphthalocyanines which contain no polar units, show a similar and low affinity for water (Figure 2). On the other hand, the aromatic diether-linked polyphthalocyanine containing the sulfone moiety has a stronger attraction for water, which must be related to the presence of the polar sulfone group in the molecule.

The maximum absorption of water by the decanediamide-linked polyphthalocyanines amounts to 7 wt. % at room temperature. This compares with 3.7 wt. %, 1.3 wt. % and 1.1 wt. % water absorption observed for the aromatic diether-linked polyphthalocyanines derived from bisphenol S, bisphenol A and bisphenol A6F, respectively.

A similar scheme of synthesis can be envisioned for other classes of phthalocyanines making possible the design of polymers with a wide variety of connecting chain structures. Moreover, the new reaction pathway is short and simple and takes advantage of inexpensive starting materials. Thus, in addition to new structural variations, the cost of these polymers can be expected to be competitive with that of other high temperature polymeric systems.

CONCLUSION

Work on the Resin Synthesis Task of this program has been completed; however, evaluation of materials generated in this phase of the program continues under other program tasks. As indicated above, this program has given impetus to new developments which are being investigated more intensively elsewhere.

REFERENCES

1. "High Performance Composites and Adhesives for V/STOL Aircraft," First Annual Report, Willard D. Bascom and Luther B. Lockhart, Jr., Editors, Task A, Resin Synthesis, J. R. Griffith and J. G. O'Rear, NRL Memorandum Report 3433, pp 7-13 (Dec. 1976).

2. "High Performance Composites and Adhesives for V/STOL Aircraft, Second Annual Report, Willard D. Bascom and Luther B. Lockhart, Jr., Editors, Synthesis of Phthalocyanine Resins, J. R. Griffith and J. G. O'Rear, NRL Memorandum Report, pp 15-20 (Feb. 1978).

3. J. R. Griffith, J. G. O'Rear and T. R. Walton, "Phthalonitrile Resins," in Copolymers, Polyblends, and Composites, Advanc. Chem. Ser., No. 142, 458 (1975).

4. T. R. Walton and J. R. Griffith, "The Thermal Stability of Phthalocyanine and Polymeric Phthalocyanine in Air," Applied Polymer Symposium, No. 26, 429 (1975).

5. T. R. Walton, J. R. Griffith and J. G. O'Rear, "Phthalocyanine Resins: A New Class of Thermally Stable Resins for Adhesives, Coatings and Plastics," Adhesion Science and Technology, Vol. 9b, 665 (1975).

6. T. R. Walton, J. R. Griffith and J. G. O'Rear, "Phthalocyanine Resins. A New Class of Thermally Stable Resins for Adhesives, Coatings and Plastics," 168th National American Chemical Society Meeting, Atlantic City, NJ, Preprints, Division of Organic Coatings and Plastics Chemistry, Vol. 34, No. 2, 446 (Sept. 1974).

7. T. R. Walton, J. R. Griffith, J. G. O'Rear and J. P. Reardon, "Electrical Conducting Polymers from Phthalocyanine Resins," 174th National American Chemical Society Meeting, Chicago, IL, Preprints, Division of Organic Coatings and Plastics Chemistry, Vol. 37, No. 2, 180 (Sept. 1977).

8. T. M. Keller and J. R. Griffith, "The Synthesis and Polymerization of Fluorinated Phthalonitrile Monomers," 176th National American Chemical Society Meeting, Miami Beach, FL, Preprints, Division of Organic Coatings and Plastics Chemistry, Vol. 39, 546 (Sept. 1978).

9. T. R. Walton and J. R. Griffith, "The Thermal Stability of Phthalocyanine and Polymeric Phthalocyanine in Air," Applied Polymer Symposium, No. 26, 429-435 (1975), John Wiley and Sons (1975).

10. F. J. Williams and P. E. Donahue, J. Org. Chem., 42, 3414 (1977).

11. J. R. Beck, R. L. Sobczak, R. G. Suhr and J. A. Yahner, J. Org. Chem. 39, 1839 (1974).

12. H. M. Relles, C. M. Orlando, D. R. Heath, R. W. Schluenz, J. S. Manello and S. Hoff, J. Polym. Sci., 15, 2441 (1977).

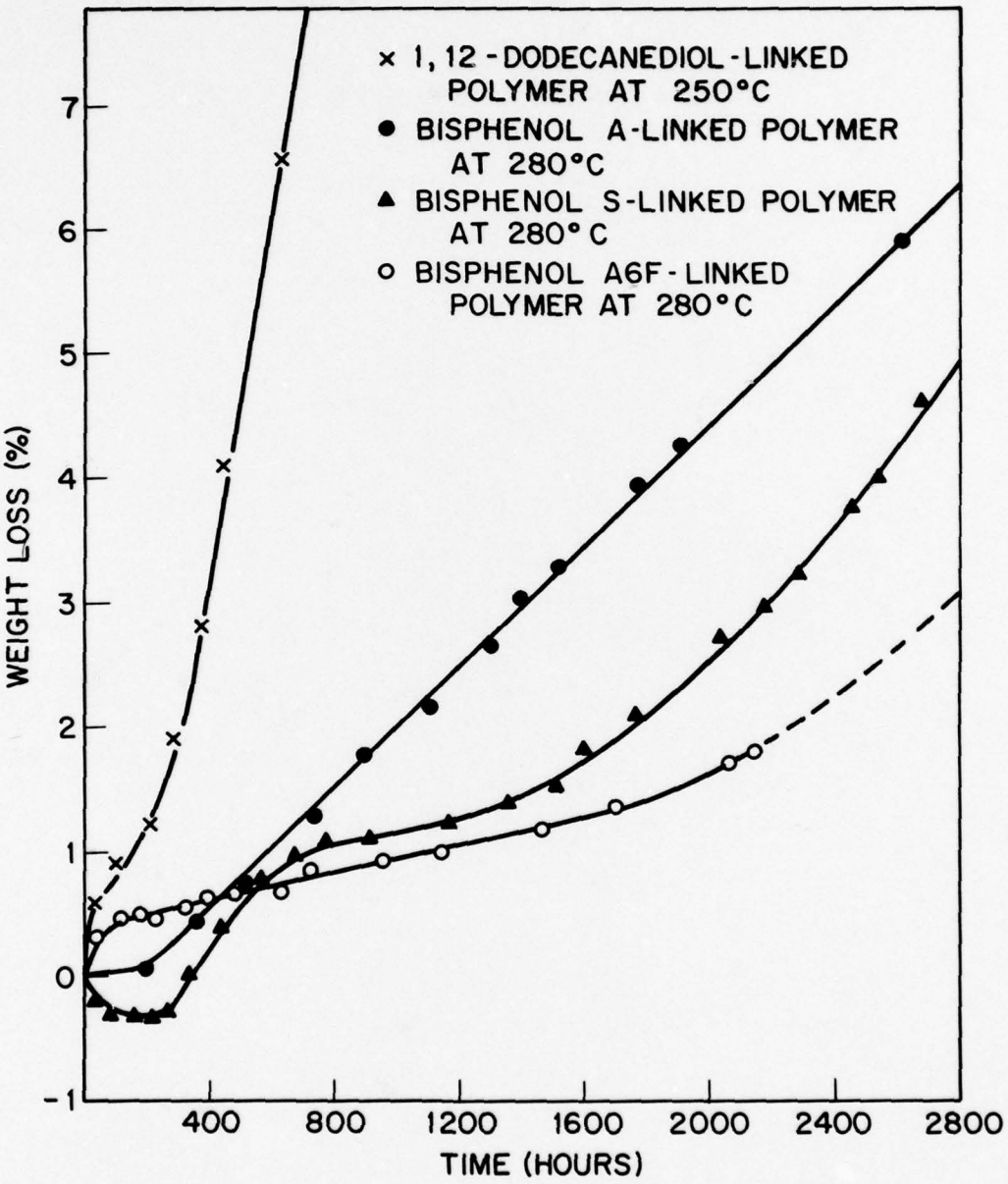

Fig. 1 - Weight loss at elevated temperature of diether-linked polyphthalocyanines

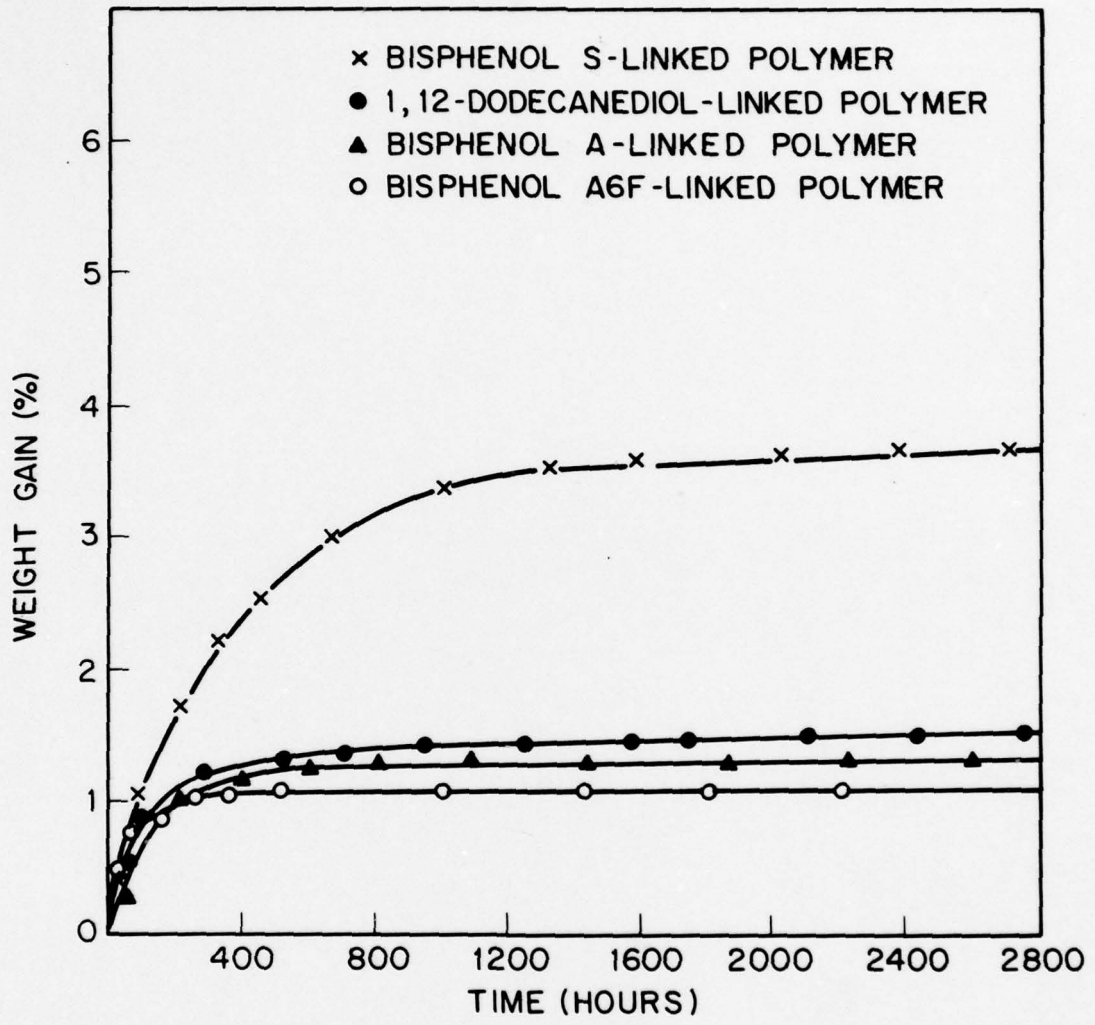

Fig. 2 - Water absorption of diether-linked polyphthalocyanines on immersion in water at room temperature

THERMOMECHANICAL PROPERTIES OF HIGH-PERFORMANCE POLYMERS

W. D. Bascom, J. L. Bitner, R. L. Cottington and C. M. Henderson
Polymeric Materials Branch
Chemistry Division

INTRODUCTION

Among the more important mechanical property requirements of the matrix resins in composites for advanced aircraft are stiffness (high modulus) and toughness (high fracture energy). In this task the effects of temperature and thermal aging on these properties are determined for a variety of candidate polymers. In addition, the moisture absorption of these polymers has been measured both before and after thermal aging.

Most of the modulus and fracture energy results have been reported previously (1,2). In this report the emphasis is on the effect of thermal aging on fracture energy and moisture absorption. However, some fracture energies are given for polymers not previously tested. Also, results are presented on the interlaminar fracture energy of graphite composites which illustrate the effect of the matrix resin toughness on composite toughness.

EXPERIMENTAL

The following paragraphs describe the methods used to prepare resin specimens for fracture testing. Plates of cured resin having a thickness of 0.3 to 1.3 cm are required for the fracture tests and in many instances special cure schedules or molding condition had to be employed. Also, when the resins were available only as laminating lacquers, procedures had to be developed to remove solvent and obtain the resin as a powder suitable for compression molding.

NARMCO 5208 (Narmco Materials, Inc., Costa Mesa, CA)

This tetrafunctional epoxy is essentially tetraglycidyl methylenedianiline (TGMDA) cured with diaminodiphenyl sulfone (DDS) along with some minor constituents (1). The resin powder was obtained from the manufacturer and cured in open pans (~15 X 15 cm) to give plates ~0.6 cm thick. It was convenient to melt the resin powder and pour the melt into the cure pans. The cure schedule, recommended by the manufacturer, involved a stepwise increase in temperature to avoid overheating due to the reaction exotherm. The schedule used was 20 hrs at 93°C, 3 hrs at 121°C, 2 hrs at 149°C, 2 hrs at 177°C and 4 hrs at 200°C.

Hexcel F-178 (Hexcel Corp., Dublin, CA)

This resin is an addition polyimide based on the bismaleimide of methylene dianiline and is supplied as a waxy powder. The resin was melted and poured into ~15 X 15 cm pans and cured at 135°C for 1 hr, 177°C for 1 hr and 246°C for 3 hrs to give plates up to 0.6 cm thick. It was found (2) that this cure schedule gave an undercured product and that a 24-hr post-cure at 240°C is desirable.

C_{10} phthalocyanine (NRL-developed polyphthalocyanine; manufactured by Eastman Organic Chemicals, Rochester, NY)

The resin readily melts at 180-200°C and was cured in open pans (~15 X 15 cm) to thicknesses of up to 1.3 cm. An initial cure at 200°C was followed by a post-cure at 220°C for 48 hrs.

Gulf T-600 (Gulf Oil Chemicals Co., Houston, TX)

This acetylenic polyimide resin was originally developed for the Air Force by Hughes Aircraft Co., Culver City, CA. As supplied by Gulf, the resin powder had been B-staged too far to allow specimen preparation in open pans or by hot compression molding. The resin cured too rapidly to allow flow and consolidation of the powder. Thin specimens (<0.3 cm) could be prepared by compression molding at 250°C and 7 MPa for 2 hrs. Specimens for fracture tests were prepared for this study by Hughes using a less B-staged resin.

Ciby-Geigy NCNS (NASA-developed; manufactured by Ciba-Geigy Corp., Plastics and Additives Div., Ardsley, NY)

As with the Gulf T-600, the advanced state of cure of this polytriazine resin made the preparation of fracture specimens difficult. Nonetheless, it was possible to obtain reasonable consolidation of the powder by compression molding at 170°C and 11 MPa for 1 hr to give disks 0.4-0.5 cm thick. The disks were post-cured at 204°C for 3 hrs and 224°C for 2 hrs. The molding temperatures mentioned here and elsewhere in this report were measured by a thermocouple imbedded in the mold.

PMR-15 (NASA-developed; manufactured by Ciba-Geigy Corp.)

The polyimide resin powder was prepared from its precursor constituents, 5-norbornene-2,3-dicarboxylic anydride (NBA), 3,3',4,4'-benzophenone tetracarboxylic dianhydride (BTDA) and 4,4'-methylene dianiline (MDA) which were obtained from Eastman Organic Chemicals. The NBA (98 gm) and BTDA (201 gm) were dissolved in methanol (190 cm^3) by refluxing for 1 hr. The MDA (183 gm) dissolved in methanol was added to the mixture of the anhydrides. The majority of the methanol was removed by vacuum evaporation at low temperature (30-40°C) to give a viscous syrup. The remaining alcohol was removed by placing the syrup in

aluminum pans and heating at 130-145°C for 1 hr in an evacuated (5 mm Hg) oven to form a glassy foam. Best results were obtained by limiting the syrup batch to 50 gm and allowing the syrup to heat for 5 minutes before starting the evacuation. The foam was pulverized in a blender and then B-staged at 230°C for 2 hrs. Test specimens were prepared by compression molding at 316°C for 30 minutes at 7 MPa. The plates were post-cured at 316°C for 16 hrs.

ASTREL (Carborundum Plastics, Inc., Atlanta, GA)

Specimens of this thermoplastic polyarylsulfone were prepared by compression molding. The resin powder was heated up to 340°C in 2.25 hrs at 35 MPa. There was a noticeable drop in pressure between 270-300°C which suggests melting and consolidation. At 340°C heating was discontinued but the pressure maintained until the mold cooled to 150°C.

UDEL P1700 (Union Carbide Corp., New York, NY)

Specimens were prepared by melting pellets of the thermoplastic polysulfone in an open aluminum dish. Only a few tests were made on this polymer since inordinately high fracture energies were obtained and it was suspected that a large plane-stress component was contributing to the measurement.

Upjohn 2080 (Upjohn Co., New Haven, CT)

The thermoplastic polyimide molding powder was dried at 135°C for 3 hrs. Compression molded specimens were prepared by heating the powder up to 328°C in 55 minutes at 14 MPa. The heat was then turned off but the pressure maintained until the mold cooled to 235°C.

Amoco 4000T (Torlon 4000T, Amoco Chemicals Corp., Chicago, IL)

The thermoplastic polyamide-imide molding powder was dried at 250°C for 1 hr. Specimens were compression molded by heating up to 325°C in 1.5 hrs at a pressure of 0.35 MPa. Pressure was removed at 200°C.

DuPont NR150B2 (DuPont Co., Plastics Products and Resins Dept., Wilmington, DE)

This thermoplastic polyimide is available only as a laminating lacquer in ethanol/N-methylpyrrolidone (75/25 wt %) solution. Consequently, solid resin was produced using procedures recommended by the manufacturer which were similar to the methods described above for PMR-15. The lacquer had a solids content of 48 wt % and was too viscous to attempt solvent removal by flash evaporation. Approximately 40 gm of lacquer was placed in aluminum pans and heated in a vacuum oven (5 mm Hg) at 200°C for 1 hr to produce a glassy foam. The foam was pulverized in a blender and then oven-dried at 270°C for 15 minutes and 371°C for 30 minutes. The powder was compression molded by heating up to 390°C in

3 hrs at minimum pressure (~0.35 MPa). At 390°C a pressure of 14 MPa was briefly applied (10 min) and then reduced to 0.35 MPa. The pressure was fully removed when the mold cooled to 300°C.

RADEL R-5000 (Union Carbide Corp., Moorestown, NJ)

This thermoplastic polyarylsulfone was not readily available as a molding powder except as a TiO_2-filled variety. Consequently, flat plate stock that had been prepared by injection molding was obtained from the manufacturer. The plate thicknesses were 0.3, 0.6, 1.3 and 2.5 cm. At the recommendation of the manufacturer, the plates were annealed at 149°C for 16 hrs and then at 213°C for 8 hrs to remove residual stress.

RYTON PPS (Phillips Petroleum Co., Bartlesville, OK)

Attempts to fabricate test specimens of this polyphenylene sulfide polymer by compression molding were unsuccessful. Round disks were prepared by the manufacturer for the fracture testing reported here.

ICI P300 (ICI United States, Inc., Wilmington, DE)

Plates of this thermoplastic polyethersulfone prepared by injection molding were supplied by the manufacturer. Square compact tension specimens were cut from these plates for fracture testing.

FRACTURE ENERGY MEASUREMENT

The fracture energies ($\mathcal{G}_{I_c}$, critical strain energy release rates) of the various resins were measured using rectangular (3) or round (4) compact tension specimens. The specimen configurations are shown in Figure 1. The rectangular specimen had W = 2.5 cm and the round specimen had W = 3.8 cm. The specimen thicknesses ranged from 3-6 mm.

The end of the saw cut was shaped into a dovetail and a precrack was formed by tapping the edge of the dovetail with a sharp blade. In most instances this operation produced a precrack which arrested in the full thickness of the specimen beyond the dovetail (Figure 2). It was not always certain that a precrack had formed when a specimen was tapped. However, post-failure examination of the specimen revealed the precrack position as a parabolic "halo" marking across the specimen thickness. Specimens which did not exhibit this halo usually gave high $\mathcal{G}_{I_c}$ (2-10X) values compared to companion test specimens. Presumably a precrack had not formed and so these high values were disregarded.

The expression for $\mathcal{G}_{I_c}$ given in Figure 1 assumes plane-stress conditions at the crack tip. Actually, a condition of plane strain

would be more accurate for most of the tests and so the fracture energies were calculated using

$$\mathcal{G}_{I_c} = Y^2 \frac{P_c}{EW^2 b^2} a (1-\nu^2) \qquad \text{Eq. (1)}$$

which assumes pure plane-strain conditions. The question of plane stress vs plane strain is discussed in a later section. In Equation 1, ν is Poisson's ratio and was assumed to be 0.35 for all polymers. The tensile modulus, E, was calculated from the shear modulus, G, measured at 25°C using the torsion pendulum.

A method has been developed (5) for determining the interlaminar fracture energy of composites. The specimen configuration, shown in Figures 3 and 4, is a double-cantilever beam, width-tapered for constant change of compliance with crack length. The fracture energy, $\mathcal{G}_{I_c}$, is given by

$$\mathcal{G}_{I_c} = \frac{12 P_c^2}{E_b h^3} \left(\frac{a}{b}\right)^3 \qquad \text{Eq. (2)}$$

where P_c is the failure load, E_b the bending modulus, and h, b and a are the thickness, width and crack length, respectively (see Figure 3). The taper is usually cut so that $a/b = 3$ although other ratios have been used.

RESULTS

FRACTURE ENERGIES

Most of the resin fracture energies have been reported previously (1,2). The earlier results along with recent additions are presented in Table I. All values were calculated assuming plane-strain conditions, i.e. Equation 1. The $\mathcal{G}_{I_c}$ value for the polysulfone, UDEL P1700, is taken from the work of Gales and Mills (6).

Fracture tests of the polyarylsulfone, RADEL, using specimens cut from 0.32-cm thick plates gave extraordinarily high $\mathcal{G}_{I_c}$ values (> 20 KJ/m^2). It was suspected that failure was occurring in essentially a plane-stress mode and this suspicion was strengthened by the clearly evident shear lips on the failure surfaces.

It is well known (7) that the contribution of plane stress to the failure mode, relative to the plane-strain contribution, decreases with increasing specimen thickness. Consequently, fracture tests were conducted using specimen thicknesses from 0.32 cm up to 2.5 cm. In order to avoid inelastic bending that might occur at the high loads expected for the thicker material, the specimens used in this study were

6.30 cm in length and height compared to the 3.15 cm used in the other fracture tests. Thus, the dimension W (Figure 1) was increased from 2.54 cm to 3.08 cm.

The RADEL specimens could not be precracked by tapping the edge of the dovetail with a blade. All this procedure accomplished was to form a short cut into the dovetail section. Consequently, different methods of precracking were tried. As might be expected, a short notch in the dovetail gave ambiguous results, primarily because the notch width was so much less than the specimen width. Calculation of the fracture energy using Equation 1 assumes the crack width and the specimen width to be the same.

Two other methods of precracking were tried: (a) eliminating the dovetail and notching the end of the saw cut with a sharp razor blade, and (b) notching the dovetail with a sharp razor blade and then mechanically popping in a crack while preventing its advance by clamping the end of the specimen.

The test results obtained thus far are presented in Figure 5. The data indicate a strong dependence of $\mathcal{G}_{I_c}$ on specimen thickness. Also, the two methods of precracking give different fracture energies. The specimens with pop-in cracks gave higher $\mathcal{G}_{I_c}$ values except for the tests with 2.5-cm thick specimens.

Although more data is needed, the effect of the precrack can be rationalized. Neale (8) has shown that compact tension specimens with pop-in cracks give high $\mathcal{G}_{I_c}$ values because of the curved, "thumbnail" contour of the crack front. The reversal in the $\mathcal{G}_{I_c}$ for the 2.5-cm specimens may have been due to failure initiating at a localized region of the razor notch instead of a simultaneous initiation over the entire notch. There was visual evidence that this had occurred and, if so, would result in erroneously high $\mathcal{G}_{I_c}$ values since failure initiated from a crack width considerably smaller than the specimen width.

The data in Figure 5 do not approach a lower limit in fracture energy which can be identified as the plane-strain fracture energy, $\mathcal{G}_{I_c}$. There are data analysis methods (9) which can be used to obtain $\mathcal{G}_{I_c}$, and this will be done when more data are available. Similarly, an analysis (8) will be used to correct the data obtained using pop-in precracks. For present purposes the lowest $\mathcal{G}_{I_c}$ value obtained, ~2.0 kJ/m^2, will be taken as an approximate $\mathcal{G}_{I_c}$ for RADEL R-5000.

The interlaminar fracture energies of graphite-fabric composites with the TGDMA/DDS epoxy (NARMCO 5208) and the thermoplastic polysulfone (UDEL P1700) as the matrix resins are given in Tables II and III, respectively. These measurements were made using the width-tapered double-cantilever beam specimen (Figures 3 and 4). By tapering the specimen in the width direction (rather than the usual height direction) a crack can be propagated between lamina to give a "Mode I"-like failure which is matrix dominated. A direct comparison between resin and composite fracture energies, however, is not usually meaningful because the composite failure inevitably involves some contribution from the rupture of fibers during crack initiation and propagation. Furthermore, the fibers often cause the crack front to deviate from planarity so that a true Mode I failure is not obtained. Nevertheless, the results for composites made with different resins can be compared to evaluate the relative toughness of the different resins when in a composite matrix. The results shown in Tables II and III indicate that the composite made with the thermoplastic resin had significantly better fracture behavior in matrix-dominated failure modes.

THERMAL AGING STUDIES

It was shown earlier (2) that aging the Hexcel F-178 polyimide and the C_{10} polyphthalocyanine caused a marked decrease in fracture energy, i.e. an embrittlement. Moreover, both the high temperature modulus and the glass transition temperature increased with heat soaking. This would suggest that during the time interval studied in these tests, thermal aging produced additional polymerization and/or cross-linking and these reactions dominated any thermal degradation that occurred.

Thermal aging tests of other candidate resins and polymers have been conducted and the results are presented in Table IV. The thermoplastic polyimide (UPJOHN 2080) and polyamide-imide, TORLON 4000T, did not show any loss in toughness up to 260°C. At 280°C both showed evidence of vapor evolution and presumably decomposition. The specimens expanded into a pillow shape which indicates softening and generation of a vapor which could not escape through the skin.

The thermoplastic polyimide (NR150B2) did not show any significant decrease in $\mathcal{G}_{I_c}$ until aged at 325°C for 240 hr; even at 350°C this polymer retained considerable toughness.

The PMR-15 thermosetting polyimide began to show a significant decrease in $\mathcal{G}_{I_c}$ at 350°C. The acetylenic polyimide T-600 specimens developed numerous surface cracks after 10-day aging at 350°C. Some of the specimens were too distorted to be used for testing. The $\mathcal{G}_{I_c}$ value reported in Table IV, although showing no loss in toughness, represents the average of only a few limited tests, and should not be considered conclusive.

MOISTURE UPTAKE

The maximum water absorption of several polymers and the effect of thermal aging on absorption were measured. Specimens approximately 2.5 cm X 1.3 cm X 0.6 cm were first dried over molecular sieve to constant weight and then placed over distilled water in closed containers at ~25°C. The increase in weight with time is shown in Figures 6-9.

The effect of thermal aging on the water uptake by the C_{10}-polyphthalocyanine and the F-178 polyimide is shown in Figures 6 and 7. For both polymers the more extensively heat-soaked materials exhibited a higher initial rate of uptake and, in the case of the polyimide, a higher equilibrium absorption. The polyphthalocyanine did not reach absorption equilibrium in the 80 days covered by the data in Figure 6. Test data taken over a 400-day period (Figure 8) indicate an equilibrium value of about 6% for this resin given a 48-hr post-cure at 240°C.

The results in Figure 9 show the NR150B2 and the PMR-15 polyimides reaching equilibrium uptake of about 3.5%. Thermal aging at 300°C for 480 hrs caused a slight decrease in the equilibrium absorption of the NR150B2, but substantially increased the PMR-15 absorption to an equilibrium value of about 5%. The 2080 polyimide and the 4000T polyamide-imide exhibited a relatively slow rate of water absorption and had not reached equilibrium after 100 days (Figure 10).

DISCUSSION

The fracture energy of polymers is often determined by the extent of plastic deformation that occurs at the crack tip before the crack propagates. The highly crosslinked epoxies, polyimides and other thermosetting polymers have little capacity for plastic deformation and so exhibit low $\mathcal{G}_{I_c}$ values (Table I). The thermoplastic polymers, on the other hand, are capable of considerable plastic deformation and usually have high fracture energies relative to the thermosetting polymers. Plastic deformation generally involves the extension of polymer segments between entanglements or crosslink points and thus plasticity is limited in materials with a high density of such points. In addition, factors such as free volume, chain stiffness, presence of bulky side groups, etc., affect the mobility of molecular segments and thereby influence a material's capacity for plastic flow. As the data in Table I indicate, there is a great deal of variability in the toughness of the different thermoplastic polymers, and much of this variation can be attributed to differences in molecular structure.

Thermal aging of the thermosetting polymers advances the cure, increases the crosslinking, and so reduces even further the capacity for plastic flow and the toughness. This was shown to occur for the addition polyimide (HEXCEL F-178) and the C_{10}-phthalocyanine (2). Presumably this was the reason for the decline in $\mathcal{G}_{I_c}$ of the PMR-15 above 325°C.

However, at this high temperature oxidative degradation is undoubtedly contributing to the embrittlement, as well.

The thermoplastic polyimide (UPJOHN 2080) and the polyamide-imide (AMOCO 4000T) appeared to decompose before there was any substantial loss in toughness. It should be noted that this decomposition involved an evolution of gas or vapor which distorted the specimen. However, these specimens were ~0.6 cm thick and in thin, fiber-composite laminates this vapor should be better able to escape. The reason for the decline in $\mathcal{G}_{I_c}$ of the NR150B2 above 325°C is uncertain. One possible explanation is an oxidation or decomposition reaction which promotes the formation of crosslinks.

The issue of the plane-stress contribution to the fracture energy, raised here by the tests on the RADEL polyarylsulfone, is important to engineering design. In structures fabricated using these non-reinforced polymers, e.g. as piping, enclosures, etc., the flaws from which fracture initiates are either surface scratches or small internal cracks. Under stress, these flaws are subjected to essentially pure plane-strain conditions and so the appropriate fracture design criteria is $\mathcal{G}_{I_c}$.

It has been suggested (11) that for satisfactory plane-strain fracture toughness testing the specimen thickness (6) should be greater than

$$\frac{2.5\ \mathcal{G}_{I_c}\ E}{\sigma_o^2} \qquad \text{Eq. (3)}$$

where E is the tensile modulus and σ_o the yield strength. In the case of the thermosets tested here, for which $\mathcal{G}_{I_c}$ was 0.2 kJ/m^2 or less, the minimum thickness is ~0.04 cm, assuming the σ_o ~70 MPa. This minimum thickness requirement is readily satisfied by the ~0.6 cm specimen thickness used in this work.

On the other hand, the minimum thickness is ~0.5 cm (assuming $\sigma_o \approx 70$ MPa) for the thermoplastics with $\mathcal{G}_{I_c}$ ~2.5 kJ/m^2, and so a specimen thickness of ~0.6 cm is marginal as far as meeting this requirement for plane-strain testing.

A yield strength (σ_o) of 70 MPa for the RADEL polyarylsulfone and the UDEL polysulfone is realistic and so it is important to test these materials using specimens with b > 0.5 cm. The results for the RADEL specimens with b = 1.3 (Figure 5) should give true plane-strain energies but the effect of precracking is still to be resolved.

However, many of the thermoplastics in Table I have tensile strengths of ~120 MPa, for example the UPJOHN 2080 and DUPONT NR150B2 polyimides. From equation 3 the minimum specimen thickness is 0.2 cm, and so tests of these polymers using 0.6-cm thick specimens should give true $\mathcal{G}_{I_c}$ values. Actually, in tensile tests these polyimides fail (fracture) before yielding so that 120 MPa underestimates the yield strength, σ_o, and 0.2 cm is an overestimate of the minimum specimen thickness for plane-strain testing.

The data in Table II and the work reported in reference (5) show clearly that the resin fracture energy can affect composite interlaminar toughness, at least for woven reinforcement. It should be pointed out that composite materials are especially vulnerable to interlaminar cracking, much more so than to longitudinal thru-fiber fracture. Konish et al (10) report a longitudinal fracture energy of 9.6 kJ/m^2 for a TGMDA/DDS graphite fiber, quasi-isotropic, $(0^\circ/\pm45^\circ/90^\circ)_S$, laminate compared to a 0.17 kJ/m^2 interlaminar fracture energy. Moreover, delamination is a common mode of failure of composites in the field. Consequently, resin toughness can be an important factor in the performance of fiber composites.

REFERENCES

1. High Performance Composites and Adhesives for V/STOL Aircraft, First Annual Report, W. D. Bascom and L. B. Lockhart, Jr., Eds., NRL Memo Report 3433, Dec. 1976.

2. High Performance Composites and Adhesives for V/STOL Aircraft, Second Annual Report, W. D. Bascom and L. B. Lockhart, Jr., Eds., NRL Memo Report 3721, Feb. 1978.

3. Knott, J. F., Fundamentals of Fracture Mechanics, Butterworths, London, 1973, p. 130.

4. Schutz, W., in Fracture Mechanics of Aircraft Structures, H. Liebowitz, Ed., AGARD, AG-176, NTIS, Springfield, VA, p. 371.

5. Bascom, W. D. Bitner, J. L., Moulton, R. J. and Siebert, A. R., Interlaminar Fracture of Organic-Matrix Composites, in preparation.

6. Gales, R. D. R. and Mills, N. J., Eng. Fracture Mech., 6, 93 (1974).

7. Parvin, M. and Williams, J. G., J. Mater. Sci., 10, 1883 (1975).

8. Neale, B. K., Inter. J. of Fracture, 14, 203 (1978).

9. Marshall, G. P., Coutts, L. H. and Williams, J. G., J. Mater. Sci., 9, 1409 (1974).

10. Konish, H. J., Swedlow, J. L. and Cruse, T. A., J. Composite Mat., 6, 114 (1972).

11. Brown, W. F. and Srawley, J. E., Plane Strain Crack Toughness Testing, ASTM Spec. Tech. Pub. 410 (1966).

Table I

FRACTURE ENERGIES OF MATRIX POLYMERS

THERMOSETS

Chemical Type	Commercial Designation	Fracture Energy, $\mathcal{G}_{I_c}$ kJ/m^2	T_g, °C
tetrafunctional epoxy	NARMCO 5208	0.076	260
polyimide (addition)	Hexcel F-178	0.12	360
polyimide (addition)	PMR-15 (NASA)	0.20	350
polyimide (acetylenic)	Gulf T-600	0.19	330
polytriazine	Ciba-Geigy NCNS	0.075	250
polyphthalocyanine	NRL/Eastman, C_{10}	0.19	360

THERMOPLASTICS

polyarylsulfone	Carborundum, ASTREL	3.0	350
polyarylsulfone	Union Carbide, RADEL	~2.0	-
polysulfone	Union Carbide, UDEL	3.2[a]	174
polyethersulfone	ICI, P300	0.65	230
polyimide	Upjohn 2080	0.81	326
polyimide	DuPont NR150B2	2.1	365
polyamide-imide	Amoco 4000	3.4	275
polyphenylene sulfide	Phillips RYTON PPS	0.21	-

[a]Gales, R. D. R. and Mills, N. J., Eng. Fracture Mech., 6, 93 (1974).

Table II

Fracture of TGMDA/DDS[a] Epoxy Materials

Material	Fiber Volume	Modulus	Fracture Energy, kJ/m^2
	%	GPa (psi)	
resin[b]	0	3.9 (5.7×10^5) tensile	0.076 (bulk)
resin/graphite cloth[c]	64.3	69.0 (1.0×10^7) flexural	0.36 (interlaminar)

[a] tetraglycidyl methylenedianiline/diaminodiphenyl sulfone

[b] NARMCO 5208

[c] Hexcel F-263/T-300, 13 x 12 weave

Table III

Fracture of Polysulfone Materials

Materials	Fiber Volume	Modulus	Fracture Energy
	%	GPa (psi)	$\mathcal{G}_{I_c}$ kJ/m^2
resin[a]	0	2.5 (3.6×10^5) tensile	3.2[c] (bulk)
resin/graphite cloth[b]	66.0	58.1 (8.4×10^6) flexural	2.2 (interlaminar)

[a] UDEL P1700, Union Carbide Corp.

[b] Hexcel F3T584 P1700 (P1700/181 style fabric)

[c] Gales, R. D. R. and Mills, N. J., Eng. Fracture Mech., 6, 93 (1974)

Table IV

Effect of Heat Soak on Fracture Energy

Polymer	Temperature	Time	Fracture Energy*, $\mathcal{G}_{I_c}$ kJ/m^2
Torlon 4000T	initial		3.91 ± 0.45
	240°C	240 hrs.	
	260°C	240 hrs.	2.84 ± 0.66
	260°C	480 hrs.	2.81 ± 0.70
	280°C	240 hrs.	decomposes
Upjohn 2080	initial		0.915 ± 0.036
	260°C	240 hrs.	0.711 ± 0.068
	260°C	480 hrs.	1.113 ± 0.065
	280°C	240 hrs.	decomposes
NR-150B2	initial		2.43 ± 0.38
	280°C	240 hrs.	2.38 ± 0.19
	280°C	480 hrs.	2.17 ± 0.18
	300°C	240 hrs.	2.18 ± 0.44
	325°C	240 hrs.	1.49 ± 0.12
	325°C	480 hrs.	1.24 ± 0.14
	350°C	240 hrs.	0.72 ± 0.26
	350°C	480 hrs.	0.35 ± 0.06
PMR-15	initial		0.20 ± 0.03
	260°C	240 hrs.	0.22 ± 0.06
	280°C	240 hrs.	0.18 ± 0.03
	300°C	240 hrs.	0.20 ± 0.05

Polymer	Temperature	Time	Fracture Energy*, $\mathcal{G}_{I_c}$ kJ/m^2
	300°C	480 hrs.	0.22 ± 0.06
	325°C	240 hrs.	0.17 ± 0.01
	325°C	480 hrs.	0.19 ± 0.01
	350°C	240 hrs.	0.12 ± 0.04
Gulf T-600	initial		0.22 ± 0.02
	260°C	240 hrs.	0.27 ± 0.02
	280°C	240 hrs.	0.20
	300°C	240 hrs.	0.21
	300°C	480 hrs.	0.22 ± 0.05
	350°C	240 hrs.	0.21

*Tested at ~25°C

$$\mathcal{G}_{I_c} = Y^2 \frac{P_c^2}{EW^2 b^2} \sqrt{a}$$

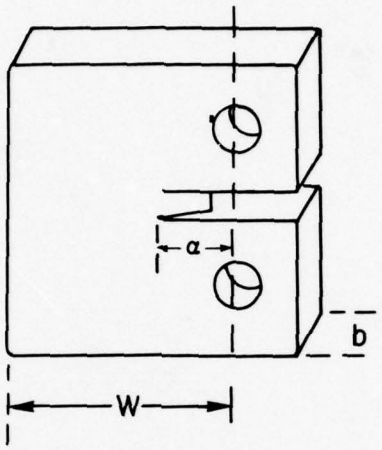

COMPACT TENSION SPECIMEN

$$Y = 29.6 - 186\, a/W + 656\,(a/W)^2 - 1017\,(a/W)^3 + 639\,(a/W)^4$$

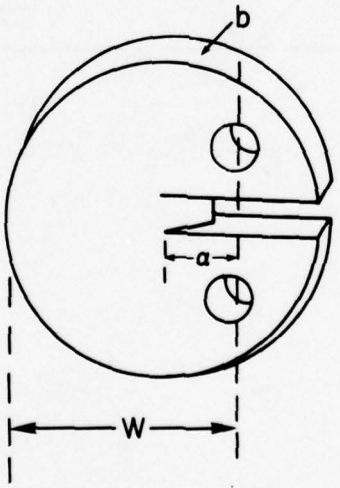

ROUND COMPACT TENSION SPECIMEN

$$Y = 30.0 - 162\, a/W + 493\,(a/W)^2 - 664\,(a/W)^3 + 405\,(a/W)^4$$

Figure 1. Schematics of square and round compact tension specimens.

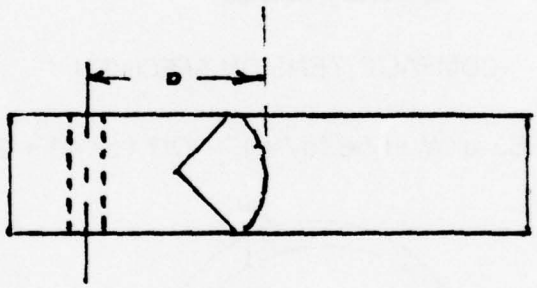

Figure 2. Drawing showing "halo" feature produced by precracking.

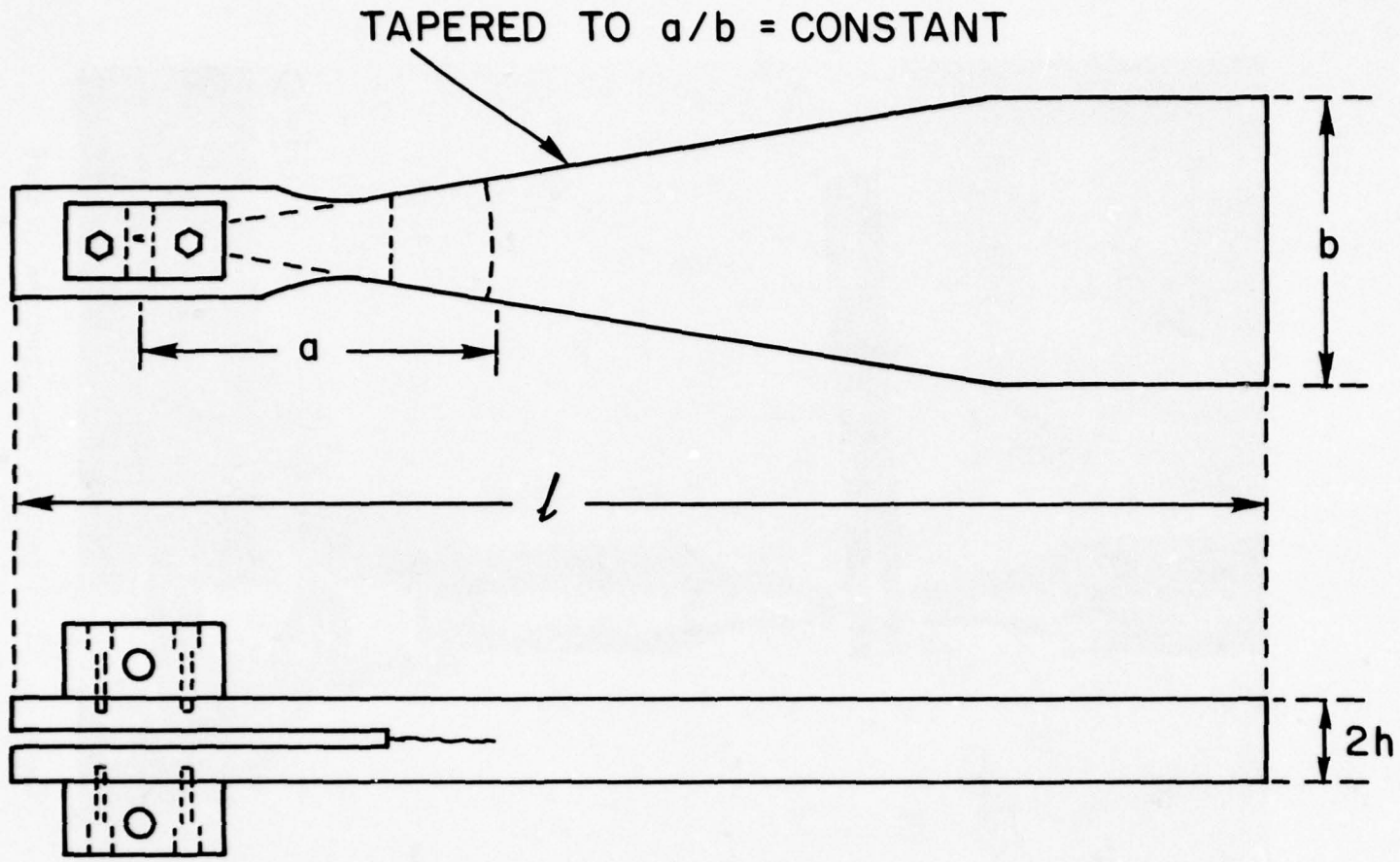

Figure 3. Schematic of width-tapered beam specimen for interlaminar fracture of composites.

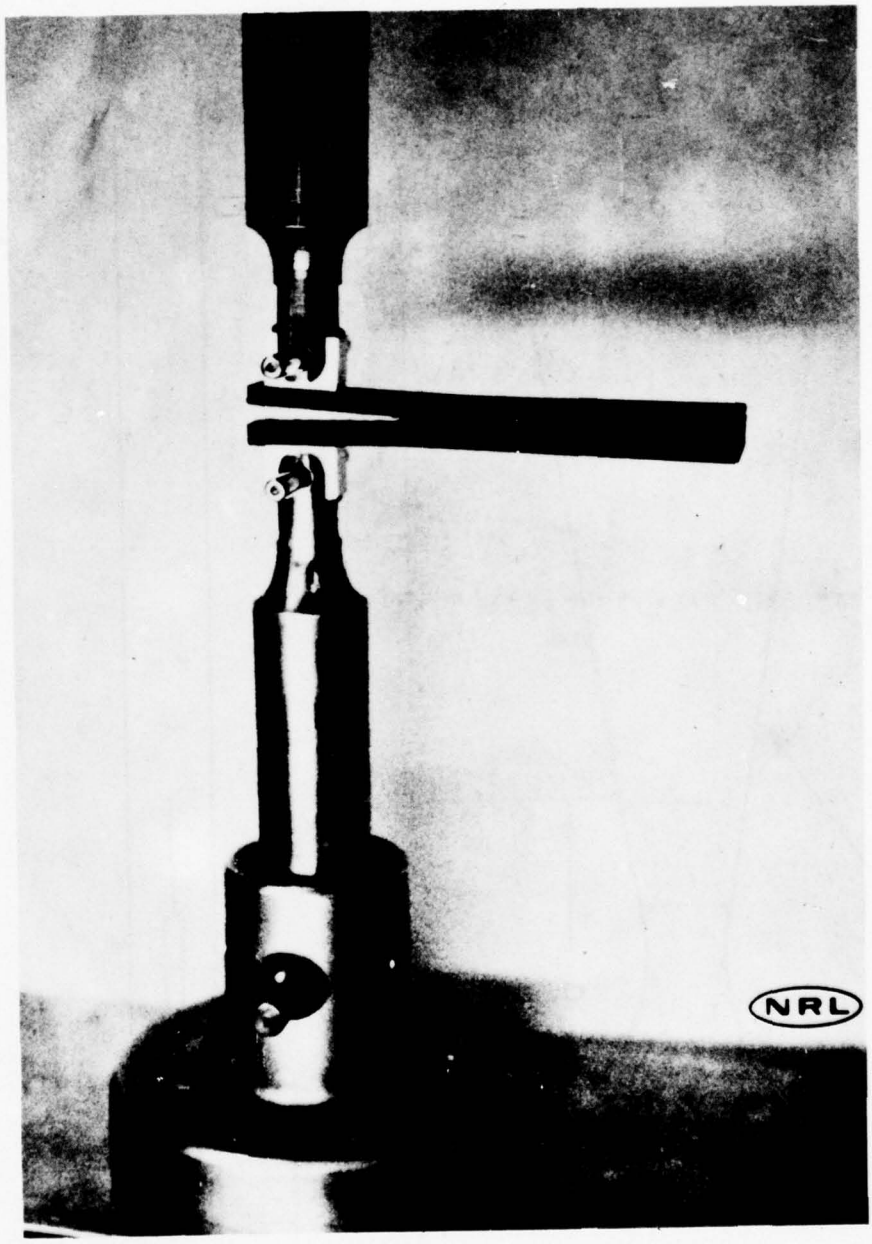

Figure 4. Width-tapered beam specimen in test.

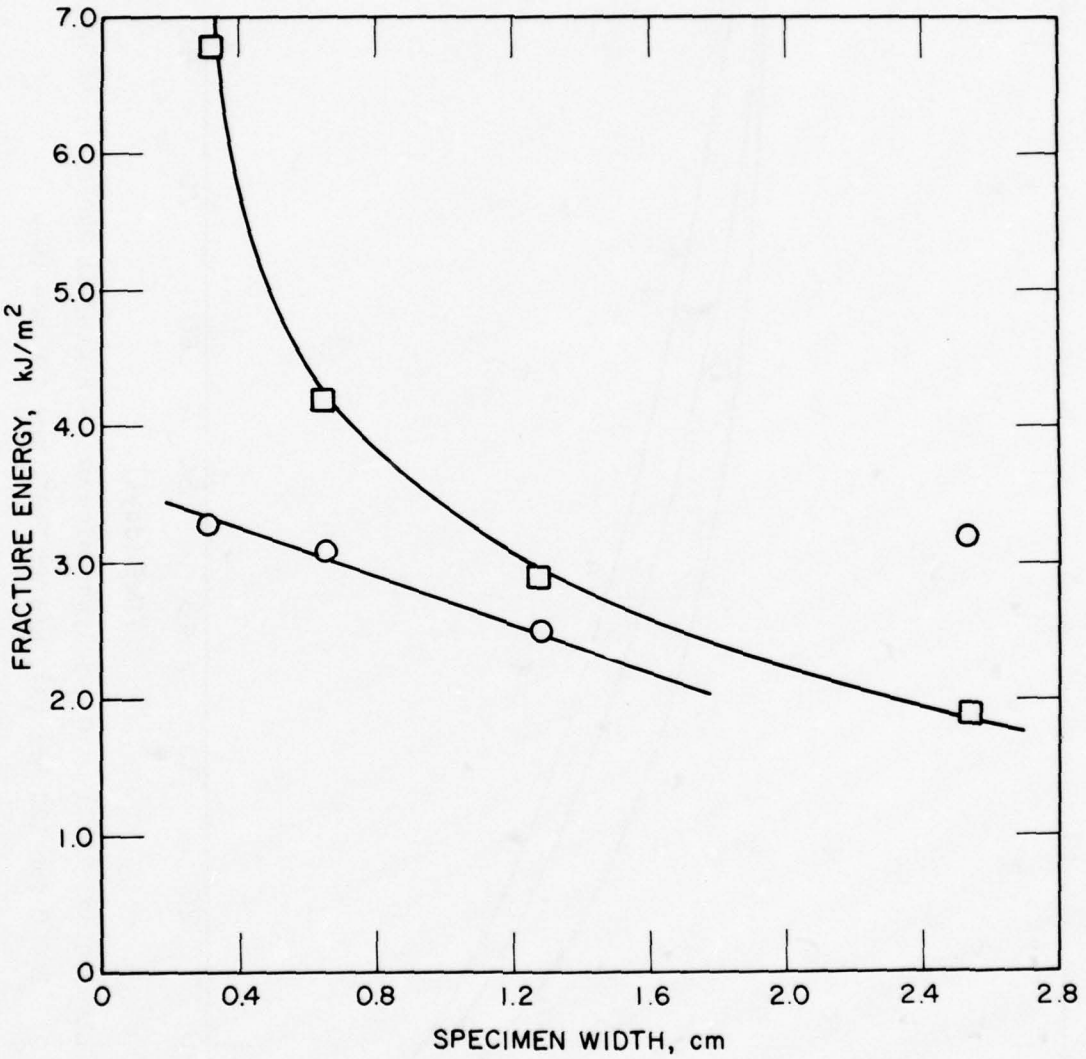

Figure 5. Effect of specimen thickness (b) on fracture energy of the polyarylsulfone, RADEL: □, pop-in precracks; 0, razor notch in saw-cut.

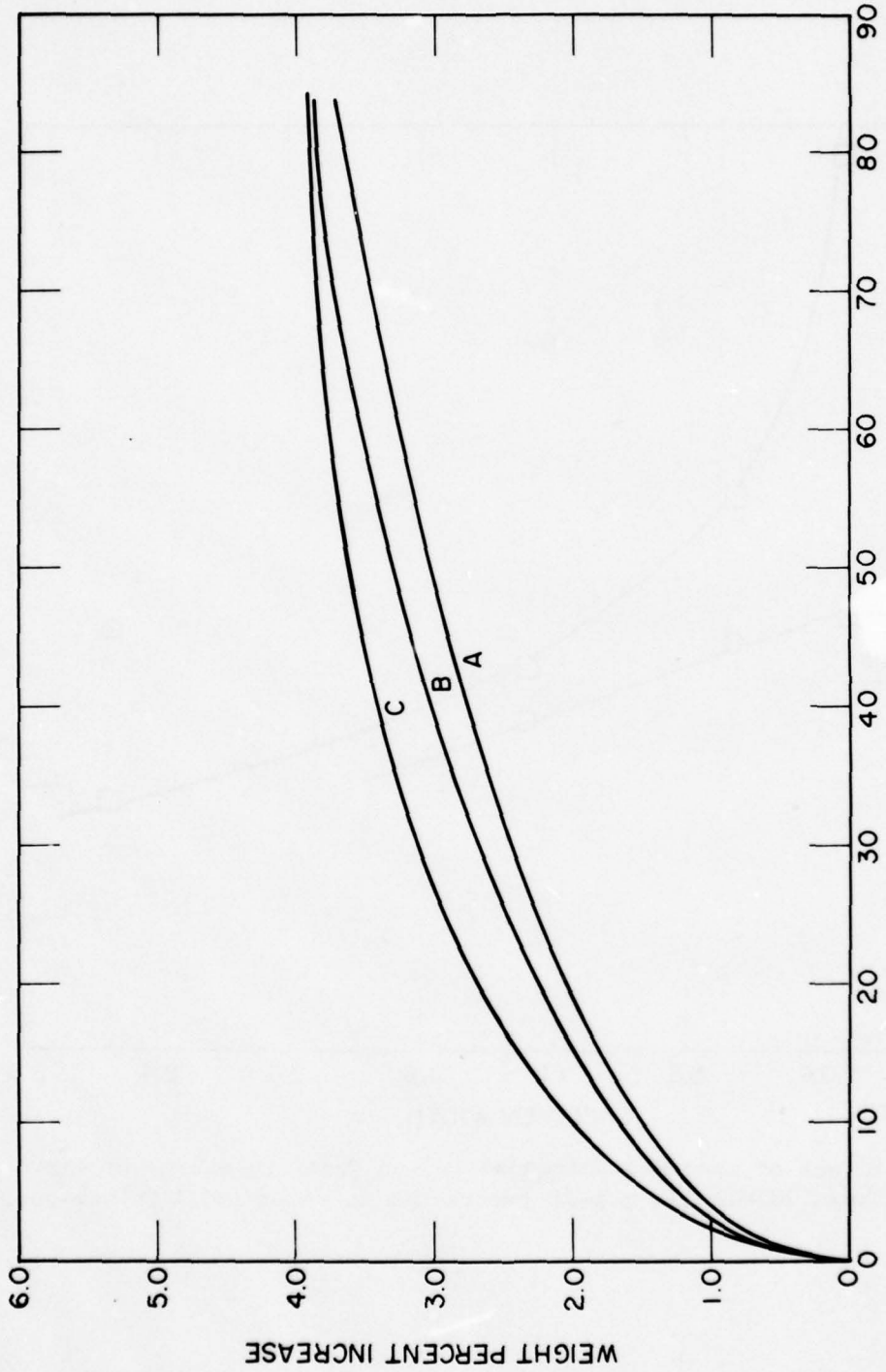

Figure 6. Water absorption (25°C) by C_{10}-polyphthalocyanine heated at 240°C for 48 hrs (A), at 240°C for 120 hrs (B), and at 260°C for 120 hrs (C).

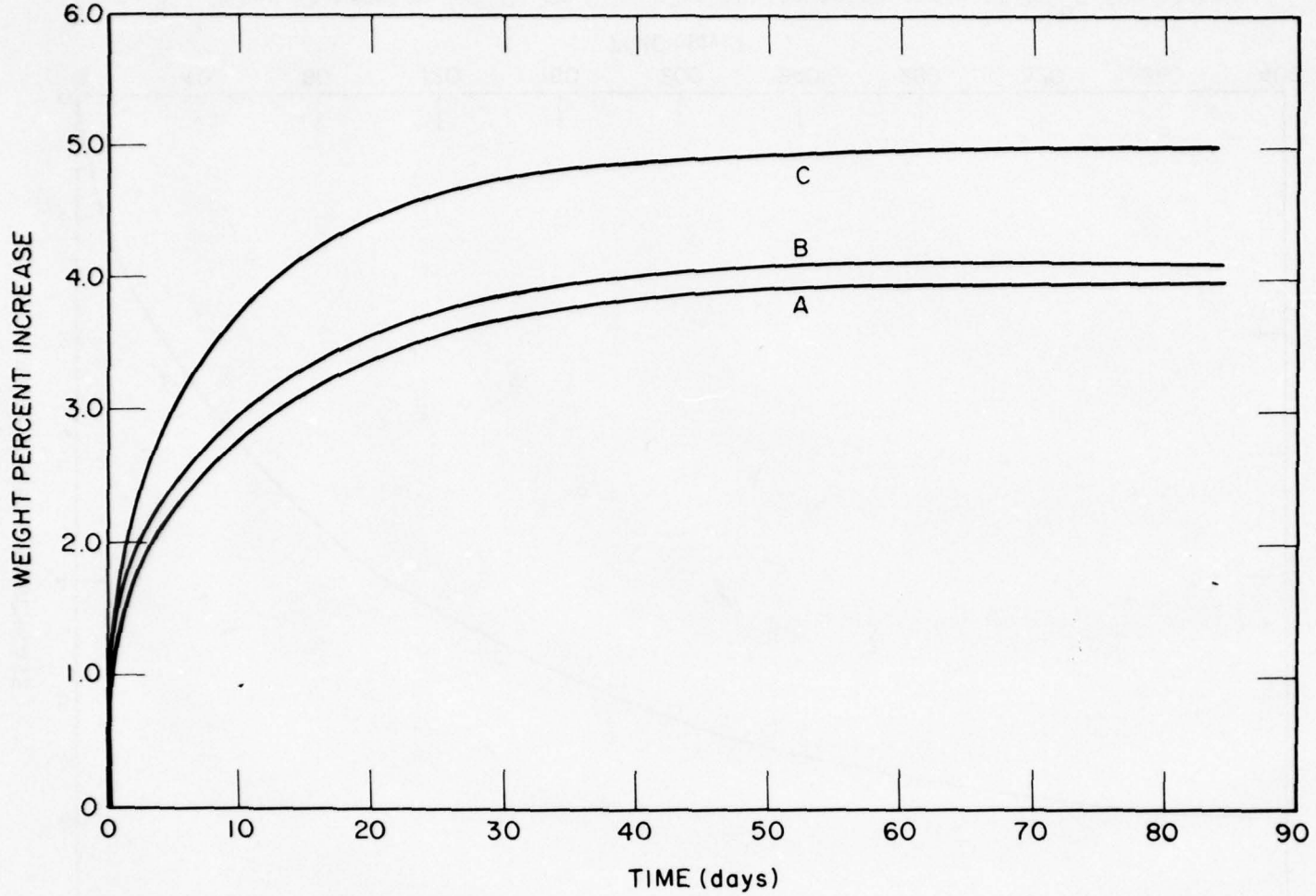

Figure 7. Water absorption (25°C) by Hexcel F-178 polyimide heated at 240°C for 48 hrs (A), at 240°C for 120 hrs (B), and at 260°C for 120 hrs (C).

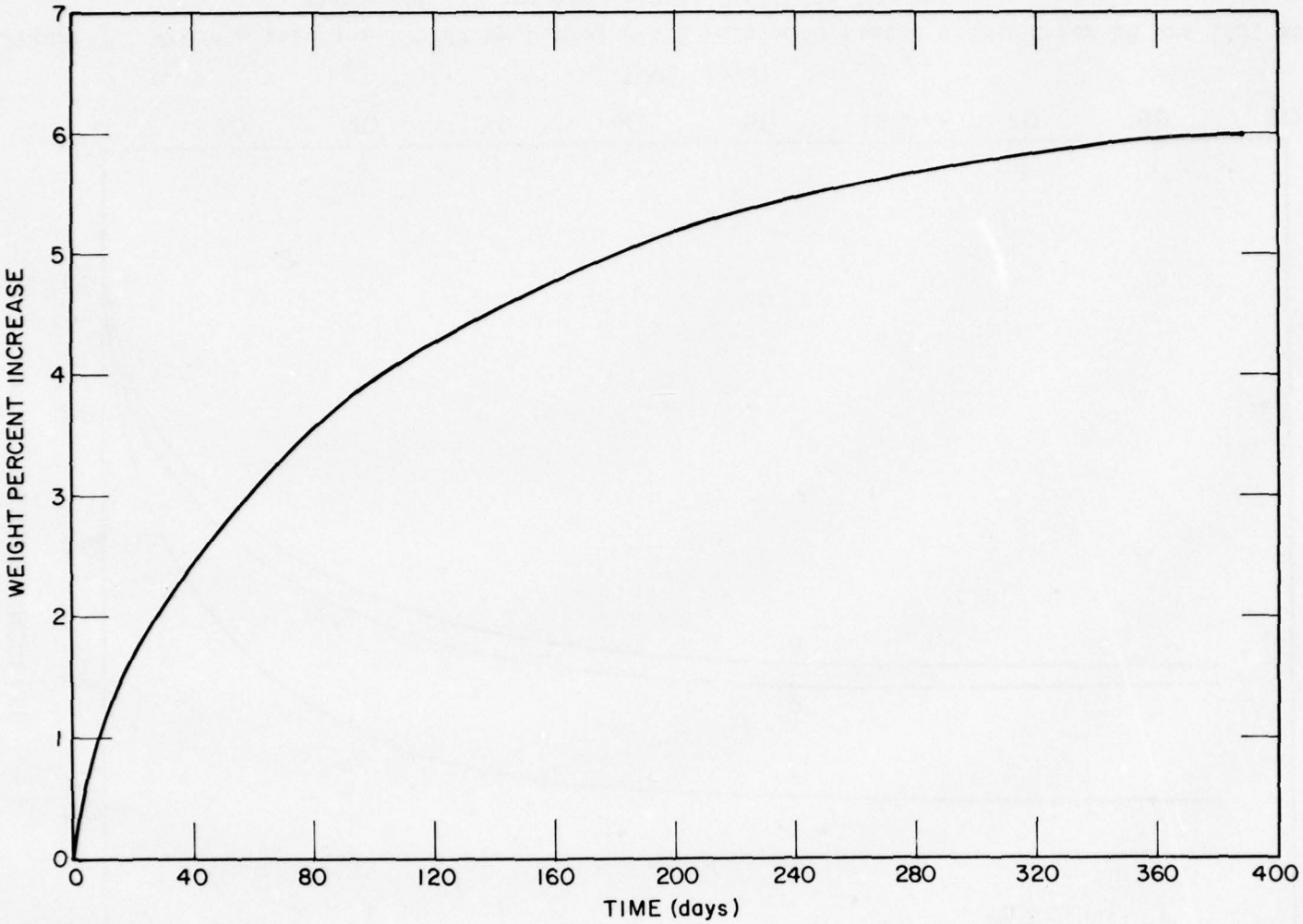

Figure 8. Water absorption (25°C) by C_{10}-polyphthalocyanine cured at 240°C for 48 hrs.

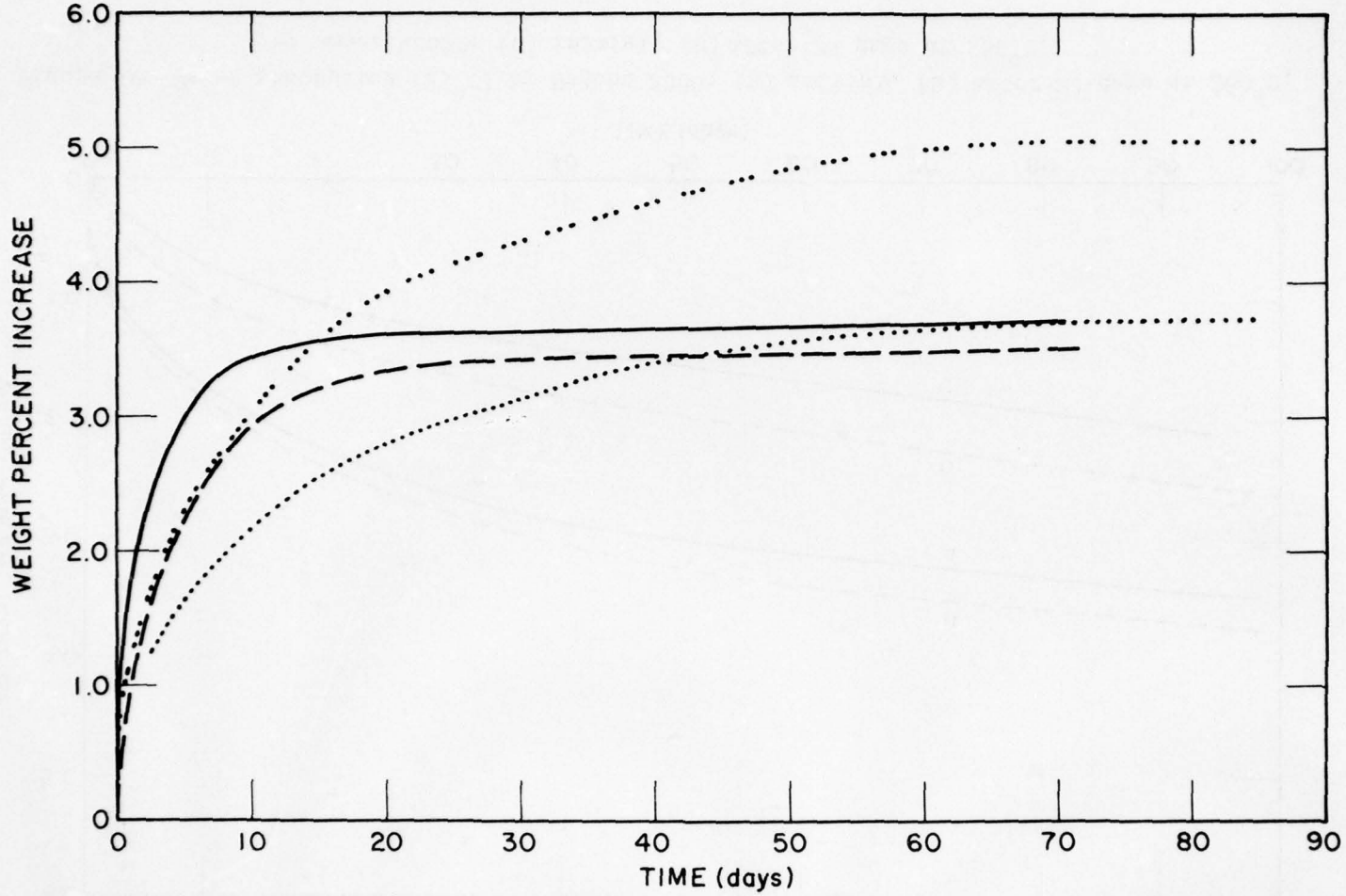

Figure 9. Water absorption (25°) by NR-150B2: (—) initial, (---) after 20 days at 300°C; by PMR-15: (····) initial cure, (··· ···) after 20 days at 300°C.

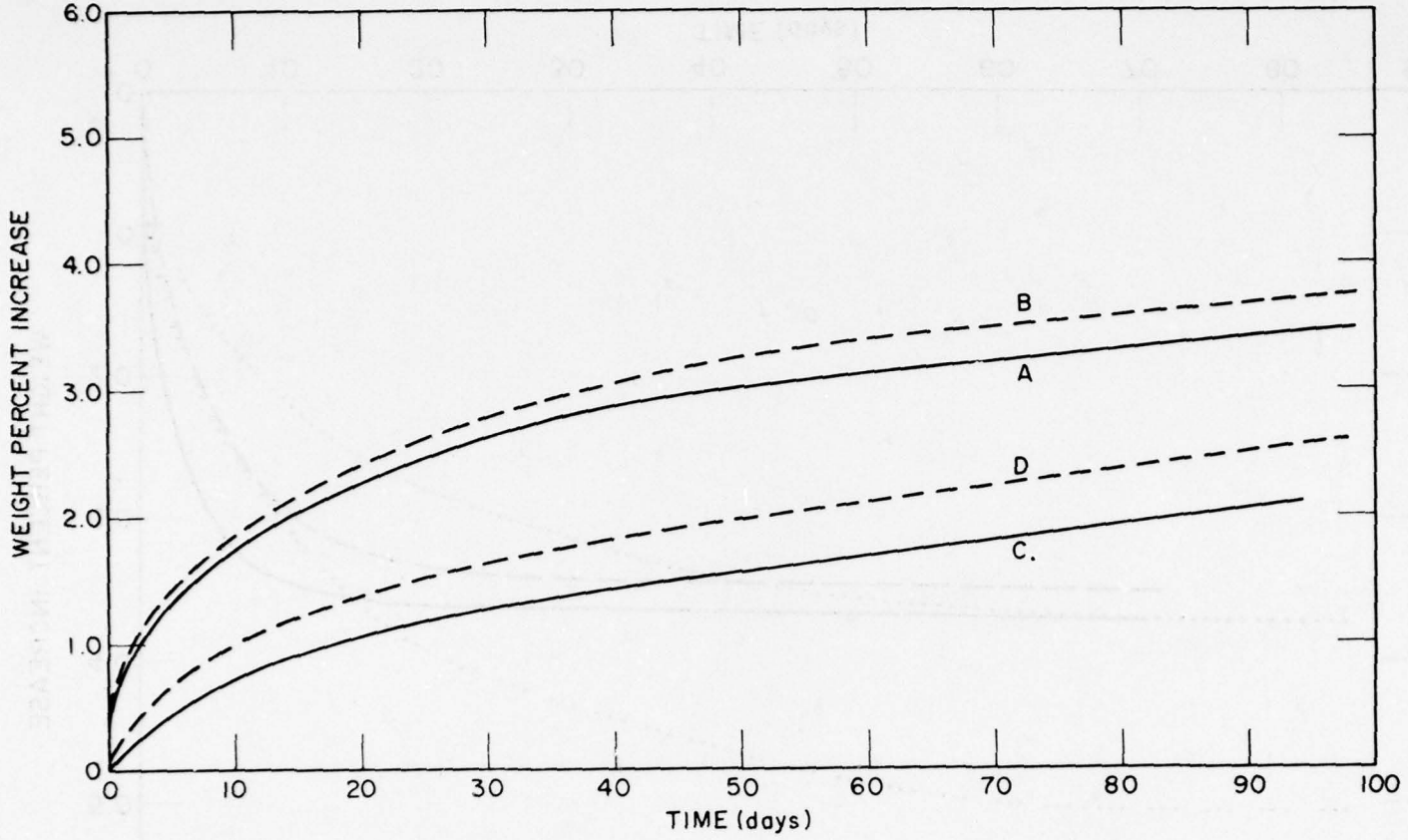

Figure 10. Water absorption (25°C) by Upjohn 2080: (A) initial, (B) after 20 days at 260°C; by Amoco 4000T: (C) initial, (D) after 20 days at 260°C.

TORSION PENDULUM ANALYSIS OF THE INFLUENCE OF MOLECULAR STRUCTURE ON THE CURE AND TRANSITIONS OF POLYPHTHALOCYANINES

J. K. Gillham
Polymer Materials Program
Department of Chemical Engineering
Princeton University
Princeton, NJ 08540

INTRODUCTION

This report follows up earlier studies (1,2) in which an automated torsion pendulum was used to investigate the transformation (cure) of a C_{10}-diamide phthalocyanine resin monomer to thermoset polymer using supported specimens [torsional braid analysis, TBA, (3)]. Cure was examined directly from isothermal plots and from transitions versus time of isothermal cure which were obtained from thermomechanical plots of intermittently cooled specimens. In the present work the influence of molecular structure on the transitions, particularly the glass transition (T_g) and a low temperature transition (T_{sec}) associated with the flexible molecular segments of the monomer and of the resulting network, has been investigated using monomers designated C_6-methyl, C_{10}, C_{14} and C_{22}-diamide phthalocyanine resin monomers.

EXPERIMENTAL

Monomers

The monomers were obtained from the Naval Research Laboratory. The chemistry of their synthesis and polymerization has been reported (4). There were:

"C_6-methyl-diamide", i.e., N,N'-bis(3,4-dicyanophenyl) 3-methylhexanediamide, mp 203-206°C.

"C_{10}-diamide", i.e., N,N'-bis(3,4-dicyanophenyl) decanediamide, mp 185-189°C.

"C_{14}-diamide", i.e., N,N'-bis(3,4-dicyanophenyl) tetradecanediamide, mp 163-165°C.

"C_{22}-diamide", i.e,, N,N'-bis(3,4-dicyanophenyl) docosanediamide, mp 144-147°C.

Torsion Pendulum

An automated, intermittently activated, freely vibrating torsion pendulum operating at about 1 Hz (3) was used for all experiments. Specimens were made by dipping a glass braid into a slurry of monomer in ethyl alcohol. After mounting the specimen in the apparatus at RT, the temperature was raised to the isothermal cure temperature at 5°C/min. Cure was monitored both continuously at the isothermal temperature and by intermittently cooling the sample and then heating back (generally at 1.5°C/minute) to the isothermal cure temperature to record the thermomechanical spectra (which were used to assign transition temperatures). All experiments were performed in dry helium.

The torsion pendulum plots display the relative rigidity ($1/P^2$, where P is the period in seconds of a freely damped wave) and logarithmic decrement $\Delta(= \ln A_i/A_{i+1}$, where A_i is the amplitude of the *ith* oscillation of a wave) versus temperature (mV from an iron-constantan thermocouple) or time. These parameters relate directly to dynamic mechanical properties in that the relative rigidity is directly proportional to the in-phase shear modulus (G') and $\Delta = \pi\tan\delta$, where δ is the phase angle between cyclic stress and strain. Transition temperatures were assigned using the peaks of the logarithmic decrement; intensities of transitions were assigned using Δ values.

RESULTS

An isothermal temperature of 250°C was selected for studying structure-property relationships since higher temperatures lead to a weak glass transition (and presumably to degradation). The present results emphasize T_g which was identified as the most dominant loss peak in a thermomechanical spectrum. Other transitions are considered more completely later. The glass transition temperatures versus time of cure at 250°C are included in Tables 1-4 and in Figures 1-4. The initial T_g for all of the monomers was less than 100°C. On heating, the glass transition temperature increased more rapidly and, after about 5 hours, reached a higher limiting temperature (designated $_{250}T_{g\infty}$) the shorter the length of the interaromatic molecular linkages. Values for $_{250}T_{g\infty}$ (see Table 5) were: C_6-methyl > 244°C, C_{10} ~ 202°C, C_{14} ~ 185°C, and C_{22} ~ 157°C. A plot of $_{250}T_{g\infty}$ versus the number of carbon atoms in the diacid used to synthesize the monomers, which is an index of segmental molecular flexibility, is shown in Figure 5. As the temperature of T_g increased with extent of cure, the intensity of T_g decreased for all four materials (Tables 1 to 4). This could lead to an uncertainty in designating T_g (see below).

Plots of isothermal cure for 5 hours at 250°C for the four monomers are shown in Figures 6A, 6B, 6C and 6D. The corresponding subsequent thermomechanical plots (250°C → -190°C) are shown in Figures 7A, 7B, 7C and 7D. Comparison of each pair of isothermal and thermomechanical plots shows that two loss "peaks" (peaks or shoulders) occur isothermally neither of which is assigned as the glass transition (vitrification), which is considered to be revealed in the corresponding thermomechanical plots at lower temperatures than the isothermal cure temperature. The first isothermal loss peak probably occurs at an isoviscous level and has been used to measure gelation times (1,2); the second "peak" presumably (2,5) corresponds to the $T_{\ell\ell}$ (or $T > T_g$) relaxation which occurs immediately above T_g. The procedure for assigning T_g is more convincingly demonstrated than in Figures 6A-6D and Figures 7A-7D by comparing the plot of isothermal cure at 220°C (Figure 8) and the subsequent thermomechanical plot (Figure 9) of the C_{14} material: there can be little doubt in this case that the intense relaxation below the temperature of isothermal cure is T_g.

The thermomechanical plots (Figures 7A, 7B, 7C and 7D) for the four materials obtained after curing at 250°C for 5 hours display two transitions below T_g. Numerical values are given in Table 6. The lower and more intense transition, designated T_{sec}, is ascribed (1,2,6) to motion of the flexible interaromatic segments. As anticipated, the more flexible the segment the more intense the mechanical loss peak: the intensity therefore increases in the order C_6-methyl < C_{10} < C_{14} < C_{22}. The least flexible segment, in the C_6-methyl, is also responsible for its loss peak being at a higher temperature (-98°C) than for its higher homologues (~ -140°C). The weaker T_{sec}' transition between T_g and T_{sec} also occurs at higher temperatures the lower the segmental flexibility; however its intensity increases relative to the background and relative to that of its T_{sec} relaxation in the order C_6-CH_3 > C_{10} > C_{14} > C_{22}. The origin of the T_{sec}' relaxation is unknown.

Just as two relaxations occur prior to vitrification in isothermal cure, so two relaxations occur above T_g (designated $T' > T_g$ and $T > T_g$) in TBA thermomechanical plots of low molecular weight material (1,2). They move quickly to higher temperatures with extent of cure, as indicated in Figures 1 to 4 for $T > T_g$ and Figures 3 and 4 for $T' > T_g$, and revealed in the corresponding thermomechanical plots (not shown here). The should be of importance to processing since they occur above T_g.

In the course of this work high resolution thermomechanical spectra of low molecular weight material were also obtained, including the following example.

Melting of the C_{14} monomer (RT → 250°C, $\Delta T/\Delta t$ 5°C/min; 250°C/5 min) and subsequent cooling ($\Delta t/\Delta t \leq 0.5$°C/min) resulted in a material the thermomechanical behavior (RT → 200°C, $\Delta T/\Delta t$ 0.5°C/min) of which is shown in Figure 10. Interpretation in terms of the sequence of transitions (designated by the loss peaks) follows:

The rigidity of the glass decreases through T_g (50.5°C), increases as a consequence of crystallization (68°C) and decreases through a series of well-defined steps (132°C, 143°C, 152°C and 163°C). The reported melting range was 163-165°C (4).

The thermomechanical spectra were reproducible. By changing the cooling conditions from the melt in the prehistory, the relative intensities of the transitions could be changed systematically.

CONCLUSIONS

An automated torsion pendulum has been used to study structure-property relationships of four phthalocyanine resins designated C_6- CH_3, C_{10}, C_{14} and C_{22}. The designation reflects the different segments between the aromatic nuclei of the monomers and of the resulting molecular networks. Cure at 250°C resulted in limiting glass transition temperatures, $_{250}T_{g\infty}$, which decreased as the segmental length and flexibility decreased: the values were C_6-CH_3 > 244°C, C_{10} ~ 202°C, C_{14} ~ 185°C and C_{22} ~ 157°C. After a standard cure of 250°C/5 hr. the thermomechanical spectra revealed two transitions below T_g: the lower (designated T_{sec}) was attributed to motions of the interaromatic molecular segments, the greater the flexibility of which, the lower and more intense the T_{sec} relaxations; the upper (designated T_{sec}') occurred at lower temperatures but with decreasing intensities (relative to the background) the greater the segmental flexibility. Two other relaxations occurring above T_g moved to higher temperatures more rapidly than T_g on cure: these bear on the processibility of the materials.

REFERENCES

1. J. K. Gillham, in High Performance Composites and Adhesives for V/STOL Aircraft, NRL Memorandum Report 3721, pp 37-59 (Ed. W. D. Bascom and L. B. Lockhart, Jr.), Naval Research Laboratory, Washington, D. C., February 1978.

2. J. K. Gillham, "Automated Torsion Pendulum Analysis of the Formation and Properties of a Polyphthalocyanine", Polymer Engineering and Science, Vol. 19, No. 4, pp 319-326 (1979)

3. J. K. Gillham, A.I.Ch.E. J., 20 (6), 1066 (1974).

4. J. R. Griffith and J. G. O'Rear, in High Performance Composites and Adhesives for V/STOL Aircraft, NRL Memorandum Report 3721, pp 15-20 (Ed. W. D. Bascom and L. B. Lockhart, Jr.), Naval Research Laboratory, Washington, D. C., February 1978.

5. J. K. Gillham, J. A. Benci and R. F. Boyer, Polymer Engineering and Science, Vol. 16, No. 5, 357 (1976).

6. W. D. Bascom, R. L. Cottington, J. L. Bitner, D. L. Hunston and J. Oroshnik, in High Performance Composites and Adhesives for V/STOL Aircraft, NRL Memorandum Report 3721, pp 23-25 (Ed. W. D. Bascom and L. B. Lockhart, Jr.), Naval Research Laboratory, Washington, D. C., February 1978.

ACKNOWLEDGMENTS

Appreciation is extended to Drs. W. D. Bascom and J. R. Griffith of the Naval Research Laboratory for providing samples of the four monomers and for their technical interactions.

TABLE 1. C_{6-CH_3}: Transitions (>RT) Versus Cure Time at 250°C

Time Min.	Plot No.	ΔT/Δt - or +	T_g °C (Δ)	T > T_g °C [Other]
	1	+		
5	2	-	92 (0.964)	111
5	3	+	92 (0.966)	110
23	4	-	138 (0.274)	246
23	5	+	139 (0.267)	223
41	6	-	186 (0.147)	>250
41	7	+	185 (0.141)	
83	8	-	212 (0.105)	
83	9	+	213 (0.0986)	
133	10	-	226 (0.0829)	
133	11	+	222 (0.0786)	
230	12	-	233 (0.0646)	[*]
230	13	+	231 (0.0605)	[*]
545	14	-	244 (0.0441)	[*]

[*] T < Tg relaxations evident in plot.

TABLE 2. C_{10}: Transitions (>RT) Versus Cure Time at 250°C

Time Min.	Plot No.	ΔT/Δt - or +	T_g (Δ) °C		T > T_g
10	1	-	60.5	(2.587)	81.5
10	2	+	60	(2.648)	79.5
28	3	-	71	(1.801)	106
28	4	+	71	(1.782)	106.5
46	5	-	99.5	(0.818)	183.5
46	6	+	99	(0.804)	182
94	8	-/+	165.5	(0.362)	
131	9	-/+	187.5	(0.283)	
269	10	-/+	199	(0.208)	
635	11	-/+	202.5	(0.139)	

TABLE 3. C_{14}: Transitions (> RT) versus Cure Time at 250°C

Time Min.	Plot No.	ΔT/Δt - or +	T_g (Δ) °C	T > T_g (T' > T_g) °C
0	1	+		
5	2	-	49 (2.218)	70 (∿ 86)
5	3*	+	49 (2.222)	67.5
5	4	-	50 (1.832)	75 (∿ 102)
5	5*	+	50.5 (1.829)	68
5	6*	+	51 (2.499)	71
23	7	-	64 (1.414)	132 (∿ 204)
23	8	+	65 (1.404)	131 (∿ 222)
33	9	-	100 (0.551)	202
33	10	+	99 (0.534)	198
66	11	-	150 (0.334)	
99	12	-	168 (0.257)	
99	13	+	169 (0.250)	
465	14	-	183 (0.137)	
465	15	+	185 (0.132)	
1005	16	-	176 (0.100)	
1005	17	+	175 (0.0986)	
1695	18	-	163 (0.0840)	
1695	19	+	161 (0.0830)	
2355	20	-	152 (0.0784)	

*See plots for multiple melting/crystallization transition.

TABLE 4. C_{22}: Transitions (> RT) versus Cure Time at 250°C

Time Min.	Plot No.	ΔT/Δt - or +	T_g (Δ) °C		T > T_g (T' > T_g) [Other] °C
5	2	-	87(?)	(0.243)	[T_{cry} 93]
5	3	+	90	(0.217)	[T_m 134]
23	4	-	58	(0.538)	124 (219)
23	5	+	60	(0.535)	129 [141/∿231]
41	6	-	71	(0.388)	184 (∿254)
41	7	+	71	(0.382)	183
89	8	-	108	(0.256)	233
89	9	+	111	(0.250)	∿226
131	10	-	128	(0.202)	
131	11	+	130	(0.200)	
296	12	-	145	(0.143)	
296	13	+	147	(0.145)	[∿50]
824	14	-	156	(0.101)	
2432	15	-	157	(0.100)	
2432	16	+	151.5	(0.0789)	[52/∿88]
5048	17	-	153	(0.0660)	
5048	18	+	148	(0.0685)	[∿48]

TABLE 5. $_{250}T_{g\infty}$ Versus Effective Number of Inter-Aromatic Carbon Atoms

Polymer	Effective Number of Carbon Atoms*	$_{250}T_{g\infty}$ (°C)
C_{6-CH_3}	5.5	> 244
C_{10}	10	∿ 202
C_{14}	14	∿ 185
C_{22}	22	∿ 157

*Effective number of carbon atoms/inter-aromatic segment is taken as the number of unbranched C atoms between the amide N atoms in the monomer, except for C_{6-CH_3} which is assigned 0.5 less than 6 because of the stiffening effect of a branched C.

TABLE 6. Polyphthalocyanines: Transitions (°C)
After 5 Hour Cure at 250°C

Polymer	T_g (Δ)	T'_{sec} (Δ)	T_{sec} (Δ)
C_6-CH_3	234 (0.180)	19 (0.0443)	-98 (0.0415)
C_{10}	194 (0.136)	3 (0.0342)	-145 (0.0858)
C_{14}	178 (0.160)	8 (0.0427)	-140 (0.155)
C_{22}	137 (0.234)	1 (0.0459)	-139 (0.229)

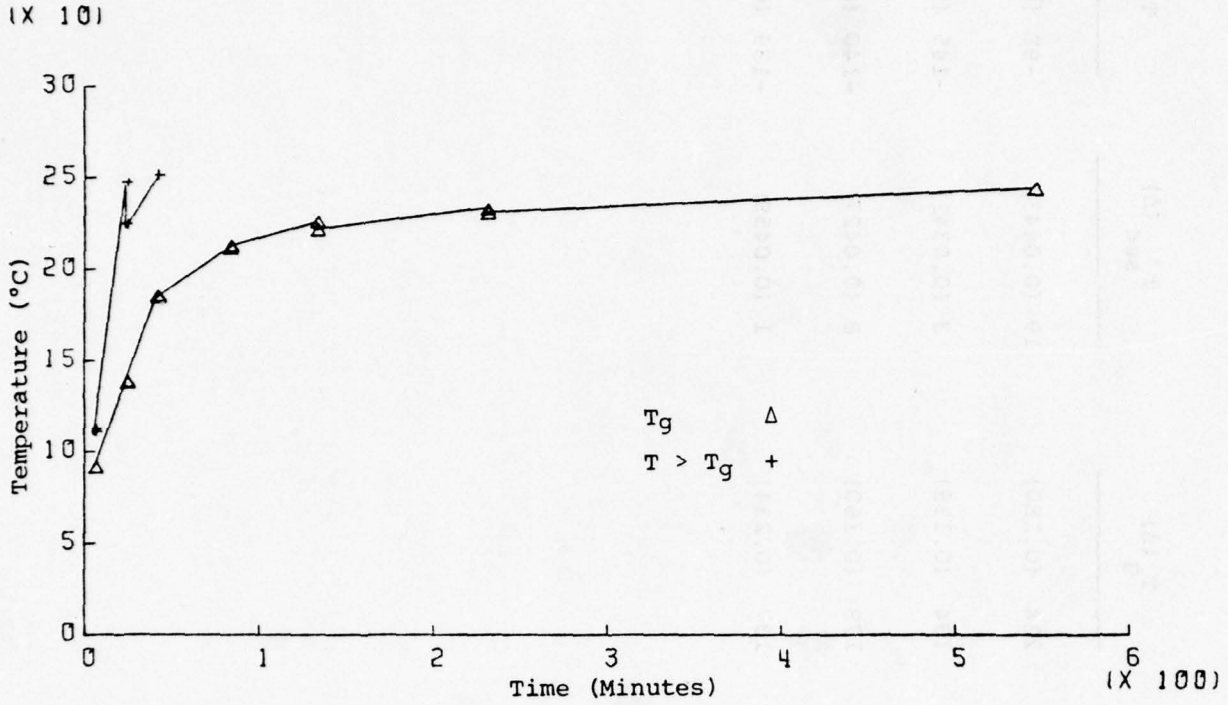

Figure 1. $C_{6\text{-}CH_3}$: Transitions (> RT) versus Cure Time at 250°C.

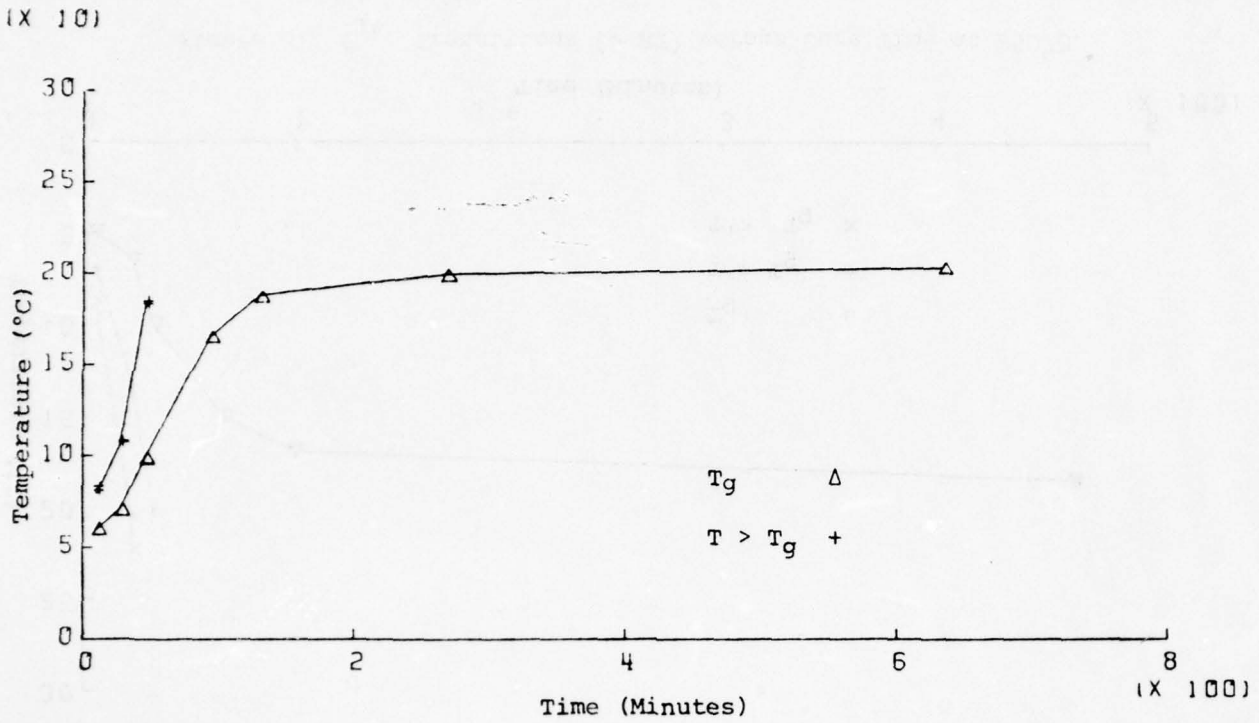

Figure 2. C_{10}: Transitions (> RT) versus Cure Time at 250°C.

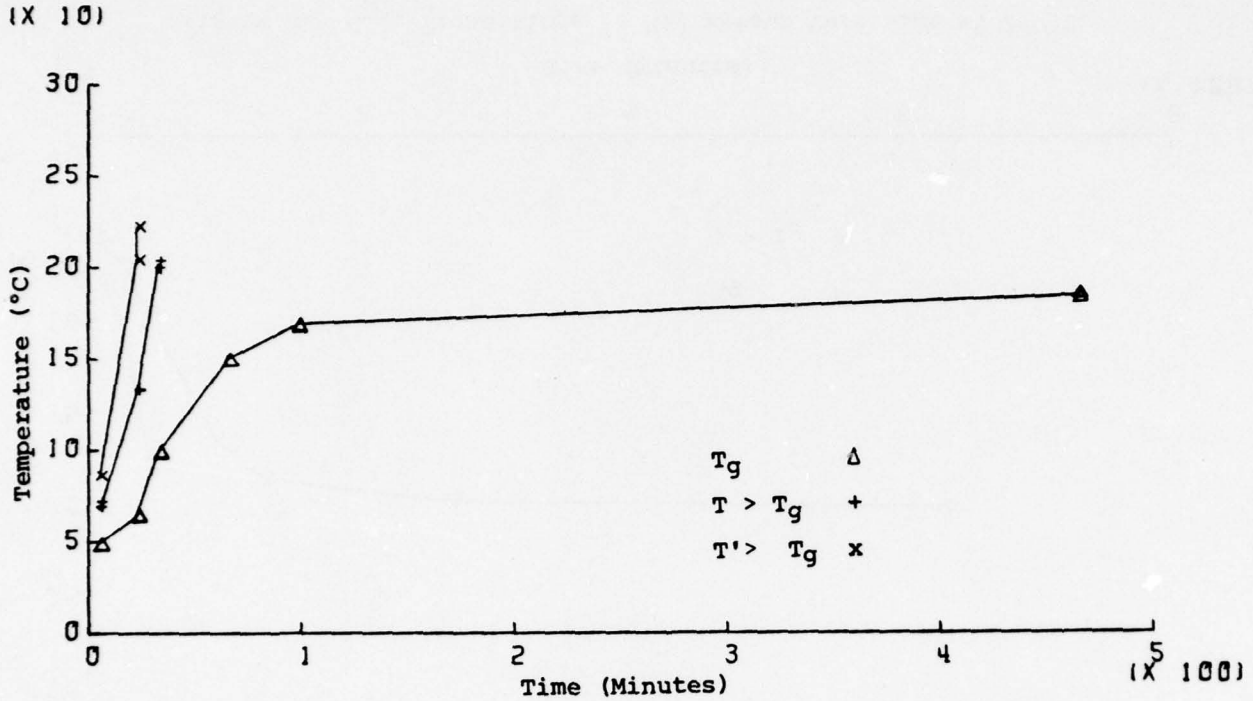

Figure 3. C_{14}: Transitions (> RT) versus Cure Time at 250°C.

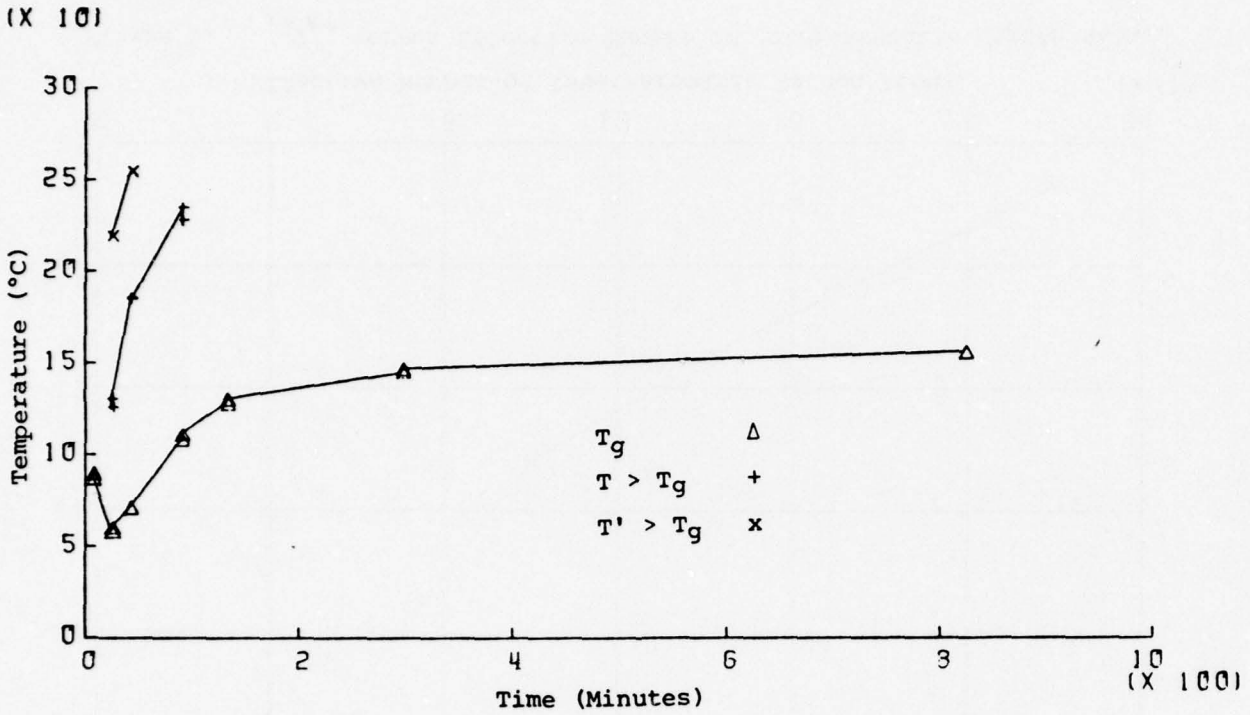

Figure 4. C_{22}: Transitions (> RT) versus Cure Time at 250°C.

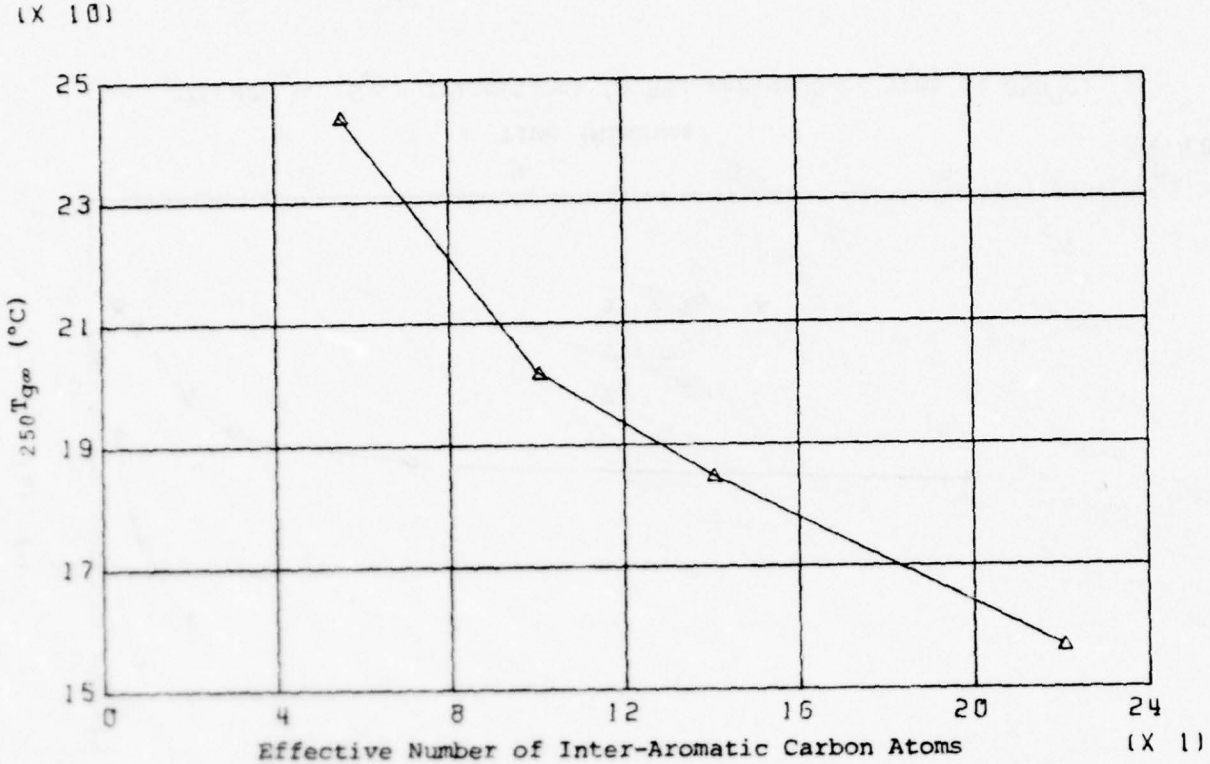

Figure 5. $_{250}T_{g\infty}$ versus Effective Number of Inter-Aromatic Carbon Atoms.

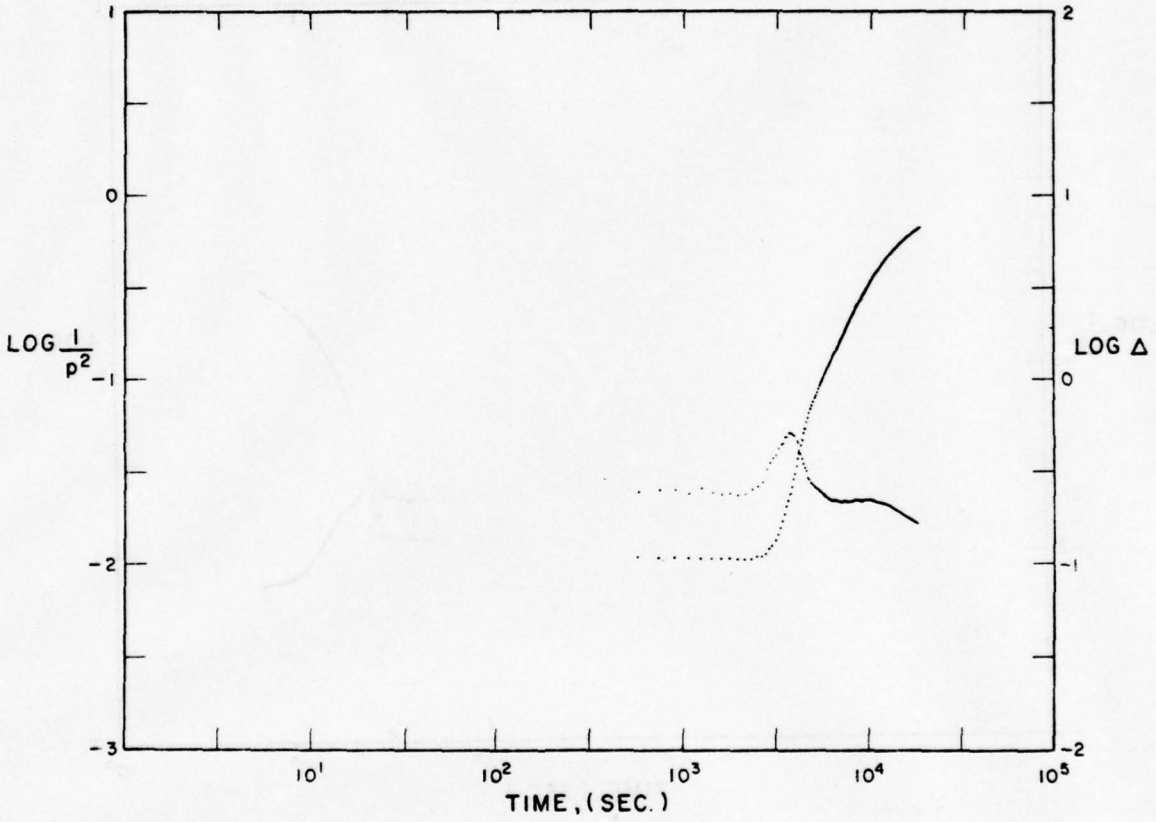

A) C_{6-CH_3}

Figure 6. Isothermal Cure (250°C/5 hr)

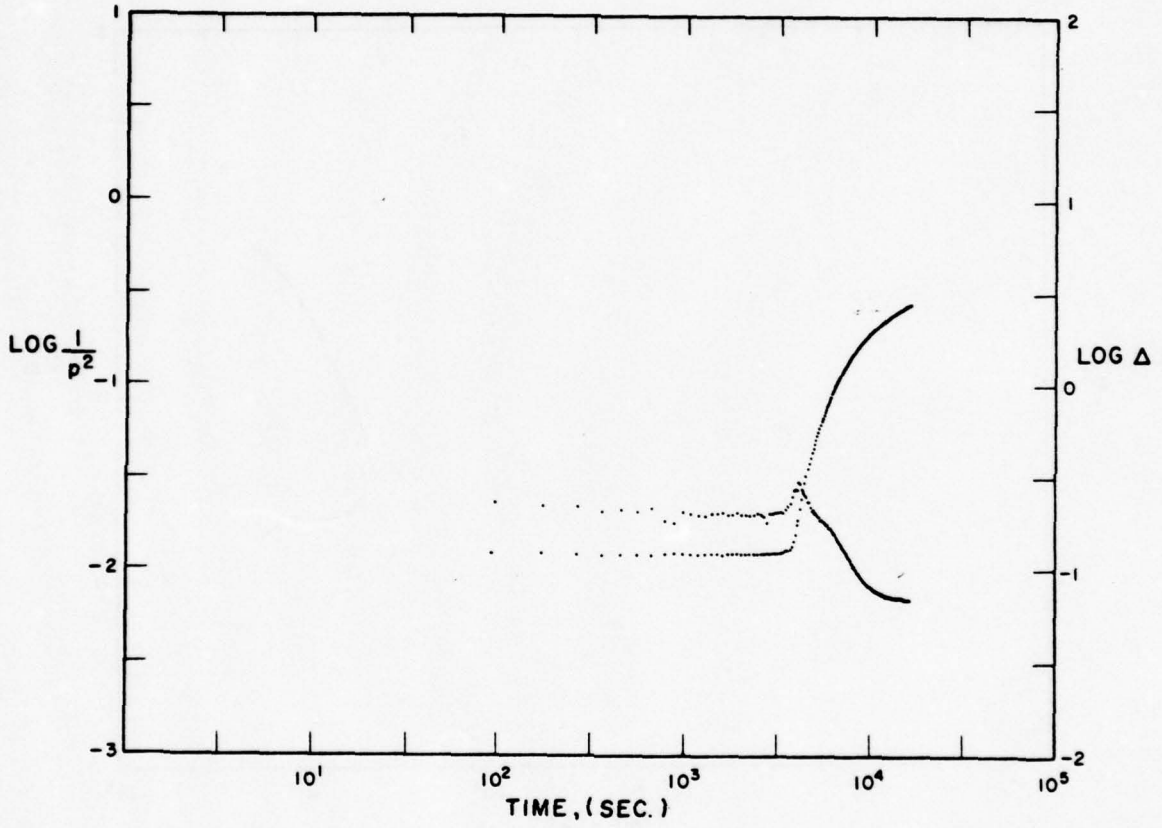

B) C_{10}

Figure 6. Isothermal Cure (250°C/5 hr)

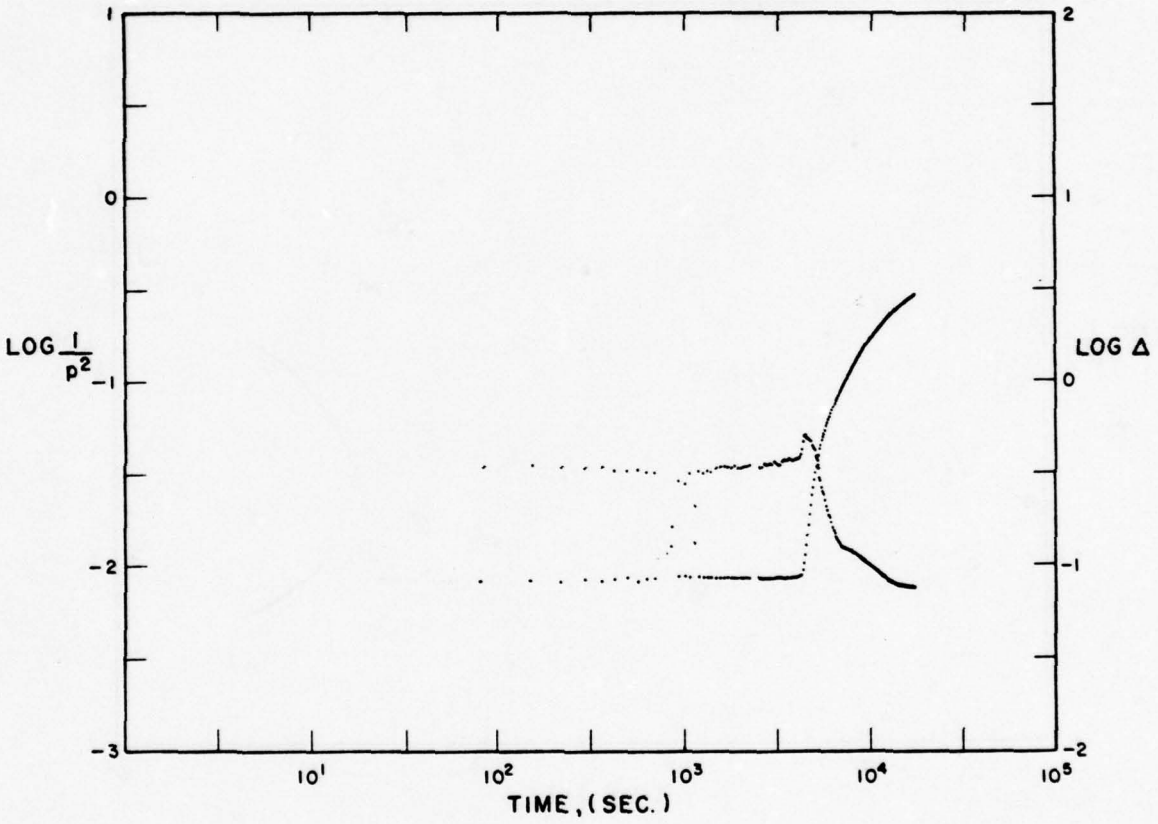

C) C_{14}

Figure 6. Isothermal Cure (250°C/5 hr)

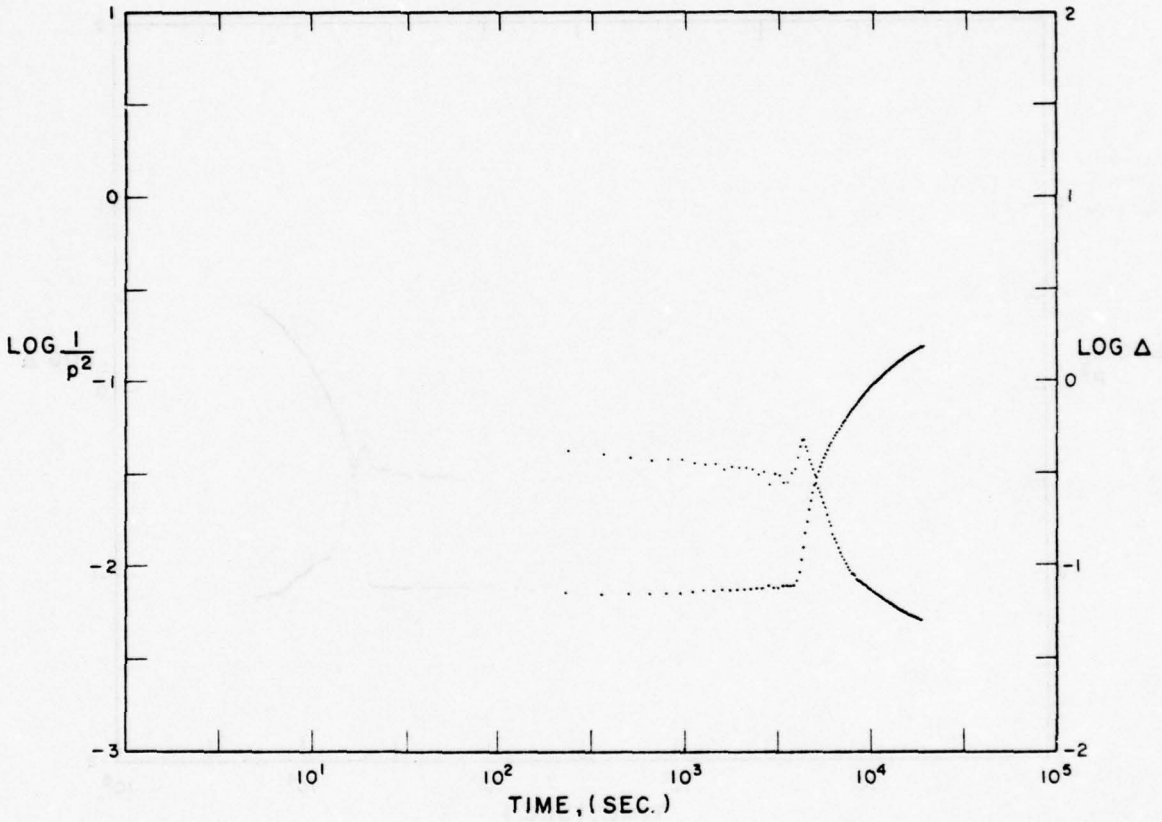

D) C_{22}

Figure 6. Isothermal Cure (250°C/5 hr)

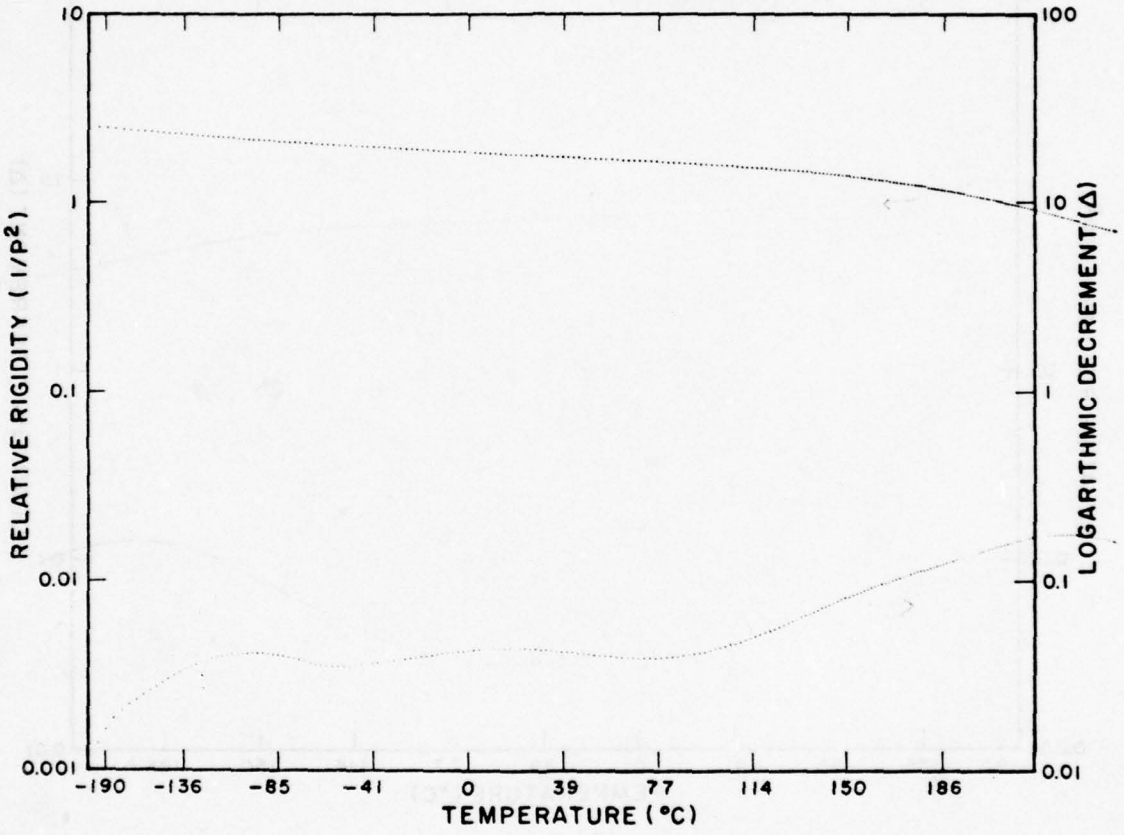

A) $C_{6\text{-}CH_3}$

Figure 7. Thermomechanical spectra (250°C → -190°C) after 250°C/5-hr cure (same specimens as for Figure 6)

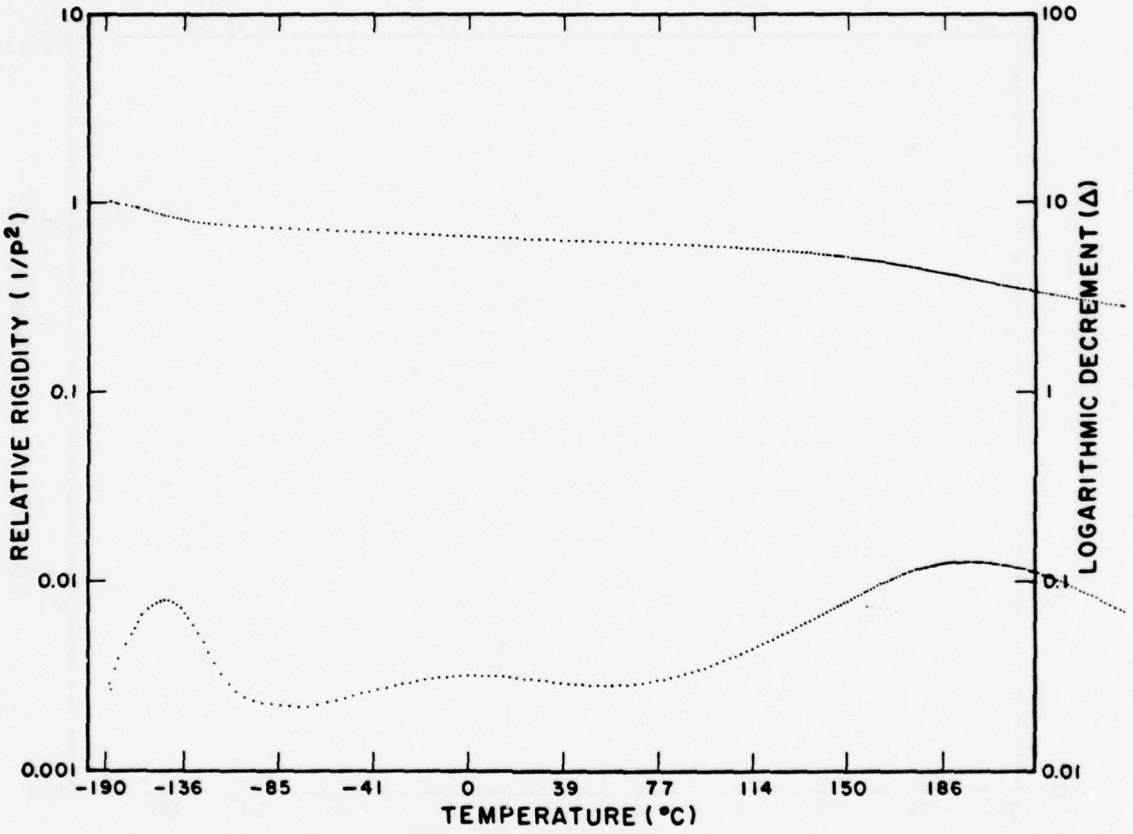

B) C_{10}

Figure 7. Thermomechanical spectra (250°C → -190°C) after 250°C/5-hr cure (same specimens as for Figure 6)

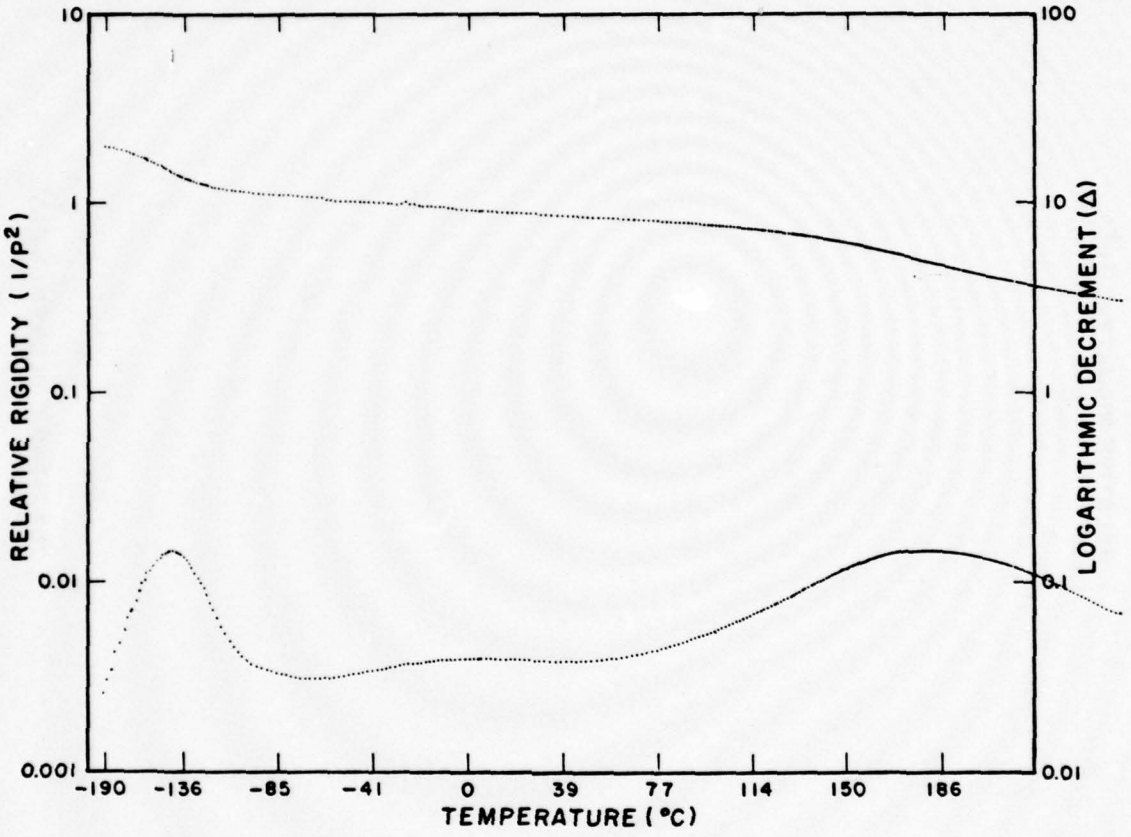

C) C_{14}

Figure 7. Thermomechanical spectra (250°C → -190°C) after 250°C/5-hr cure (same specimens as for Figure 6)

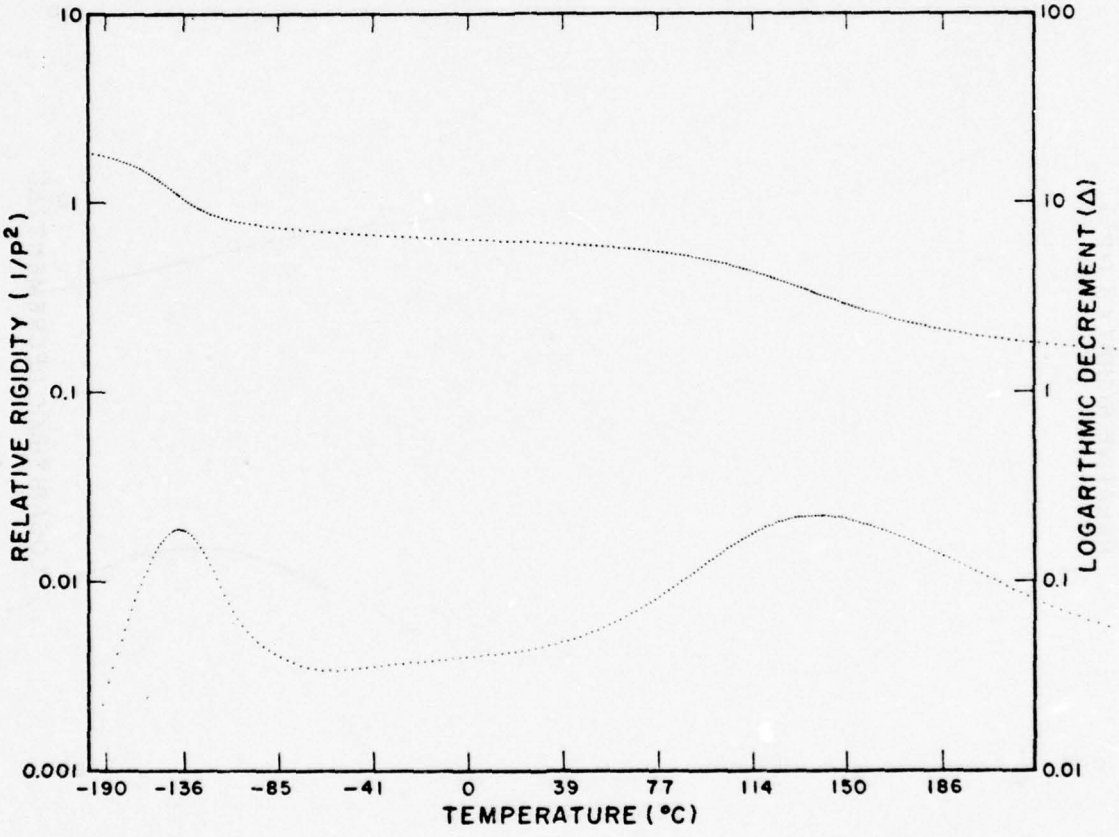

D) C_{22}

Figure 7. Thermomechanical spectra (250°C → -190°C) after 250°C/5-hr cure (same specimens as for Figure 6)

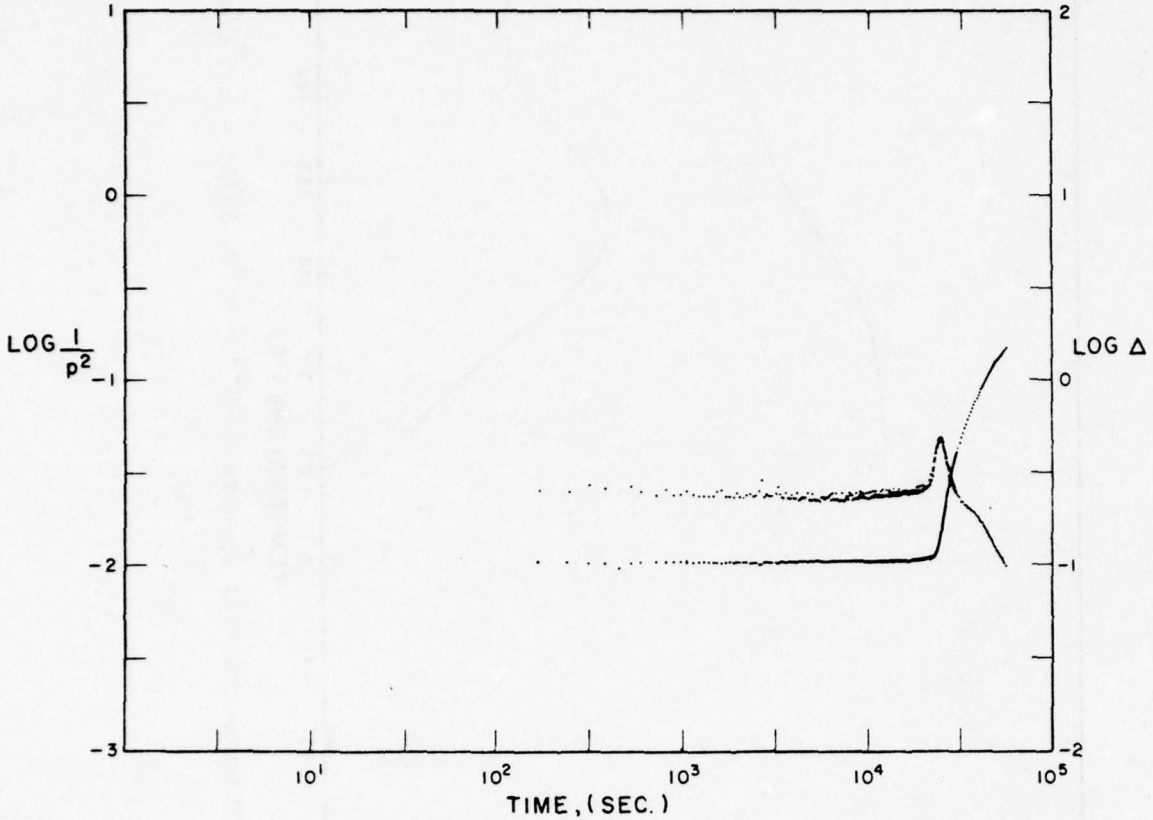

Figure 8. Isothermal cure (220°C/16.5 hr): C_{14}.

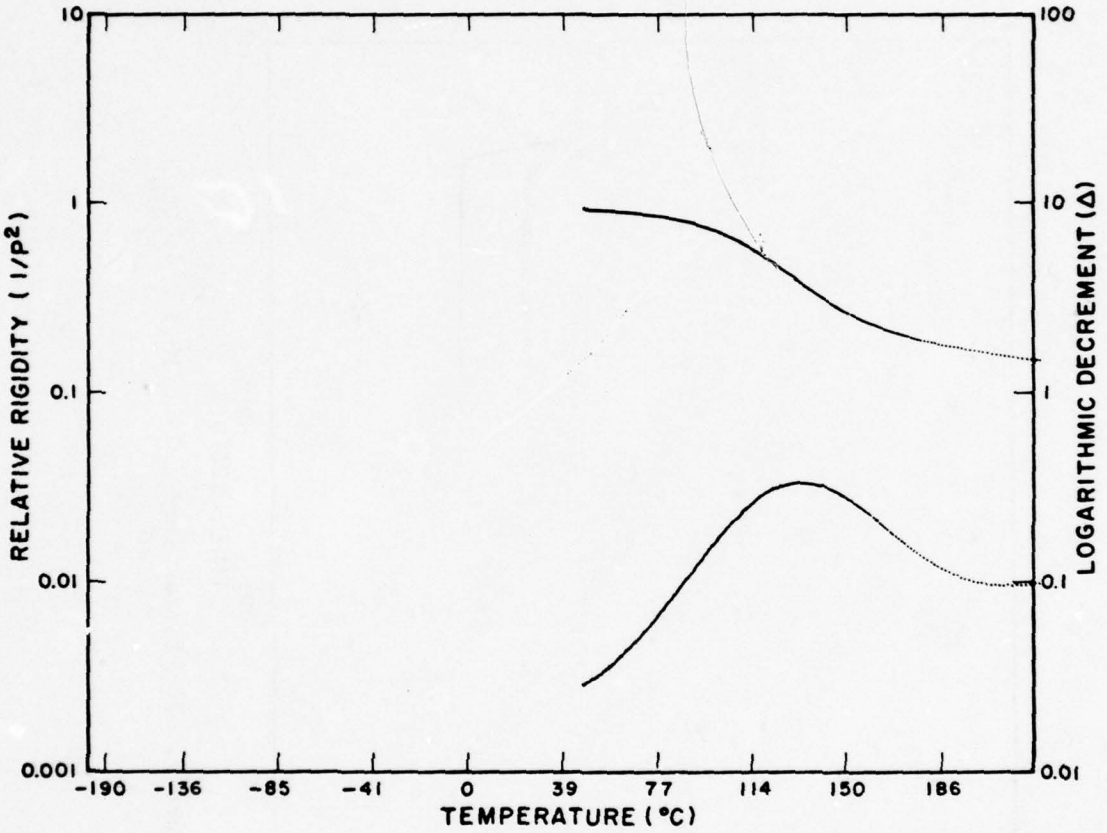

Figure 9. Thermomechanical spectra (220°C → 45°C, $\Delta T/\Delta t \leq 1.5$°C/min)

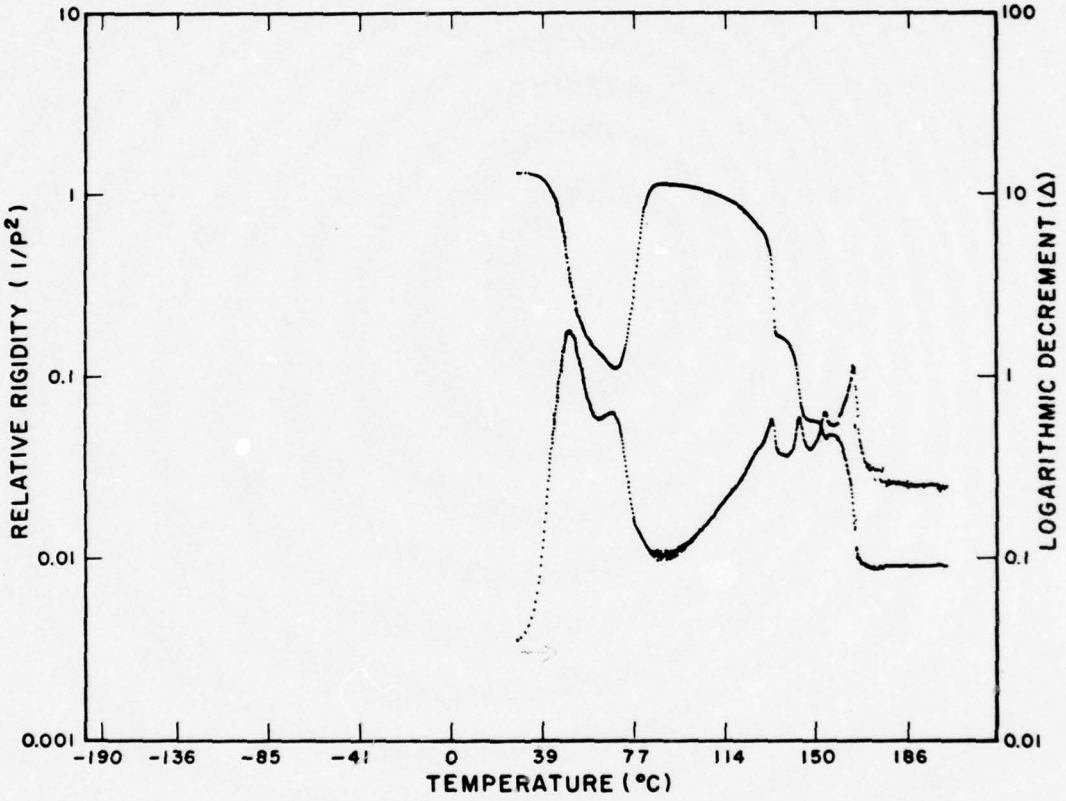

Figure 10. C_{14} monomer. Thermomechanical spectra (RT → 250°C, $\Delta T/\Delta t$ 0.5°C/min) after melting (250°C/5 min) and subsequent cooling ($\Delta T/\Delta t \leq 0.5$°C/min).

CHEMICAL CHARACTERIZATION FOR QUALITY CONTROL

C. F. Poranski, Jr. and W. B. Moniz
Chemical Diagnostics Branch
Chemistry Division

INTRODUCTION

Any program to develop or select organic polymers for aerospace applications like structural adhesives or fiber-reinforced organic matrix composites must include the development of quality assurance procedures. These procedures should cover tests to verify not only the processibility and physical properties but also the chemical composition of the polymer. Quality assurance is an integral part of the NRL V/STOL Program.

The Chemical Characterization Task is responsible for developing procedures to monitor the chemical composition of organic materials being evaluated in this program. These procedures, coupled with those being developed by the other Tasks for thermomechanical and physical properties, will be the basis of a quality assurance scheme for the resin system meeting the performance goals of the NRL V/STOL Program.

The objectives of the Chemical Characterization Task for FY-78 were: a) determine the utility of liquid chromatography for the analysis of C_{10}-diamide, b) define quality control parameters and procedures for C_{10}-diamide and other selected resin systems, and c) characterize new commercial materials of interest to the Program.

The major effort of the Chemical Characterization Task during FY-78 was focused on C_{10}-diamide. An evaluation of liquid chromatography of C_{10}-diamide systems revealed several separation and detection problems. A differential scanning calorimetry (DSC) procedure was developed which appears promising as a technique for evaluating the purity of C_{10}-diamide.

Progress was made in other areas also. A proton NMR method for analyzing TGMDA/DDS resin systems was refined.

The aging study on Hexcel F-178/T300 prepreg was completed. The carbon-13 NMR spectrum of HR-600 resin was analyzed, and a NMR method for determining epoxide equivalent weights of DGEBA-type epoxy resins was developed. These topics are discussed in more detail below.

DIFFERENTIAL SCANNING CALORIMETRY*

NRL's current procurement specifications for C_{10}-diamide require that the material melt within the range of 185°-192°C and that the melting point spread be no greater than 3°. There is no procedure specified for obtaining the melting point, and thus its determination can be somewhat subjective. In an attempt to provide a more quantitative basis for establishing melting behavior, we initiated a differential scanning calorimetry (DSC) study of the C_{10}-diamide.

The following procedure was developed using a Perkin-Elmer Model DSC 2:

1. Weigh 10 ± 1 mg into an aluminum DSC capsule.

2. Precondition the sample by programmed heating at 10°/min. to 175°C. Do not record the DSC curve. (The reason for this step is discussed below.)

3. Cool the sample to room temperature at 20°/min. in the DSC apparatus.

4. Heat the sample to 215°C at a heating rate of 10°/min., recording the curve at a gain setting which keeps the melting endotherm on scale (R20 for a 10-mg sample).

5. Evaluate the data against quality control pass/fail criteria.

Using this procedure, 17 batches of C_{10}-diamide have been examined. Table 1 gives the temperatures of the peak endotherms, as well as the melting points obtained by conventional procedures. In general, the peak endotherms are 3-5° higher than the conventional melting points. This may be due to differences in heating rates or some other instrumental factor, or it may be related to effects which are eliminated in the preconditioning step.

* This study was carried out in collaboration with Dr. Paul Peyser of the Polymeric Materials Branch.

To facilitate comparisons of peak amplitudes and shapes, the DSC curves were normalized to a common basis, scaling each curve by the ratio of sample weight to weight of standard. The standard is NRL 1, a high purity sample of C_{10}-diamide.

The endotherms of the samples varied widely, as expected from the conventional melting point data. Two classes of behavior are depicted in the accompanying figures. Figure 1 shows the curves for four samples having nominally the same peak endotherm temperature, 193.1°. Of these, sample 12B has the sharpest curve in terms of height and width. The others (10A, 11C, and 25) have distinctly lower heights, with skewing to low temperature, indicative of higher impurity content. Sample 25 shows additional very low amplitude peaks at ca. 182° and 192°.

Figure 2 depicts the range of endotherms encountered, as represented by the standard (STD, NRL 1), 12B, 21, 24, and 20. The last three samples show rather unusual "double-lobe" endotherms, with an initial peak at ca. 183°. The low amplitude endotherms of these three samples and the shift of their curves to low temperature are indicative of impurity content. For example, sample 20 was a commercial product, rejected on the basis of its low melting point. Analysis of this material by proton NMR showed that 4-aminophthalonitrile and sebacic acid were present in appreciable amounts.

The use of these results to establish the quality control criteria referred to in Step 5 of the procedure must wait on performance data currently being acquired in other parts of this program.

The second step of the procedure requires heating the sample to 175°, well below the melting region. The preconditioning is necessary to remove endotherms and exotherms which occur around 169-170°C. These peaks are most prominent in the heating curves of the reference material, a sample of C_{10}-diamide purified by several recrystallizations from ethanol. These peaks are less pronounced for the lower purity materials. They are due to solid-state phenomena believed to be associated with a sample's previous history.

HIGH-PERFORMANCE LIQUID CHROMATOGRAPHY (HPLC)

HPLC has proved to be quite useful in analyzing a wide variety of chemical systems. Once the operational parameters have been established, the method is easily

automated. Recent developments in microprocessor control and automatic sampling have made possible long-term (overnight), unattended, repetitive operation. For this reason, we have devoted some time to seeking a HPLC method for the analysis of C_{10}-diamide.

As a starting point, we assumed that the most likely impurities to be expected in commercial C_{10}-diamide would be 4-aminophthalonitrile (APN), sebacic acid (SA), and any of several solvents which might be used in the manufacturing process (dimethyl formamide, acetone, or water). A procedure was sought which would allow detection of as little as one percent of APN or SA in C_{10}-diamide, as well as reveal the presence of solvents. Two modes of liquid chromatography were investigated (reverse phase gradient elution (RPGE) and size exclusion (SEC)) with mixed results. In the RPGE work good separation of APN and C_{10}-diamide was obtained with two VYDAC reverse phase columns and a solvent system which changed linearly from 57% H_2O/43% MeOH to 45% H_2O/55% MeOH in two minutes. In a gradient mode, however, only a UV detector can be used. While both C_{10}-diamide and APN have adequate UV absorption at 254 nm or 280 nm, SA does not, and could not be detected in this mode. Moreover, there is only a limited solvent composition range for the C_{10}-diamide system. With less than 43% MeOH the C_{10}-diamide never comes through the column. At greater than 55% MeOH the C_{10}-diamide elutes quickly and cannot be separated from APN. Considerably more work would need to be done to determine the optimum solvent composition if the H_2O/MeOH solvent system is to be used.

For the SEC work we used two 100Å μ-Styragel columns, 100% tetrahydrofuran (THF) as the solvent and a differential refractometer as the detector. Two problems were encountered. Although C_{10}-diamide was separated from APN and SA, the latter two compounds were not separated. Also, the signal from SA in the refractometer was very weak, about one-tenth that of APN or C_{10}-diamide for comparable sample concentrations of 1 μg/μl. Since the maximum solubility of C_{10}-diamide in THF is ∿3 μg/μl, to detect SA at the 1% level in C_{10}- diamide, the sample injection size must be greater than 35 μl. To date, only 10-μl (containing 1 μg/μl C_{10}-diamide) samples have been used. A 100-μl sample injection loop is available, however, and will be tried.

The liquid chromatography effort has indicated two possible routes to a quality control procedure. However, a considerable amount of work is required to optimize either approach, and there may be other approaches more suitable

for this particular group of compounds. Before proceding further, therefore, we will seek advice from commercial suppliers of columns and chromatographs, hoping that their experience will speed the optimization process.

AGING OF GRAPHITE/POLYIMIDE PREPREG

In a previous report (1) we discussed results of a short-term (21 days) aging study of Hexcel F-178/T300 prepreg. In that study no change in the relative intensities of the proton NMR peaks was observed. This aging study has been continued to a total time of seven months, again with no significant difference discernible in the proton spectra of material extracted from aged prepreg. However, there were changes in the processing characteristics and mechanical properties of laminates prepared from the aged prepreg. These changes are reported in a later section of this review.

The failure of proton NMR, a very sensitive technique, to detect changes in extracts of aged prepreg may be due to the choice of solvent, acetone. The products of the chemical reactions leading to loss of tack and decreased resin flow must not be soluble in acetone. A more effective solvent will be sought if time allows.

QUANTITATIVE ANALYSIS OF TGMDA/DDS FORMULATIONS

We have previously described a proton NMR method for quantitative analysis of TGMDA/DDS formulations (2) and some initial results (3). Additional work has been done on this method and will be published in complete form elsewhere (4). The results, now spanning the range 25-50 phr, are shown in Figure 3. We are confident that, with additional work to define the accuracy and precision and to refine the procedure, the proton NMR method will be as useful as present infrared or liquid chromatographic approaches. The method is straightforward and easily adapted to the variety of TGMDA/DDS systems in use with modifications to accommodate effects due to the various additives in use. We do not plan to continue work in this area unless it becomes a specific need of this program.

CARBON-13 NMR STRUCTURAL ANALYSIS OF HR-600

HR-600 is an acetylene-terminated polyimide oligomer developed by Hughes Aircraft Company and subsequently commercialized by Gulf Oil Chemicals Company as Thermid 600. The structure (Figure 4) was originally proposed on the basis of carbon-hydrogen-nitrogen analysis, and infrared

and proton NMR spectroscopy. The carbon-13 spectrum, although fairly complex, was analyzed using data obtained from model compounds and confirmed the proposed structure (5).

C-13 NMR OLIGOMER ANALYSIS OF EPOXY RESINS

Epoxy resins based on the diglycidyl/ether of bisphenol A (DGEBA) are mixtures of oligomers of the general structure shown below:

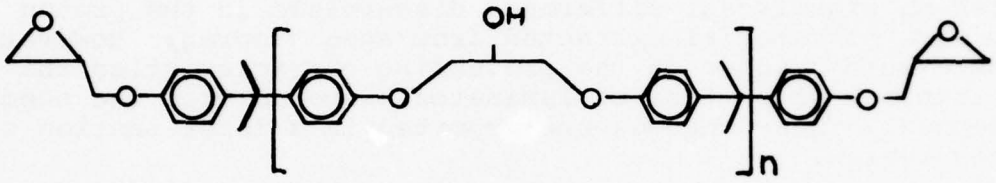

Two important processing characteristics, the epoxide equivalent weight (EEW) and molecular weight distribution, depend on the proportion of oligomers of various n's contained in the mixture. It is often necessary to determine both characteristics in order to help assure reproducible products. We have reported how carbon-13 NMR may be used to determine the EEW (6). Figure 5 shows the region of interest in the carbon-13 NMR system for two DGEBA resins. The EEW determination depends on the fact that as n increases, the relative intensities of the lines at 44 and 50 ppm (due to carbons in the glycidyl end groups) decrease relative to that of the line at 70 ppm (which is due to carbons resulting from epoxide-ring opening reactions).

Our preliminary results, shown in Table 2, indicate that the carbon-13 NMR method is promising. Work is continuing in another program to determine the analytical precision, optimize the concentration/time variables and chemically analyze the resin samples used in these carbon-13 NMR studies.

FUTURE PLANS

During FY-79 the Chemical Characterization Task will focus on methods of analysis of C_{10}-diamide prepregs and curing of C_{10}-diamide. In particular, the analysis of C_{10}-diamide prepregs will include: a) determining the

degree of staging by DSC, Fourier transform infrared, ESCA and nuclear magnetic resonance techniques, and b) determination of the amount and type of volatiles present. Investigation of the curing of C_{10}-diamide will be aimed at elucidating the mechanism of the cure and structure of the final polymer using, primarily, electron spin resonance, variable temperature NMR and proton-enhanced carbon-13 NMR.

REFERENCES

1. "High Performance Composites and Adhesives for V/STOL Aircraft, 2nd Annual Report"
   W. D. Bascom and L. B. Lockhart, Jr.
   NRL Memorandum Report 3721, February, 1978, p. 65.

2. "High Performance Composites and Adhesives for V/STOL Aircraft, 1st Annual Report"
   W. D. Bascom and L. B. Lockhart, Jr.
   NRL Memorandum Report 3433, December, 1976, p. 37.

3. "High Performance Composites and Adhesives for V/STOL Aircraft, 2nd Annual Report"
   W. D. Bascom and L. B. Lockhart, Jr.
   NRL Memorandum Report 3721, February, 1978, p. 67.

4. C. F. Poranski, Jr. and W. B. Moniz
   Proceedings of the Fifth ASTM Conference on Composite Materials: Testing and Design, ASTM, Philadelphia, PA, in press.

5. C. F. Poranski, Jr., W. B. Moniz, and T. W. Giants
   Organic Coatings and Plastics Preprints 38, 605 (1978).

6. W. B. Moniz and C. F. Poranski, Jr.
   Organic Coatings and Plastics Preprints 39, 99 (1978).

7. Y. Tanaka, A. Okada, and I. Tomizuka in "Epoxy Resins," C. A. May and Y. Tanka, eds., Marcel Decker, 1973, Chapter 2.

TABLE 1

MELTING POINTS (DEG C) OF C_{10}-DIAMIDE

SAMPLES OBTAINED BY DSC (PEAK ENDOTHERM

TEMPERATURES) AND BY A CONVENTIONAL METHOD

SAMPLE	DSC PEAK ENDOTHERM TEMPERATURE	CONVENTIONAL MELTING POINT
Standard	197.4	190-192
2	192.2	188-189
9A	192.1	184-187
10A	193.1	186-188
11A	192.6	-
11B	191.5	185-188
11C	193.1	186-189
12A	192.9	186-189
12B	193.2	187-188
12C	190.1	185-187
13A	191.9	183-187
20	183.8	175-182
21	190.7	185-187
22	193.4	186-188
23	189.3	183-187
24	191.9	-
25	193.1	187-190
26	190.5	184-187

TABLE 2

EPOXIDE EQUIVALENT WEIGHTS DETERMINED BY CARBON-13 NMR

RESIN	LITERATURE*	C-13 NMR
DER 332LC	170-175	178
EPON 826	180-188	172
EPON 828 (1)	185-192	176
EPON 828 (2)	185-192	181
EPON 828 (3)	185-192	171
ARALDITE 7071	450-530	522
EPON 1001	450-530	568
EPON 1002	600-700	686
EPON 1004	875-1025	971

* From Ref. 7.

Fig. 1 DSC curves for four samples of C_{10}-diamide having nominally the same peak endotherm temperature, 193.1.

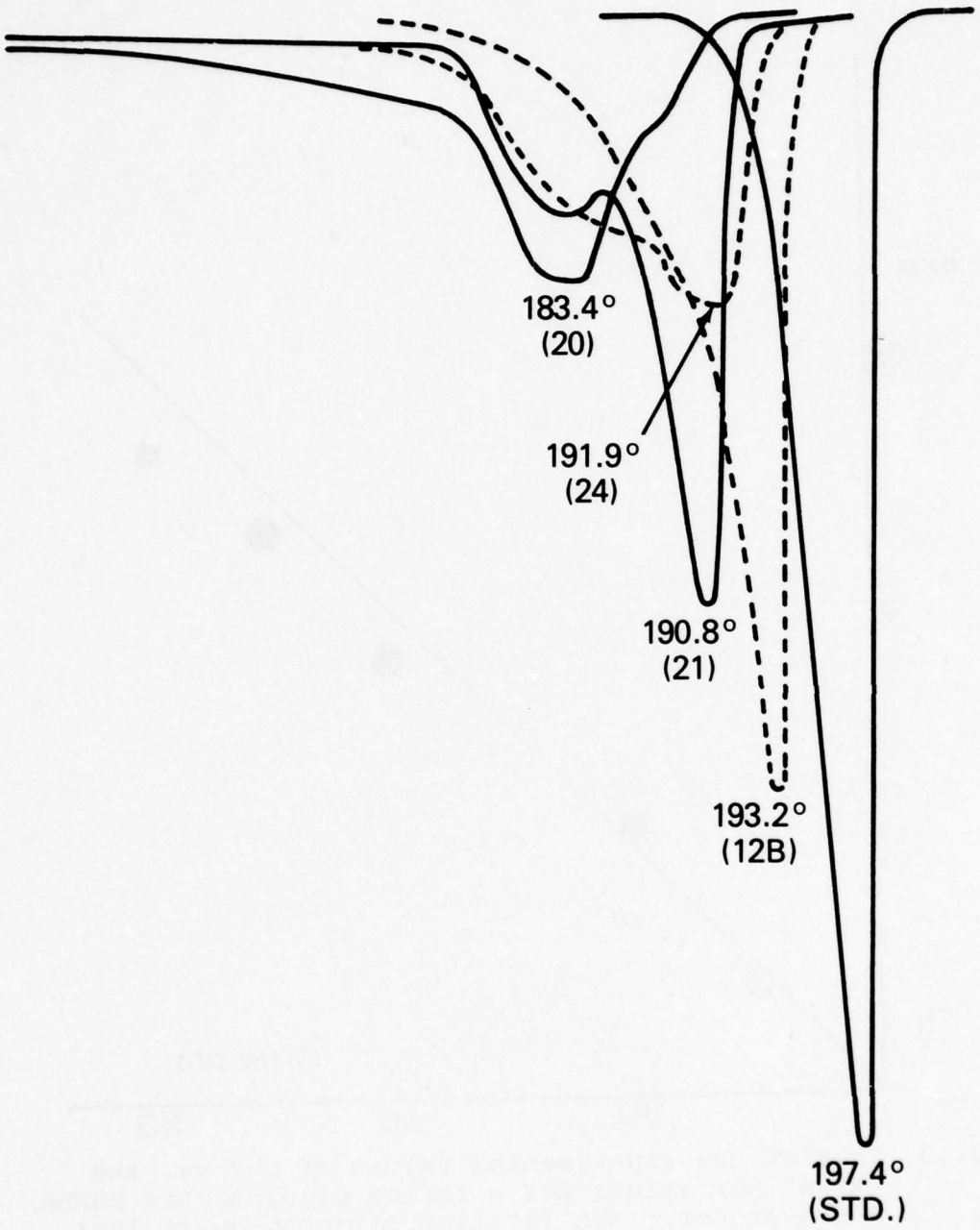

Fig. 2 DSC curves illustrating the range of endotherms encountered among 17 batches of C_{10}-diamide. The standard is a high purity standard sample (NRL 1).

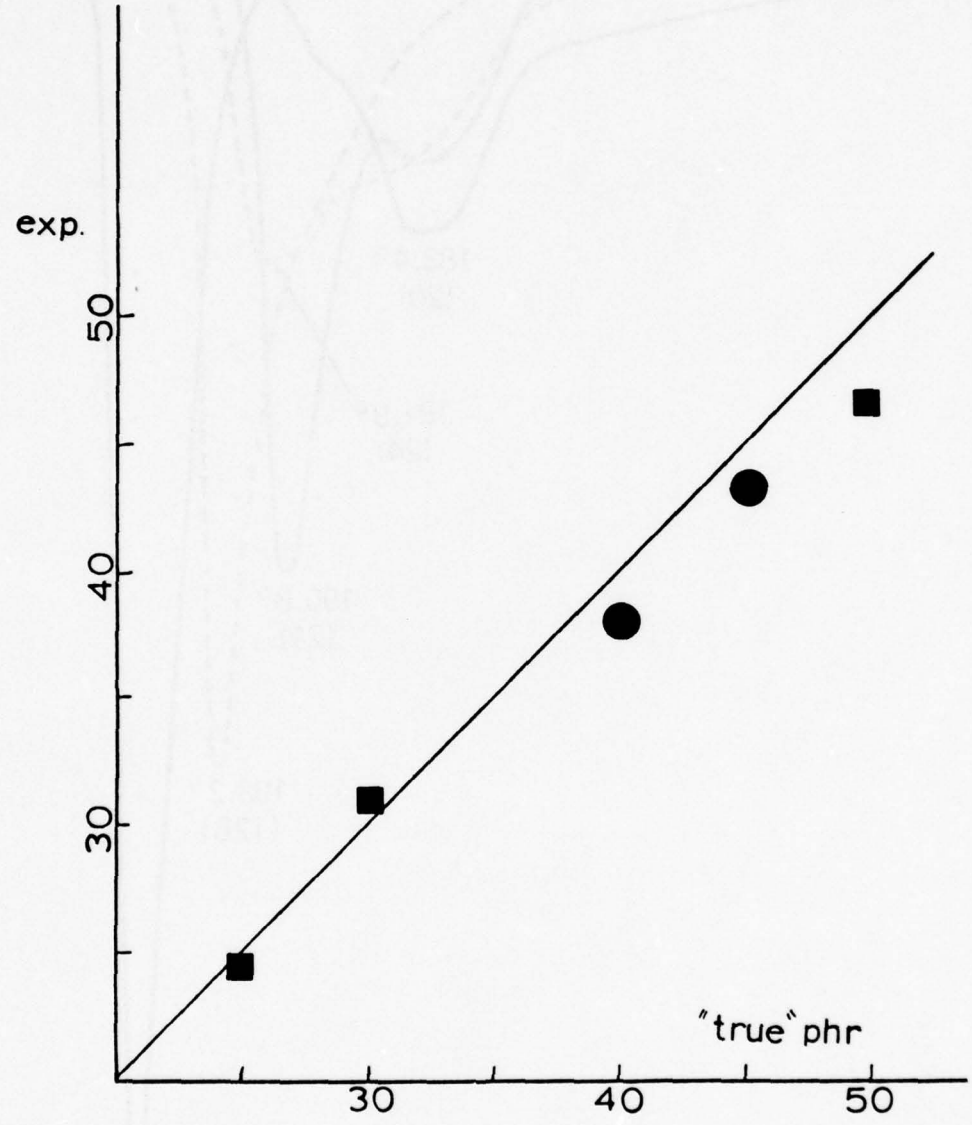

Fig. 3 Plot of the experimental values of phr vs. the "true" phr values for a series of synthetic TGMDA/DDS mixtures. The 45° line corresponds to 100% accuracy. The circles are values measured with a continuous wave spectrometer; the squares are results obtained with a Fourier transform spectrometer.

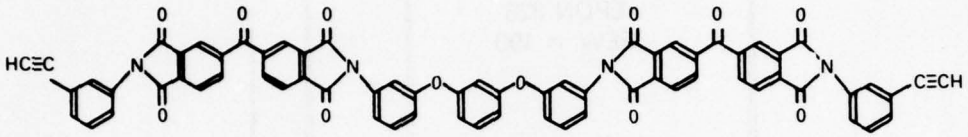

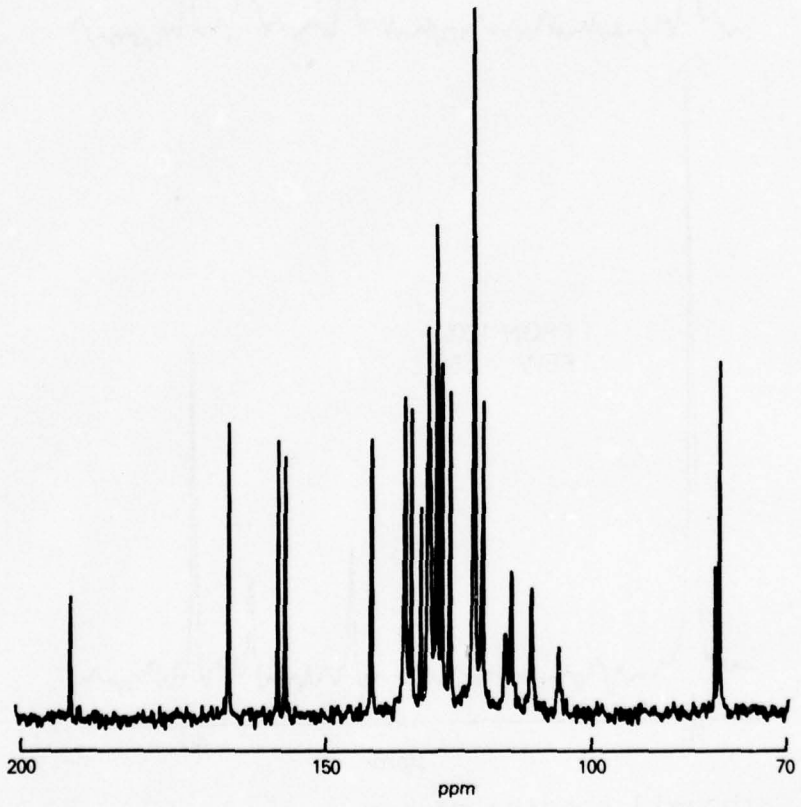

Fig. 4 Structure of HR600 and its carbon-13 NMR spectrum obtained from a saturated solution in DMSO-d_6.

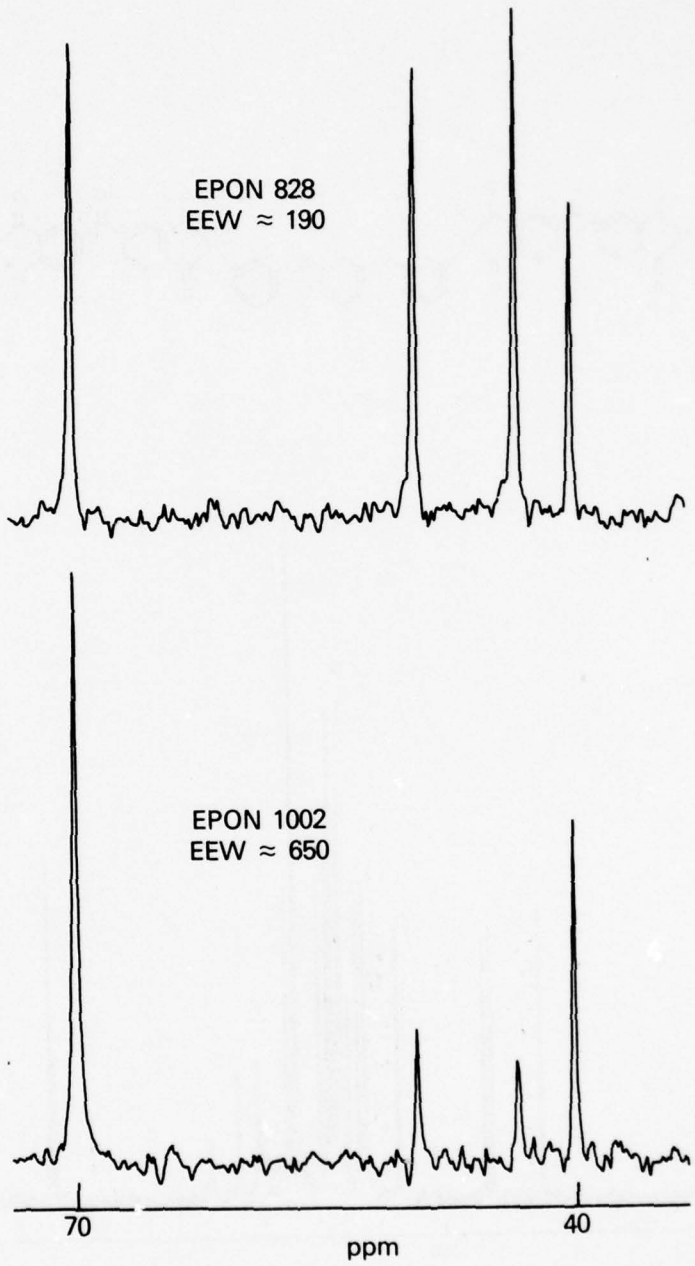

Fig. 5 Carbon-13 spectra of two epoxy resins. Note how the relative intensities of the peaks at 44 and 50 ppm decrease as the EEW increases.

RADIATION CURABLE ADHESIVES

F. J. Campbell, W. Brenner*, L. M. Johnson and J. S. Burr
Radiation Effects Branch
Radiation Technology Division

INTRODUCTION

Radiation curing of structural adhesives offers a number of potentially attractive features as compared to currently used thermal curing techniques. Probably the most significant feature is the capability of this technique to effect cures at ambient temperatures in remarkably short periods of time using electron-beam radiation. One-component systems can be used, and no formulating with catalysts, accelerators, etc. is required. In addition, pot-life problems are eliminated thereby saving time and labor. Radiation curing also helps to avoid residual thermal stresses which are often induced by curing at elevated temperatures. Other benefits which are of practical value include: less energy consumption due to the elimination of autoclaves and curing ovens; simplified processing at essentially contact pressure; avoidance of air pollution as no volatile products are evolved during cure of the 100% reactive adhesive compositions; and the capability to direct the curing energy to the bond line by portable, remote-controlled accelerators. There appears to be a very real need for broadening the scope of this novel technique for curing structural adhesives by offering fabricators a greater choice of radiation-curable adhesive compositions so as to better meet the diverse end-product requirements.

For future applications requiring longer life performance at high temperature and in severe Naval aircraft environments the effort has been directed toward the selection or formulation of adhesives that are maximized to provide this service. Variables were evaluated in both adhesive material formulation and the radiation curing process. In previous reported studies a commercially available heat-curable high temperature adhesive exhibited good bond strength when radiation cured. This was further evaluated during the current period by measurements of fracture energy as a function of cure dose. Studies to improve the performance features of laboratory formulations were also conducted so that adhesives with completely identifiable components could be achieved, and the contributions of the various constituents needed to obtain these features could be characterized. Formulation variables,

---

*Department of Applied Science, New York University

particularly those that would increase toughness of the cured adhesive were explored, and a laboratory synthesized high-temperature, water-resistant resin with this potential was included in this study through the cooperation of the Polymer Synthesis Task Group.

PROGRESS

A Commercially Available Modified Polyimide Adhesive

In the preceding progress report the results of initial tests of a modified polyimide adhesive formulation obtained commercially were reported as being significant and worthy of further evaluation (1). The single lap-shear strength of aluminum alloy test specimens that were cured by electron-beam radiation at a dose of 200 kGy (20 Mrad) were on the order of 10 MPa (1400 psi), three times greater than was obtained from polyimide resin formulations prepared in the laboratory during that period. This product, designated as LO-559, is supplied by the Loctite Corporation, Newington, Connecticut. It is described as an acrylic-modified polyimide resin, containing a peroxide catalyst and an inert filler. Curing can be obtained at room temperature by the application of a primer/activator to the metal adherend surfaces or by heat and pressure if the primer/activator is not used. A cure cycle of 30 to 60 minutes at 150°C is recommended to obtain optimum heat resistance. This material was further investigated during this report period for radiation-curing characteristics and environmental exposure effects on the radiation-cured material utilizing both single-lap shear and fracture-energy testing.

Environmental Exposure Tests:

Single lap-shear strength was utilized as the test criterion to evaluate the effects of elevated temperature aging and of long-time immersion in both water and acetone. Aluminum alloy 7075-T6 strips, cleaned by the FPL acid-dichromate etching procedure, were assembled with a 2.5-cm square lapped area utilizing a few drops of adhesive pressed sufficiently to produce about 0.125 mm bondlines. The assembly was then tightly wrapped with strapping tape to maintain this configuration during handling and curing. These specimens were cured with a 200 kGy dose of electron-beam radiation at ambient temperature in less than a minute of irradiation time with the 3-MeV Dynamitron accelerator at the Radiation Dynamics, Inc. Service Center in Plainview, NY. The aging studies consisted of testing the lap-shear strengths after the initial cure and after aging for 500-hour periods at 150°C, 177°C and 232°C, and also after immersions for 500 hours at room temperature in water and acetone. The data given in Table 1 illustrate the excellent thermal stability and resistance to these fluids.

Fracture Energy Tests:

The lap-shear strength of the LO-559 is considerably higher than that of any of the laboratory-prepared polyimide resin formulations so far tested. By examination, this was attributed to its greater toughness, achieved by the utilization of a flexibilizer and an inert filler in the formulation. Evaluation of the toughness by fracture-energy tests show this to be evident by the high test values obtained utilizing round compact-tension test specimens (2).

Utilizing fracture energy, $\mathcal{G}_{I_c}$, as the criteria, further experiments were conducted to determine the dose required to achieve optimum cure, as signified by a maximum value. Specimens were prepared by pouring 12 g of adhesive into 5-cm diameter aluminum dishes to obtain a depth of 6 mm. These were deaerated for 8 hours in a vacuum chamber, and then irradiated by 2-MeV electrons from the NRL 2-MeV Van de Graaff accelerator at a dose rate of 60 kGy per minute. Specimens were irradiated at doses of 50, 100, 150 and 200 kGy. An average of five specimens were tested at each dose to obtain the average values, which are listed as follows:

Dose (kGy)	50	100	150	200
$\mathcal{G}_{I_c}$ (J/m^2)	490	630	490	510

These results demonstrate that an optimum cure was reached at between 50 and 100 kGy and that further irradiation did not produce an over-cure, or appreciable degradation of the maximum value, at a dosage of two to four times the optimum.

Heat-Cured Loctite LO-559:

An additional study was conducted to obtain a comparison of lap-shear strength and fracture energy of heat cured LO-559 to those obtained by radiation curing. Identical specimens were cured by a heat cycle of 60 minutes at 150°C, as recommended by the manufacturer (3), cooled to room temperature and tested. The fracture energy values obtained on these specimens averaged 260 J/m^2 and the lap-shear strength averaged 8.2 MPa as compared to the 630 J/m^2 and 10.2 MPa obtained by radiation curing. Additional tests are being planned for studying the effects of specimen temperature during the radiation curing process as another variable that should be explored in the optimization of properties of radiation curable adhesives.

Experimental Modified Polyimide Adhesives

Adhesive tests of several radiation-cured experimental formulations of a commercial polyimide resin (KERIMID-601) and another commercially

available polyimide resin (Hexcel F-178) were reported in the previous report (1). Heat aging stability of these was also very good, with little or no loss of strength (determined by single lap-shear tests) after oven aging for 500 hours at 232°C, but the strength of these was only in the 3-4 MPa range. Toughness was also lacking in these materials as was evidenced by the very low fracture energies obtained (in the order of 80 J/m^2).

Since adhesive formulations are normally a very complex blend of a number of materials, each material must be selected to contribute its characteristic feature which will enhance the desired property and also be compatible with all the other components. A typical formulation will contain all or some of the following characteristic materials: base resin, reactive solvent, crosslinker, adhesion promoter, chain modifier, toughener, filler and coupling agent. The above formulations were simply a base resin, reactive solvent and crosslinker. They did not contain a toughener.

Additional experimental formulations were prepared under the current studies utilizing a rubber-forming additive for the purpose of imparting increased toughness to these modified polyimide formulations. This material was vinyl-terminated butadiene/acrylonitrile (VTBN from B. F. Goodrich). These were prepared by blending the VTBN in various proportions into two basic formulations, consisting of bismaleimide prepolymer (BMI) with a reactive monomer (oxydianiline) and one or the other of the polyfunctional monomers diallylphthalate (DAP) or triallyl isocyanurate (TAIC).

The formulations of the base resins used in these experiments were as follows:

	Formulation A
100 pts	BMI
10 pts	ODA
40 pts	DAP
	Formulation B
100 pts	BMI
10 pts	ODA
40 pts	TAIC

Determining the optimum proportions of VTBN for maximum toughness and thermal aging stability was then performed by testing single lap-shear strength on specimens which utilized the various formulations as

adhesives. These specimens were prepared with aluminum alloy 7075-T6 adherends prepared as described earlier and irradiated with a 200 kGy dose.

Specimens were tested after the initial cure without aging and also after aging at 150°C, 177°C and 232°C for 500-hour periods. Five specimens were tested for each data point reported. The results of these experiments are presented as curves for each of the aging temperatures on plots in Figure 1 for the Formulation A variations and in Figure 2 for the Formulation B variations. The curves of single lap-shear strength versus parts VTBN show that maximum strength was obtained with 50 parts VTBN in each of the formulations. It is also evident that the thermal aging stability of both formulations is very good up to a temperature between 177°C and 232°C. Further experiments are planned to study fracture energy in order to obtain the relationship between the two properties for these formulations.

Fluoropolyacrylate Resin

From the experience gained by studies of commercially available products it was determined that an eventual program goal should be to develop an adhesive formulation from components selected to impart maximum operating temperature stability, water absorption resistance and sufficient toughness to assure high bond strength. In previous work it was determined that an essential key to this achievement lies in the synthesis of a rubber-forming pre-polymer that, when formulated with a polyimide preparation, will radiation cure into a dispersed two-phase system, similar to the CTBN toughening of epoxy resins. A particularly promising candidate for this purpose was developed by the Organic Synthesis Task Group, namely the acrylated cis-trans fluoropolyol resin that was initially described by Griffith and O'Rear in the previous report of this program (4). The initial specimen obtained was a 100% esterified polymer that readily crosslinked upon irradiating with γ-rays in the NRL ^{60}Co Source. Test specimens receiving doses of 50 and 200 kGy were tough, clear solids which had about the same T_p, in the vicinity of 300°C. T_p was measured with a Thermomechanical Analyzer (Dupont Model 943) employing the normal penetration probe. Further studies of the very limited quantity of this material were conducted by mixing it with various polyfunctional monomers that would maximize the crosslink density. In the ratios of 20 parts crosslinker to 100 parts polymer all but one formed clear solutions, and all crosslinked to hard, strong solid specimens. The results obtained are described in Table 2. The significance of the surface being either dry or tacky while all are hard in the bulk of the specimens indicates that oxygen inhibits the curing reaction to some degree. This will not affect the adhesive application for these formulations but could prevent their utilization as composite resins, where surface characteristics are as important as the bulk properties.

These materials, though tough, were not the flexible materials desired as toughener additives which could increase fracture energy of the radiation-cured polyimide resin. Subsequently, the Organic Synthesis Group provided us with small quantities of the two newly prepared resins described in their report elsewhere in this document. One of these had been 100% esterified, as before, and the other had only 10% of the available hydroxy groups esterified. Each material was poured into a small vial and irradiated to doses of 50 and 100 kGy in the NRL ^{60}Co Source. The 100% resin crosslinked to a tough, clear solid (except for a tacky surface) at both doses, while the 10% resin was a very soft, stringy, self-healing rubber material. There was no noticeable difference between the 50 and 100 kGy doses specimens of each material, indicating that 50 kGy would be sufficient for a complete cure. Since this type of material is being studied as a potential toughening additive for radiation-cured high temperature adhesives, it was evident that an acrylic esterification of somewhere between 10% and 100% will be needed to obtain a rubber of the required hardness.

Additional experiments were conducted to determine whether a rubber of the desired characteristics could be obtained by blending these two resins in various proportions or whether another esterified resin of an intermediate level was needed. Blends in the proportions shown in Table 3 were prepared and irradiated in the NRL ^{60}Co Source to a dose of 50 kGy to achieve crosslinked materials which exhibited a range of hardness from very hard to very soft. Temperature stability was again determined by T_p measurements. These measurements and descriptions of the hardness of each crosslinked blend are given in the Table. From these observations it appeared that the desired properties might be achieved by a 50:50 blend of the two materials. However, the lack of strength and elongation of this material indicates that it is not suitable when prepared by this method. A better rubber would probably be obtained if the acrylated groups were more uniformly distributed on the polymer chain, and it appears that the degree of esterification should be in the range of 50% to 80% acrylated. Future preparations will provide sufficient material for making formulation variable studies by fracture energy and lap-shear strength specimens.

Water Absorption Measurements

One of the desired properties of these resins for use in adhesives and composites is low water absorption since the presence of water in conventional adhesives has been found to promote stress corrosion and seriously decrease strength. It may also cause permanent damage if freezing occurs. Thus, a study was initiated to determine the equilibrium water content of several of the above materials when exposed to water vapor. Specimens of these materials which were suspended in a near 100% RH atmosphere were weighed periodically and the weight-gain vs. time were plotted. The radiation cure dose was also a variable in this study. After 120 days of exposure the water content had reached

near maximum for the polyimide formulations, while the 100% acrylated fluoropolyol (AFP) showed no weight gain even after the 120-day exposure. The cure doses and percent weight increases for these specimens are listed in Table 4.

When more of the partially acrylated fluoropolyol resins become available they will be blended into polyimide base adhesives and composite matrices, and the effect of this addition on the resistance to water absorption of the radiation-cured materials will be evaluated.

CONCLUSIONS

It has been demonstrated that the electron-beam radiation curing process will produce cured adhesives having many of the properties desired for high-performance service.

In a study of one adhesive that is commercially available for heat-cure processing, the radiation cured properties have been shown to be superior to the heat cured, providing the radiation processing variables are optimized. It was also significant to observe that this material is not degraded by an overdose of two to four times greater than the required cure dose. It is therefore a product that can be recommended for further evaluation as a radiation curable adhesive.

Initial tests of a high temperature, water-resistant acrylated fluoropolymer resin synthesized at NRL showed it to have promising characteristics as an adhesive component. More of this material in intermediate degrees of acrylate esterification should be prepared for further evaluation as the toughener in high temperature, water-repellent adhesives.

This task on radiation curable adhesives has been terminated.

REFERENCES

1. F. J. Campbell, W. Brenner, L. M. Johnson and M. E. White in High Performance Composites and Adhesives for V/STOL Aircraft, Second Annual Report, NRL Memorandum Report 3721, pp. 79-92, Naval Research Laboratory, Washington, D. C., February 1978.

2. W. D. Bascom, R. L. Cottington, J. L. Bitner, D. L. Hunston and J. Oroshnik, ibid, pp. 23-25.

3. LDS-LO-559, Laboratory Data Sheet on High Temperature Adhesive LO-559, Loctite Corporation, Newington, CT 06111.

4. J. R. Griffith and J. G. O'Rear, in High Performance Composites and Adhesives for V/STOL Aircraft, Second Annual Report, NRL Memorandum Report 3721, pp. 15-20, Naval Research Laboratory, Washington, D. C., February 1978.

Table 1

Effects of Aging on Electron Beam Cured Modified Polyimide Adhesive (Loctite LO559)

Test Specimens: Single lap-shear with 7075-T6 aluminum adherends

Cure Dose: 200 kGy

Single lap-shear strength at room temperature

	MPa (psi)				
Initial	After 500 hr aging in medium				
	air @ 150°C	air @ 177°C	air @ 232°C	water @ RT	Acetone @ RT
9.9	10.4	10.2	9.2	8.9	9.4
(1430)	(1510)	(1480)	(1340)	(1290)	(1360)

Table 2

Effect of Adding Polyfunctional Monomers on the Radiation Cured Properties of a 100% Esterified Fluoropolyacrylate Resin

Monomer	Dose (kGy)	Appearance	T_p
triallyl isocyanurate	50	hazy, hard, dry surface	300°C
triallyl isocyanurate	300	hazy, hard, dry surface	325°C
diallyl phthalate	50	clear, hard, tacky surface	305°C
diallyl phthalate	300	clear, hard, tacky surface	310°C
triallyl cyanurate	50	clear, hard, tacky surface	360°C
triallyl cyanurate	300	clear, hard, dry surface	310°C
trimethylolpropane trimethacrylate	50	clear, hard, dry surface	325°C
trimethylolpropane trimethacrylate	300	clear, hard, dry surface	310°C

Table 3

Effect of Blending to Achieve Partially Esterified Fluoropolyacrylate Resins on the Radiation Crosslinked Properties

Percent Composition		Appearance	T_p
100% Esterified	10% Esterified		
100	0	hard, clear, strong	310°C
75	25	hard, clear, strong	300°C
50	50	hard rubber, clear no strength, no extensibility	300°C
25	75	soft rubber, clear no strength, no extensibility	25°C
0	100	very soft stringy rubber, clear	not measurable

Table 4

Water Absorption of Radiation Cured Materials

120 Days at 100% RH

Specimen	Cure Dose (kGy)	% H_2O Gain
LO-559	100	3.5
LO-559	150	3.3
LO-559	200	2.7
100% AFP	50	0.0
100% AFP	100	0.0

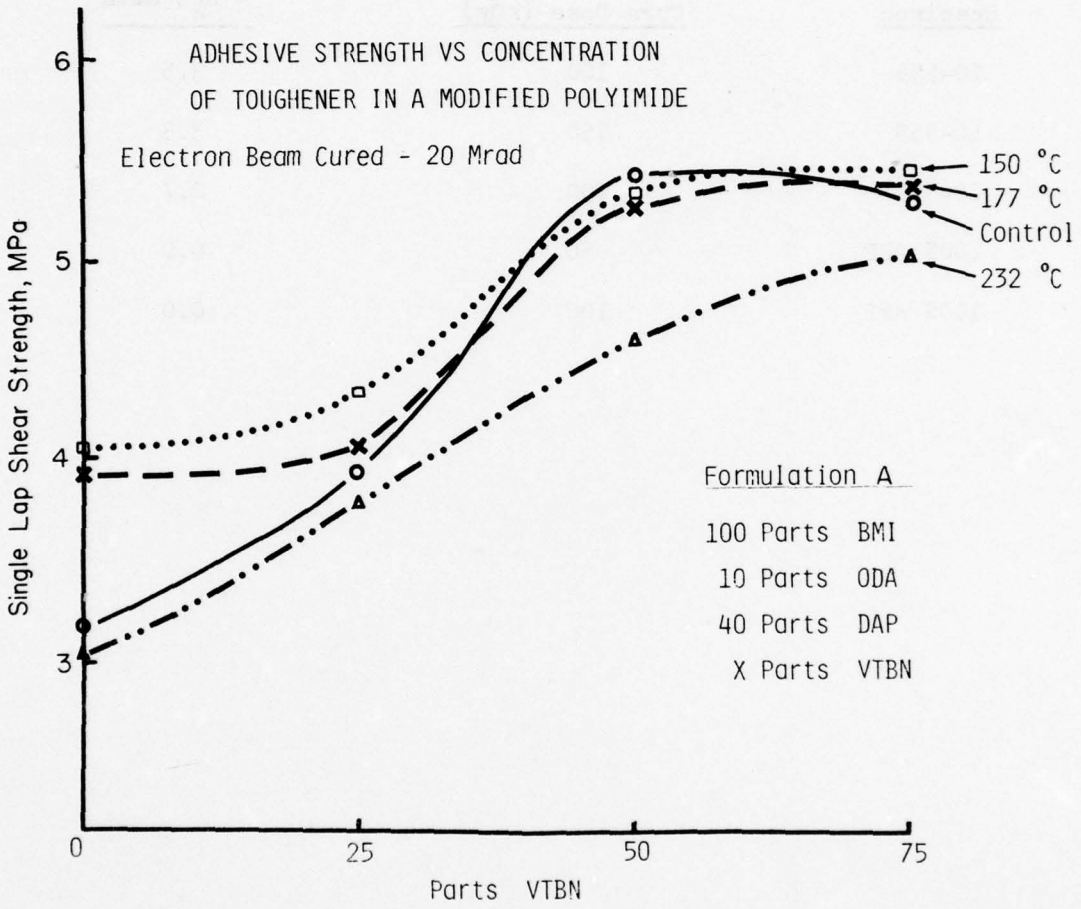

Fig. 1. Adhesive Strength vs Concentration of Toughener in a Modified Polyimide. Formulation A, Electron Beam Cured 200 kGy (20 Mrad).

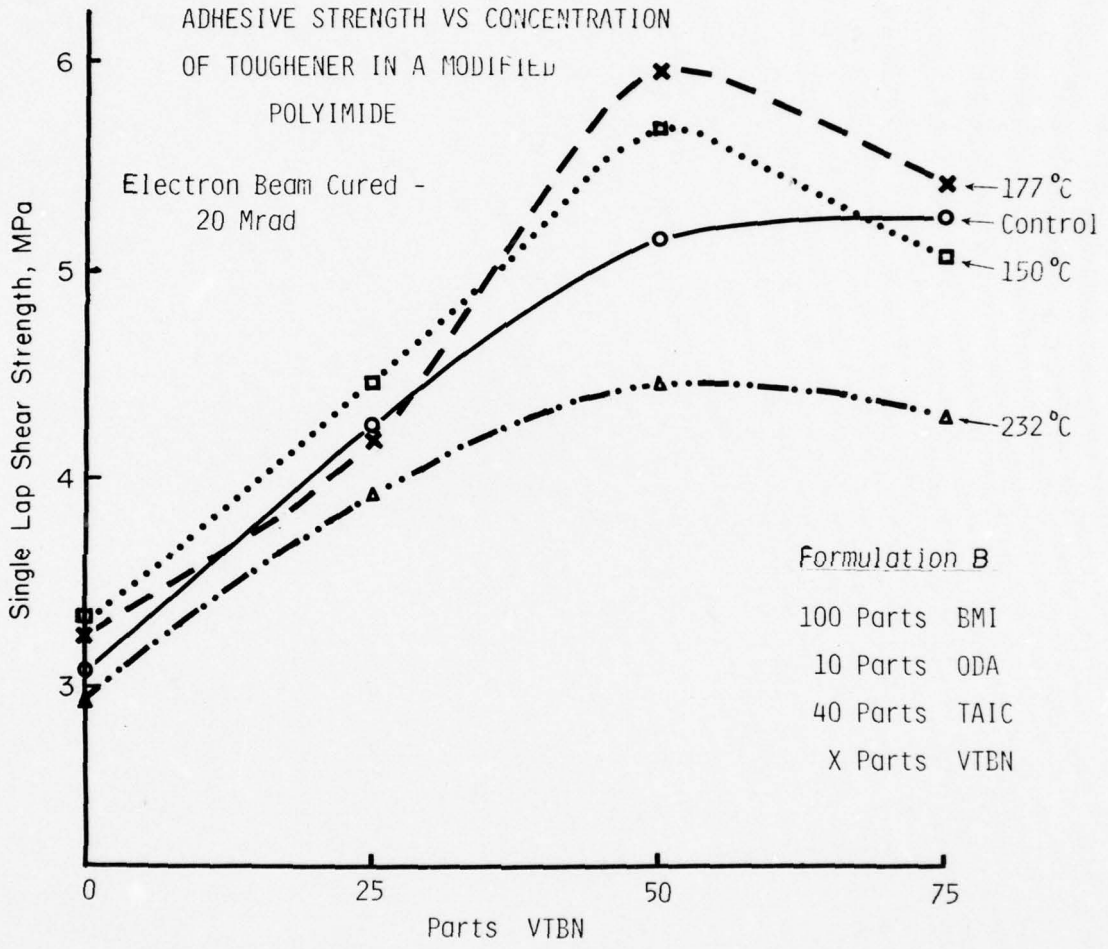

Fig. 2. Adhesive Strength vs Concentration of Toughener in a Modified Polyimide. Formulation B, Electron Beam Cured 200 kGy (20 Mrad).

CURE ANALYSIS AND FABRICATION TECHNIQUE FOR ADVANCED COMPOSITE MATERIALS

R. Y. Ting and H. C. Nash
Polymeric Materials Branch
Chemistry Division

INTRODUCTION

The objective of this task is to develop fabrication conditions for the preparation of fiber-reinforced resin-matrix composites of interest to the V/STOL Program. This includes the identification and controlling of critical steps in the fabrication process. Once the processing parameters are determined, laminates are fabricated, characterized and delivered for testing in the Design Optimization Task.

The fabrication of fiber-reinforced composites involves a complex combination of physical and chemical processes. Basically, it begins with the hand lay-up of a predetermined number of prepreg plies in proper sequence and orientation. The lay-up is then subjected to a properly designed curing cycle and a consolidation process. Important considerations are given to the dwell time, cure temperature, applied pressure, the type and amount of bleeder material and the design of dam and vacuum bag. Lastly, the laminate is post-cured for a given length of time at a fixed post-cure temperature.

To ensure the quality of the laminates produced, laminate density and void/fiber/resin volume fractions are determined before the laminates are delivered for testing. Standard tensile tests are also performed on an Instron Rheometer. The details of these characterization techniques were described in an earlier report (1).

LAMINATE FABRICATION

Three composite systems are to be fabricated in this task. While the reinforcement was fixed to be Thornel 300 graphite fiber (T-300), three resin systems were selected for comparison: an epoxy system (NARMCO 5208), a polyimide resin (Hexcel F-178) and the C-10 phthalocyanine resin developed earlier at NRL (2). The fabrication of both the 5208/T-300 and F-178/T-300 angle-ply laminates has been completed. Conventional vacuum-bag techniques were used and sample cures carried out in a hydraulic press. The details of sample lay-up, fiber orientation and laminate properties were given in previous reports (1,3). Fiber/Resin volumetric contents were determined by an acid

AD-A069 611 NAVAL RESEARCH LAB WASHINGTON D C F/G 11/2
HIGH PERFORMANCE COMPOSITES AND ADHESIVES FOR V/STOL AIRCRAFT.(U)
MAY 79 L B LOCKHART
UNCLASSIFIED NRL-MR-4005 NL

2 OF 2
AD
A069611

END
DATE
FILMED
7-79
DDC

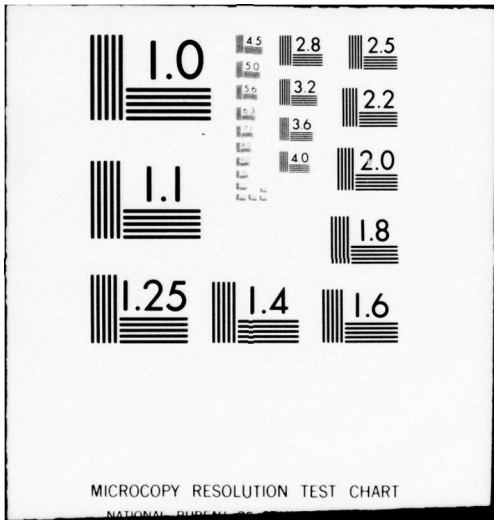
1.0
1.1
1.25
1.4
1.6
1.8
2.0
2.2
2.5
2.8
3.2
3.6
4.0
4.5
5.0
5.6
6.3
MICROCOPY RESOLUTION TEST CHART

digestion method (4); the samples prepared were essentially void-free. Table I shows the density data and acid digestion results of F-178/T-300 laminates. The apparent void content is generally less than 0.5%.

C-10/T-300 CURE ANALYSIS

Because necessary equipment for large-scale prepreg production is not available in-house, the prepregging of the C-10 phthalocyanine/graphite fiber (C-10/T-300) system was developed in collaboration with two commercial sources: namely, U. S. Polymeric Chemicals, and the Composites Division of the Ferro Corporation. Both the hot-melt prepregging technique and a resin/solvent slurry technique were demonstrated to be capable of successfully producing 12-inch wide prepreg tapes. However, only the latter technique yielded the required 38-42% resin content in the prepregs. This material was therefore chosen for preliminary cure analysis. Dimethylformamide was the solvent selected for prepreg preparation, resulting in a final product with about 6% volatiles. The prepreg had a dark green color, and the general appearance was dry and brittle. Sufficient tack for easy lay-up could be developed by heating the material briefly at 130°C.

DSC and TGA Studies

Thermal analysis was carried out to obtain information about the behavior of the prepreg material prior to laminate fabrication. Techniques used included differential scanning calorimetry (DSC) and thermal gravimetric analysis (TGA). A Perkin-Elmer DSC-2 unit was used to perform DSC scans over the temperature range of 310°K (37°C) to 500°K (227°C) at a heating rate of 10°C/min under a dry nitrogen atmosphere. A DuPont 900 Series TGA unit was used to analyze sample weight loss as a function of temperature over the temperature range of 20°C to 350°C. The sample was heated at a rate of 5°C/min and was continuously purged with dry nitrogen at a flow rate of 100 ml/min.

The result of DSC scans is shown in Figure 1. The top trace is a "null-reference" baseline, obtained by placing an empty aluminum micropan in the DSC system. The bottom trace is from a pure, uncured C-10 phthalocyanine resin used in making the prepregs. It can be seen that an endothermic peak appears at 186°C indicating the melting of the resin. An exthotherm at 197°C may be related to the onset of cure, which seems to extend continuously into the higher temperature region. This behavior is very much different from the cure of an ordinary epoxy resin, where a distinct and sharp exotherm is always present and recovers to the baseline level indicating the completion of cure (5). The area under this exotherm is usually used to develop the resin cure kinetics (6). However, such a technique is not applicable for C-10 phthalocyanine because of the anomalous cure behavior shown in Figure 1. The middle trace is that for the prepreg material. It shows two sharp endotherms at low temperatures, perhaps related to the release of some unknown, low boiling volatiles. A series of additional endotherms

appear at 124°C, 145°C and 174°C. These peaks are generally broad, each covering some 20 degrees in temperature. The low peak at 145°C may be identified with the release of DMF added during prepregging. (DMF has a boiling point of 152.8°C). The other peaks, appearing at temperatures lower than 186°C, the melting point of pure C-10 phthalocyanine, are believed to be related to the melting of resin oligomers. The melting temperature of this resin is known to be depressed greatly by B-staging (1). The multiple melting behavior of B-staged phthalocyanine was also observed by Gillham (7,8) in a dynamic mechanical study using an automated torsion braid technique.

In order to further identify the nature of the observed DSC endotherm peaks, TGA was performed to examine material loss as a function of temperature. This result is shown in Figure 2. Substantial weight loss is found in the temperature range of 50°C to 90°C, suggesting that the DSC endotherms in the same range are indeed related to release of volatile organics and/or moisture. The further weight loss observed near 150°C shows DMF evaporation; the amount is nevertheless small. Rapid weight loss begins to take place beyond 275°C. This perhaps limits the curing temperature, at least initially, to no more than 260°C (500°F).

The fabrication of unidirectional laminates using the C-10 phthalocyanine/ graphite prepreg was carried out based on the DSC and TGA results. The initial difficulty to be overcome was the readiness of resin flow. According to the DSC record, the material begins to melt partially around 124°C. Since this melting takes place before DMF is completely released, the added solvent greatly increases resin flow, and hence makes it difficult to retain the resin in the composite sample. Previous experience in curing the pure C-10 resin indicated that this material required a very long cure time (2). This requirement is also evident from the results of the DSC and dynamic mechanical studies (8) on pure C-10 phthalocyanine.

Slow-Cure Procedure

A "slow" cure procedure was therefore developed. A dynamic dielectric technique was employed to monitor the curing of the composite sample. For the cure study, a 6" X 6" (15.2 X 15.2 cm) unidirectional sample, either eight or sixteen plies, was first laid up by hand. Two aluminum-foil electrodes, 2" X 2" (5.1 X 5.1 cm) in size, were used for the dielectric monitoring. The electrodes, one on the top and one on the bottom, were separated from the sample with a thin polyimide film as electrical insulation. Connections were made from the electrodes to an Audrey III Dielectrometer, which continuously measured both the sample capacitance and dissipation factor as a function of cure time and temperature. The capacitance is directly proportional to the real part of sample complex dielectric permissivity, k^*, whereas the dissipation factor is the ratio of the imaginary to the real part of k^*. The dynamic dielectric analysis is analogous

to a dynamic mechanical measurement in that the capacitance is analogous to the mechanical storage compliance and the dissipation factor to the loss tangent (9). Therefore, the results of this analysis can be related to rheological changes in the curing of a thermoset resin. Analog signals from the Audrey Dielectrometer were continuously recorded on a Hewlett-Packard Model 7132A chart recorder. Temperature was measured by an iron-constantan thermocouple placed next to the sample. The complete lay-up was placed in a polyimide vacuum bag and the heating/pressure cycle carried out in a Wabash hydraulic press, where in situ dielectric monitoring was performed at a fixed frequency of 10^3 Hz.

Figure 3 shows the record of in situ dynamic dielectric monitoring of a typical cure cycle based on these considerations. The sample was quickly heated up to 140°C under full vacuum. Very small and gradual increases in capacitance and dissipation were observed once the temperature had reached the 140°C level. These changes indicated the escape of volatiles and perhaps the melting of some crystalline entities (10). After two hours, the temperature was further increased to 190°C in an attempt to fully melt the sample. A sharp increase in capacitance accompanied by a dip in dissipation indicated the completion of melting and perhaps some further release of volatiles. The minimum in the dissipation curve might be related to the flow of matrix resin. The further increase in dissipation was indicative of the onset of cure at this temperature. However, torsion pendulum studies showed that the gelation time at 201°C is about nine hours (8). Therefore, this portion of the cure cycle allowed for development of a very low gel fraction, but led to complete escape of the volatiles. The condensation of the solvent could be easily observed through the polyimide bag during this period. After ninety minutes at 190°C, the system was brought to the final cure temperature of 250°C. The discontinuity in the capacitance and dissipation curve was the point when 100 psi pressure was applied and vacuum released. Increasing temperature and applied pressure caused the capacitance to decrease while the dissipation rapidly increased. These changes were indicative of the gelation process (10). With or without pressure, the gelation time was about 25-30 minutes in this case, as opposed to 45 minutes measured in the torsion braid study of the pure resin (8). Both the capacitance and dissipation gradually levelled off after ninety minutes at the final cure temperature. The very slight increase in dissipation beyond this point suggested a slow but continuing solidification of the composite sample. Heating was discontinued after 2.5 hours and the sample was allowed to cool slowly under pressure. The press cycle totaled 6.5 hours. Post-cure was carried out at 260°C for 22 hours.

Variations from the described cycle were allowed in different runs by changing the amount of vacuum, length of each temperature cycle, and the time and the amount of pressure applied to the sample. The fiber contents for samples fabricated by using these "slow" cure cycles were determined. Fiber-volume contents generally fell into the 68-70%

range. The resin contents were 20-26%. On the average there was a 5.5% void content. The low resin content may be attributed to the effect of DMF solvent which caused excessive resin flow. Both DSC and TGA results suggested that the amount of escaped volatiles was small. The chemical structure of phthalocyanine apparently allowed a large portion of added solvent to be "trapped" in the resin. By using a "slow" cure cycle, the resin had sufficient time to flow and thus was lost from the sample. This was evident by examining the wetting of bleeder and vent plies by the resin. The resin loss was not reduced even if the vacuum was reduced to 4-5 psi. The high void content may be caused by excessive staging, which was evident from laminate appearance. The applied pressure never exceeded 150 psi in fabricating these unidirectional composite samples. Even so, for high pressure cases, it was found that fibers were somewhat squeezed outward and distorted from the originally aligned zero-degree direction.

Fast-Cure Procedure

The most effective procedure was to use modified "fast" cures which completely eliminated the 190°C heating period shown in Figure 3. The sample was heated to 150°C under full vacuum for two hours then brought quickly to the 260°C cure temperature. In situ dielectric measurement was used to determine the gel point, which is indicated by the maximum of the dissipation curve in Figure 3. At this point 100-125 psi pressure was applied to ensure optimum solidification. Samples prepared in this manner generally had a fiber volume content of about 62-64%, and a matrix content of 33-34%. The void content was reduced to less than 2.5%. It is felt that such a modified "fast" cure would not only eliminate the resin-starved condition and fiber-distortion problem in laminates cured slowly, but further reduction in laminate void content could also be achieved. This is perhaps most important since in most applications involving composite materials fracture processes usually dominate in composite failure. Results of preliminary tests seem to indicate that an extended post-cure cycle (48-54 hours at 245°F) is needed to optimize laminate mechanical properties. More extensive studies are currently underway to examine this effect.

AGING STUDY OF F-178/T-300 PREPREG

A major difficulty in handling many prepregs is that the material must be stored at very low temperatures (i.e. -20°C). The shelf life of these prepregs is generally only a few weeks at room temperature and only a few months at freezer temperatures. Presumably, continual B-staging occurs at room temperature and, at the same time, the resin may degrade by absorbing moisture from the atmosphere. Also, since before lay-up for fabrication the prepreg must warm up to room temperature, it could absorb moisture through condensation.

A short-term aging study (21 days) on F-178/T-300 prepregs reported earlier (3) showed no obvious change in material mechanical

properties or chemical composition as a result of aging. The aging period was therefore extended up to 28 weeks and the results are reported here.

Fresh prepreg material was cut, packed in kits and stored at room temperature in three environmental chambers controlled at 16%, 50% and 95% relative humidity, respectively. The kits were essentially small aluminum shelves with 17 open slots. Each kit therefore contained seventeen pieces of prepgeg, 15 cm X 15 cm in size with one piece in each slot. At the end of each four-week period, a kit was removed from storage and a 16-ply laminate prepared on the same day. The extra sheet of aged prepreg from each kit was used for proton nmr analysis, (see Chemical Characterization Task).

Unidirectional 16-ply laminates were fabricated in a Wabash Press using conventional vacuum bag techniques. The processing included a full-vacuum cycle at 121°C (250°F) and a pressure cycle at 177°C (350°F) with a pressure of 6.9 X 10^5 Pa (100 psi). Samples were post-cured at 249°C (480°F) for 10 hours. The curing cycle was kept the same for processing all aged samples.

Samples were cut from the laminate and tests were carried out to determine if any change occurred in their mechanical properties relative to composites prepared from unaged prepreg. The short-beam shear test (ASTM-D 2344) was chosen to determine the interlaminar shear strength, a resin-dominated property. The flexure test (ASTM-D 790) was selected to measure the laminate flexural strength and modulus, which are fiber-dominated properties. The dimensions of the shear samples were 0.5" X 0.16" X 0.08", whereas the flexural samples were 2" X 1" X 0.08". Tests were carried out on an INSTRON testing machine at a crosshead speed of 0.05 in/min.

Figure 4 shows the flexural strength of the graphite/polyimide composite plotted as a function of the prepreg aging period. It can be seen that laminate flexural strength steadily decreases as aging continues. The effect is more pronounced at higher humidity levels. After twenty weeks of aging at 95% relative humidity, the flexural strength is reduced by nearly 25% from that of the original control sample. The same tread is followed by the flexural modulus data.

Figure 5 presents the interlaminar shear strength data as a function of prepreg aging time. In this case, the results show a rapid increase in shear strength initially as aging proceeds which becomes stabilized at a level approximately 55% higher than that of the initial control. The increase seems to be independent of the humidity level at which prepreg samples were aged.

At first glance these results seemed surprising because any resin degradation taking place due to moisture absorption in the prepreg should lead to a poorer resin-dominated property such as interlaminar

shear strength. The fact that interlaminar shear strength was improved and flexural properties deteriorated may be resolved by considering some physical changes to the prepregs which occurred during aging.

First of all, during the aging period the prepreg material clearly showed a steady loss of tack. As aging continued, the prepreg gradually became dry and brittle, making it difficult to keep all plies properly aligned and adhered during lay-up. Secondly, the bleeding during curing was greatly reduced for aged samples. Wetting of the bleeder plies became less and less, particularly around the corners of the square plies, as aging continued. These changes seem to suggest that the amount of resin flow was greatly reduced due to aging. It is possible that exposure to high humidity caused little or no chemical degradation in the resin system; results of proton nmr spectroscopy seem to confirm this (see Chemical Characterization Task). On the other hand, room temperature storage produced a prepreg material that was excessively B-staged. The aged prepregs essentially had a higher degree of crosslinking than a fresh sample at the beginning of the fabrication process. This represented a higher molecular weight species, having a greater melt viscosity and thus lower flow when subjected to the same temperature/pressure cycles during fabrication. Laminate density measurements and fiber/matrix volume determinations by the acid degestion technique confirmed this. These results are given in Figures 6 and 7, respectively. The higher resin content may be responsible for the observed increase in interlaminar shear strength.

AGING STUDY OF C-10/T-300 PREPREG

The polymerization of C-10 phthalocyanine resin is thermally activated at about 200°C, and the resin, because of its chemistry, is extremely stable at lower temperatures. Therefore, room temperature storage should have virtually no effect on the chemical composition or processing behavior of this resin. This chemical property is a great advantage when considerations are given to such problems as storage requirements and quality control. An aging test for C-10/T-300 prepreg similar to that described above is currently underway in an attempt to demonstrate this property. Additionally, interruptions in the cure cycle will be programmed to determine the extent of "forgiveness" of this material to fabrication/processing discontinuities.

REFERENCES

1. J. V. Gauchel and H. C. Nash, in High Performance Composites and Adhesives For V/STOL Aircraft, W. D. Bascom and L. B. Lockhart, Jr., ed., NRL Memo Report 3433, December 1976.

2. T. R. Walton, J. R. Griffith and J. G. O'Rear, ACS Organic Coatings and Plastics Preprints, 34, 446 (1974).

3. R. Y. Ting and H. C. Nash, in High Performance Composites and Adhesives for V/STOL Aircraft, W. D. Bascom and L. B. Lockhart, Jr., ed., NRL Memo Report 3721, February 1978.

4. ASTM Standard Test D3171-76.

5. L. W. Crane, P. J. Dyne and D. H. Kaelbles, J. Polym. Sci., Polym. Letter Ed., 11, 533 (1973).

6. J. F. Carpenter, SAMPE Ser., 21, 783 (1976).

7. J. K. Gillham, contribution to this report entitled "The Influence of Molecular Structure on the Cure and Transitions of Polyphthalocyanine."

8. J. K. Gillham, ACS Organic Coatings and Plastics Preprint, 38, 598 (1978).

9. N. G. McCrum, B. E. Read and G. Williams, Anelastic and Dielectric Effects in Polymeric Solids, John Wiley, New York, 1967.

10. C. A. May, D. K. Whearty and J. S. Fritzen, SAMPE Ser., 21, 803 (1976).

Table I

PHYSICAL PROPERTIES OF HEXCEL F-178/T-300 LAMINATES

Plate Number	Orientation	Density (g/cm^3)	Volume Fraction		
			Fiber	Resin	Void
211	Quasi	1.581	0.6326	0.3668	-0.0024
212	37.5°	1.577	0.6221	0.3799	-0.0020
213	22.5°	1.585	0.6318	0.3712	-0.0030
214	30°	1.567	0.6181	0.3764	0.0055
215	30°	1.585	0.6422	0.3562	0.0016
216	45°	1.576	0.6176	0.3844	-0.0020
217	45°	1.579	0.6260	0.3746	-0.0006
218	15°	1.564	0.6334	0.3519	0.0147
219	37.5°	1.570	0.6251	0.3736	0.0013
220	22.5°	1.576	0.6399	0.3523	0.0078
223	0°	1.590	0.6394	0.3643	0.0037

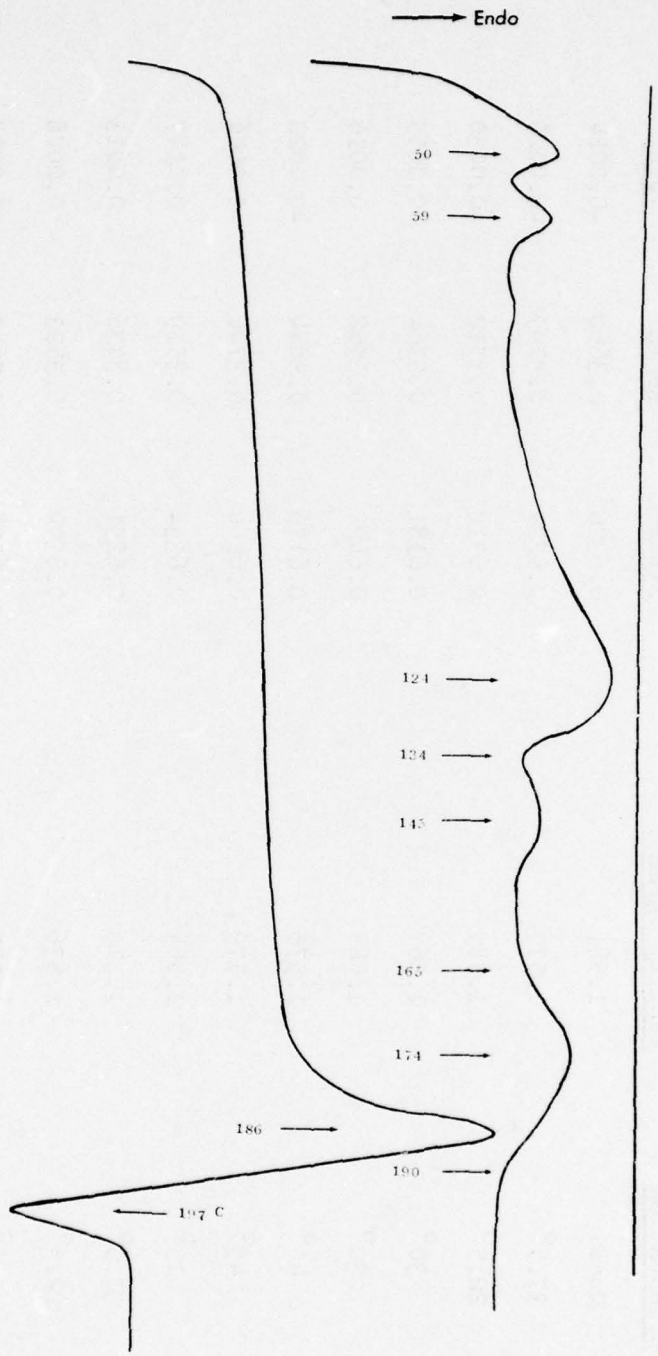

Fig. 1 - DSC record of C-10 phthalocyanine resin (bottom trace) and prepreg (middle trace). The top trace is the baseline obtained with an empty sample pan.

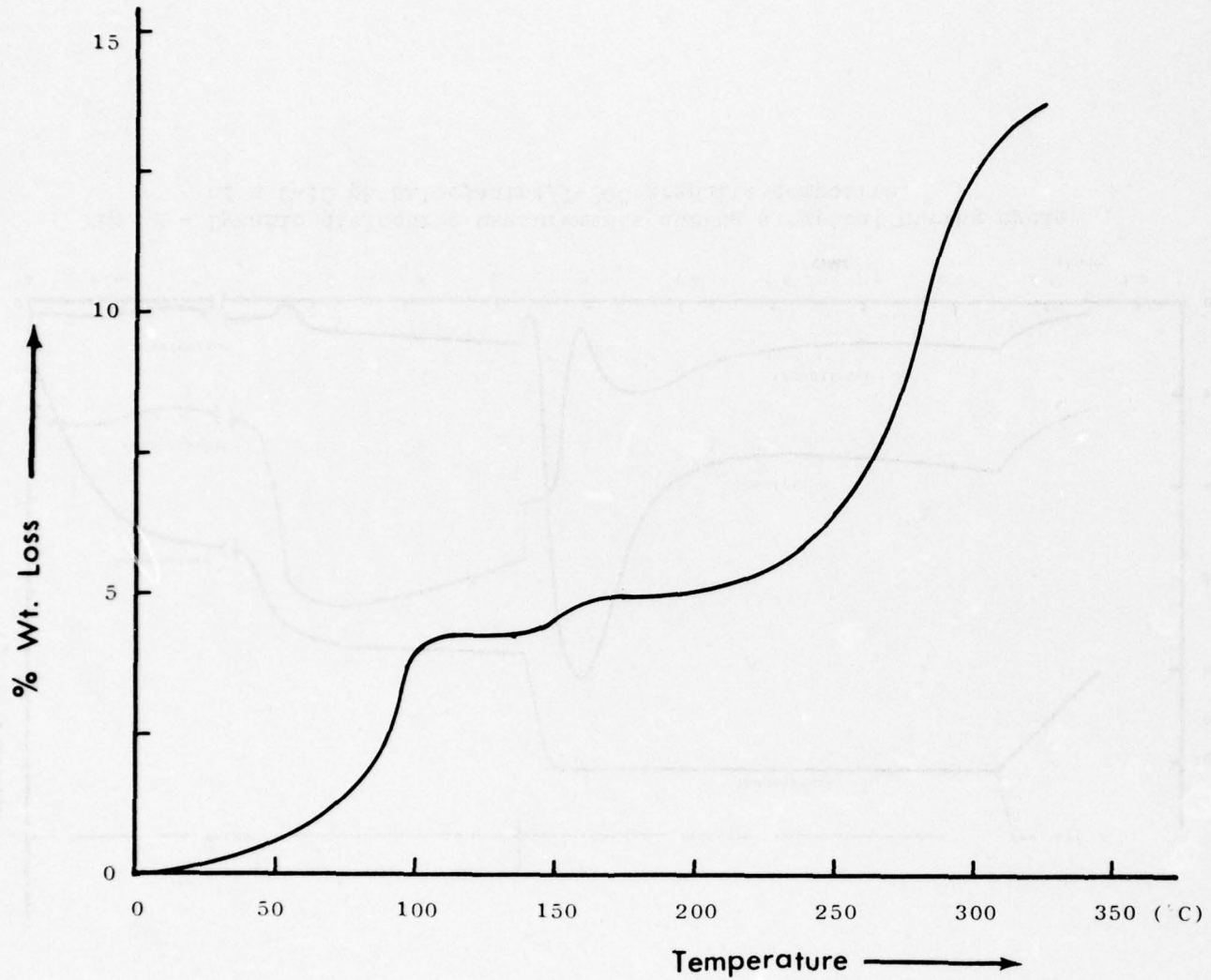

Fig. 2 - Percent weight loss of C-10 phthalocyanine/T-300 graphite prepreg as a function of temperature.

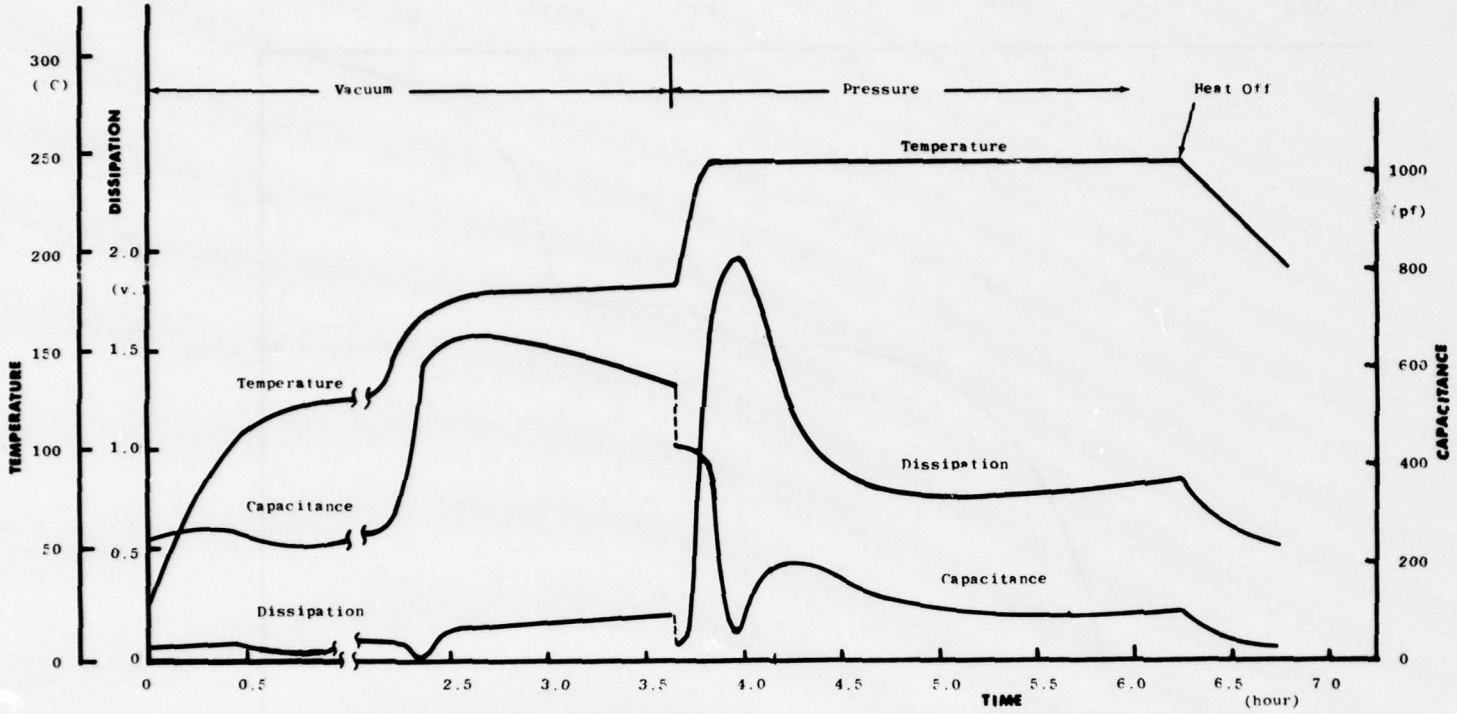

Fig. 3 - Dynamic dielectric measurements during a typical curing cycle of a C-10 phthalocyanine/T-300 graphite composite.

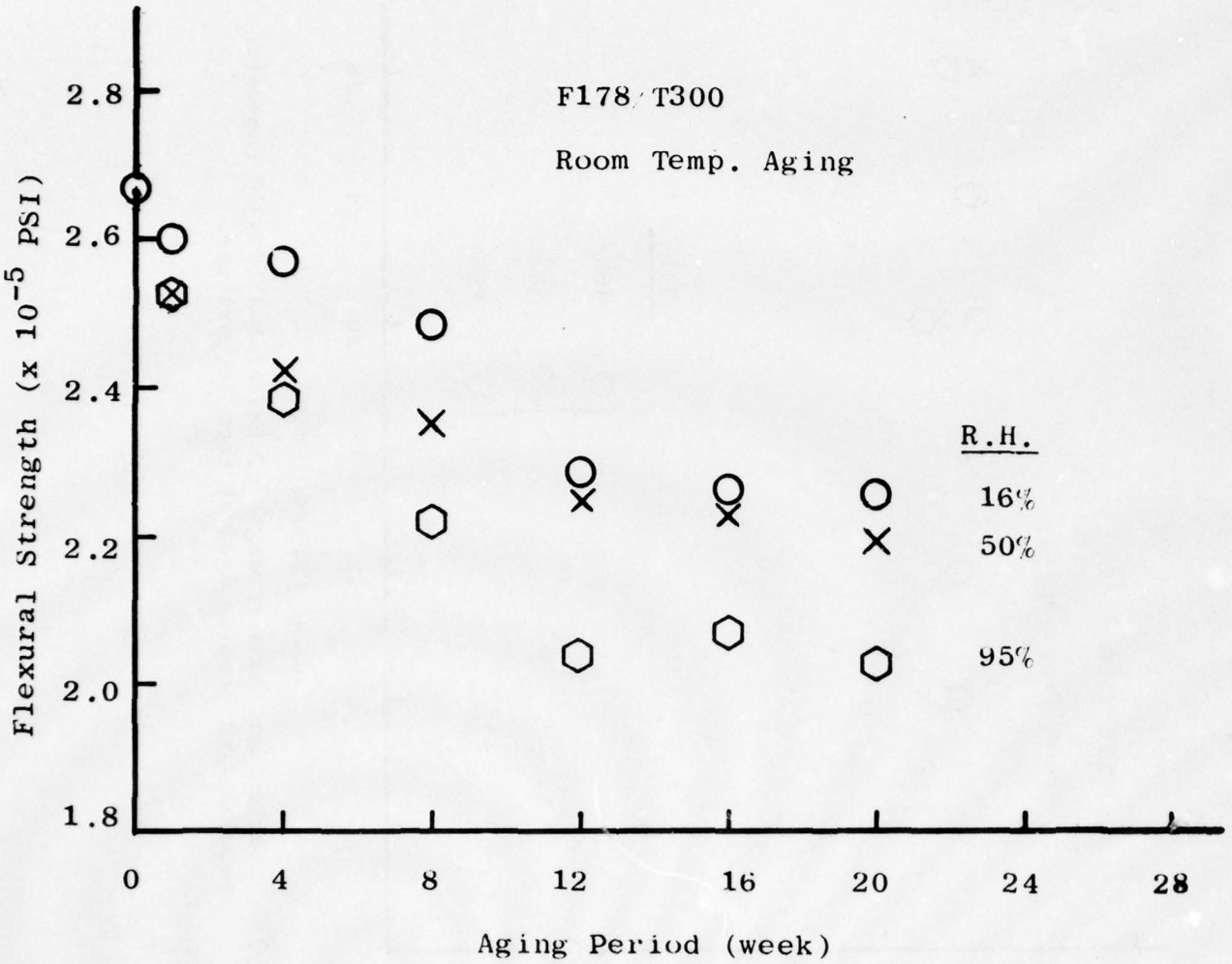

Fig. 4 - Flexural strength of Hexcel F-178/T-300 composite as a function of prepreg aging period at room temperature.

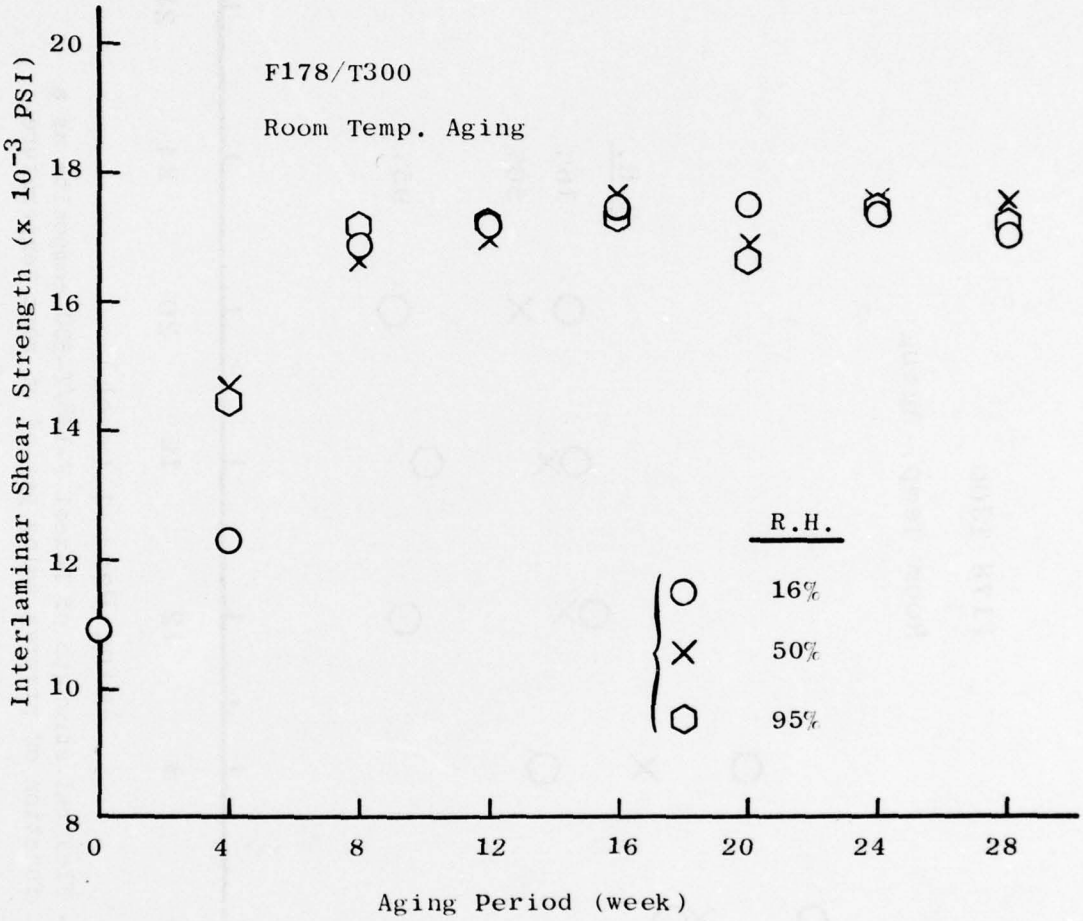

Fig. 5 - Interlaminar shear strength of Hexcel F-178/T-300 composite samples from prepreg aged at room temperature.

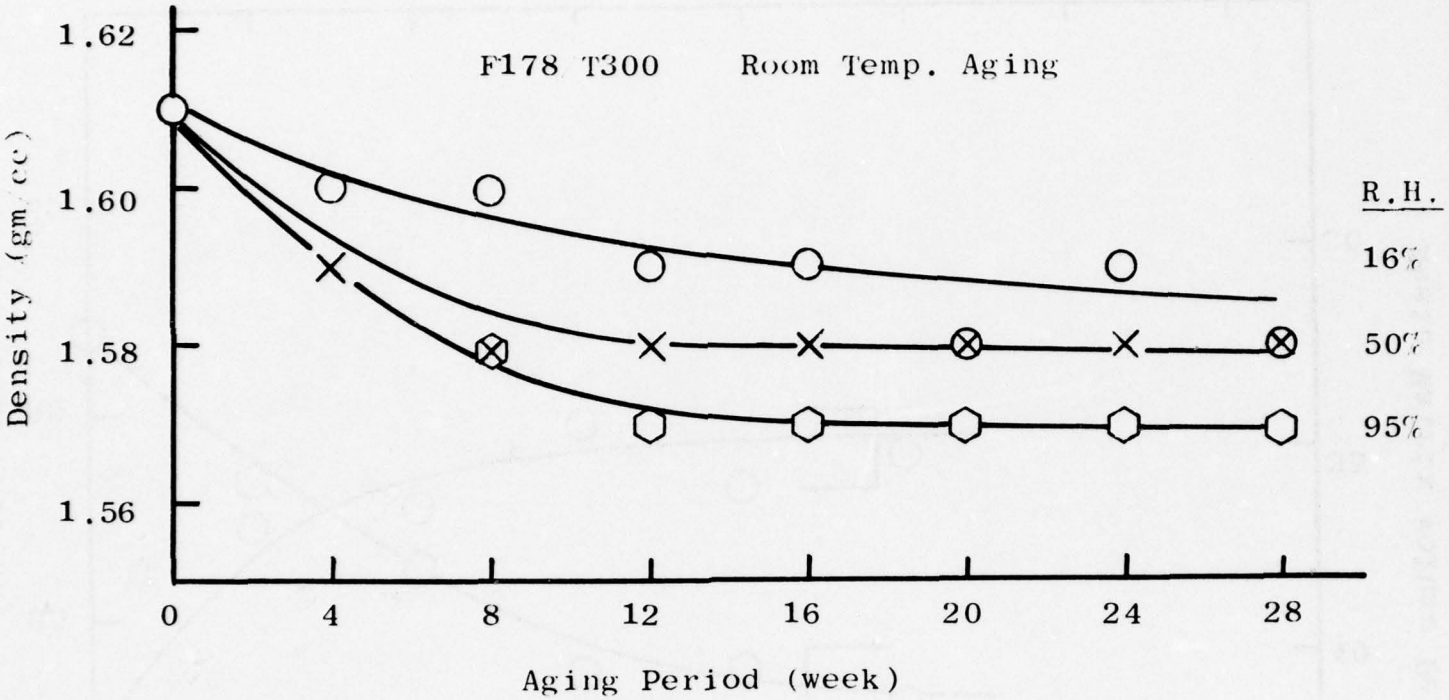

Fig. 6 - Density of F-178/T-300 composite as a function of prepreg aging at room temperature.

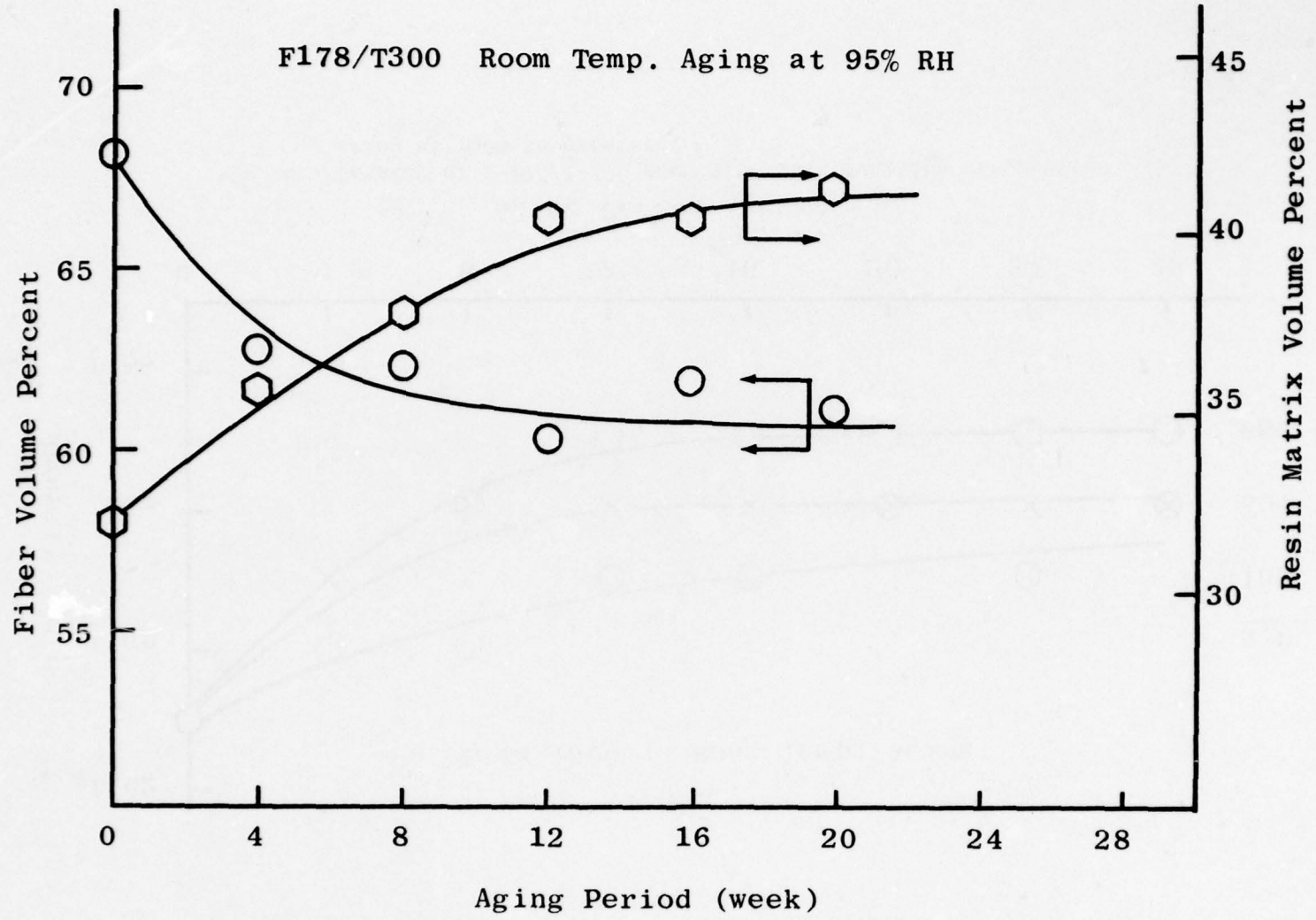

Fig. 7 - Volumetric fractions of fiber (T-300) and matrix (F-178) vs prepreg aging period at room temperature and 95% RH.

FAILURE CRITERIA FOR COMPOSITE STRUCTURES

P. W. Mast, D. R. Mulville, L. A. Beaubien
S. A. Sutton, R. W. Thomas, J. Tirosh and I. Wolock
Mechanics of Materials Branch
Ocean Technology Division

Part I. Failure Criteria for Composites

Part II. Failure Criteria for Adhesive Joints

PART I. FAILURE CRITERIA FOR COMPOSITES

INTRODUCTION

This task deals with the development of failure criteria for structural composites, using resin matrices discussed in the prior tasks, and demonstration of the applicability of these criteria in structural components. Fracture tests are being conducted on small test coupons in a unique in-plane loader developed at NRL, referred to in the first annual report [1]. A large base of experimental data is obtained under complex loads to simulate service conditions. A concept of similar strain fields was developed for predicting failure in structures, based on data obtained on test coupons in the in-plane loader, as described in the second annual report.[2] This concept states that if the strain field in the region of interest in the structure is similar to that previously observed in a test coupon, the loads that caused failure initiation in the test coupon will also cause failure in the structure. Several tests were reported which demonstrated the validity of this prediction technique. Results reported in this section include extensive fracture tests on a graphite/epoxy composite of varying reinforcement angles and under a broad range of in-plane loads. Additional tests are also reported on the validation of the fracture prediction technique developed, using a box beam as the structural component.

IN-PLANE LOADER TESTS

Additional fracture tests were conducted using the in-plane loader described in the first annual report [1]. The type of loadings produced are shown in Figure 1 - horizontal displacement, vertical displacement, and rotation. The earlier tests conducted on Thornel 300/Narmco 5208 graphite/epoxy composite were all in one octant of load space (Figure 2), with tension, positive rotation and positive shear. In the current tests on T300/5208, the loading

was extended to four octants to include negative rotation and compression, for the included fiber angles of 30°, i.e. (± 15°), 45°, 60°, 75° and 90°, and for a quasi-isotropic layup (0, ±45, 90°). Tests were also conducted in the first octant only for included angles of 105°, 120°, and 135°. In addition tests were conducted on a series of T300/F178 graphite/polyimide composites, mainly in the first octant, for included angles of 30°, 45°, 60°, 90°, and for a (0, ±45, 90°) layup. Fabrication conditions for the 5208 composites were given in reference 1, and for the F178 composites in reference 2.

The results for the T300/5208 tests are shown in Figures 3-11. The angles θ_1 and θ_2 are defined in Fig. 2. θ_1 is a measure of the ratio of vertical displacement to horizontal displacement, or in octants I and II, of tension to positive shear. Thus $\theta_1 = 0°$ signifies pure positive shear and $\theta_1 = 90°$ signifies pure tension. $\theta_1 = -90°$ signifies pure compression. θ_2 indicates the rotation, which is positive or counterclockwise in octants I and IV, and negative or clockwise in octants II and III. The vertical direction on the figure is the magnitude of the displacement and rotation necessary to initiate fracture and is designated as r, as shown in Figure 2.

There are a number of criteria that can be used in determining the point at which failure initiates. Basically, fracture initiation is defined as the point at which there is a significant increase in the non-recoverable strain energy in the specimen. This increase in the dissipated energy is attributed to the initiation of fracture. The value for the displacements and rotation at this point is referred to as r, the critical displacement, or the displacement for fracture initiation. In some cases, the non-recoverable strain energy does not increase suddenly as r increases, and the point of fracture initiation is not as clearly defined. In these cases, some other criterion must be selected, such as the point at which the load or displacement changes sharply. In the current tests, initiation was defined as the point at which there was a 10 lb (4.5 kg) drop in the load in two successive readings, which are taken 0.1 second apart during the test. Selection of this parameter was based on the examination of curves obtained for load, displacement, and dissipated energy versus time for the specimens tested. A different parameter will be examined to determine its effect on the conclusions. Each vertical line in Figures 3-11 represents the results of a single test. The reproducibility of the test data is quite apparent. The com-

plexity of the fracture process in composites is also apparent from the range of the critical displacements observed as the loading conditions are changed. It should be pointed out again that the absolute values of r will vary with the criterion selected for fracture initiation.

It is apparent that comparing the fracture toughness of different composite materials is not a simple process, since the toughness varies with the applied loading. It thus becomes a matter of comparing a large number of points and it is often difficult to express such a comparison simply. The data obtained during the course of each test - i.e., loads and displacements - is stored in a computer. It is not necessary to print the data shown in Figs. 3-11 in order to use it in predicting the fracture behavior of a structural component. Such figures are useful for visualization but not necessarily for utilization.

Failure surfaces can be prepared from this data and these are shown in Figures 12-21. In comparing the results for T300/5208 composites as the included angle is increased, the following is observed : (1) For most loading cases in both octants I and II, as the included angle increases from 30° to 120°, r increases by as much as 200%, except from the cases where $\theta_1 = 0$ - i.e., pure shear - which appears to be a transition region (2). In quadrants III and IV, - i.e., compression loading - there is no significant effect of reinforcement angle over the range studied, except for the cases where $\theta_2 = 45^{\circ}$. For these loadings, the critical displacement decreased as the reinforcement angle increased from 30° to 90°.

In comparing the quasi-isotropic (Q) configuration ($0, \pm 45, 90^{\circ}$) to the angle ply laminates, the following was observed: (1) In octant I, the critical displacements for Q were approximately the same as those for the 120° angle ply laminates, except for the tests at $\theta_2 = 0$, where the values for Q were generally greater. (2) In octant II, the displacements for Q were generally much greater than those for the angle-ply laminates with included angles up to 90°, the highest tested. (3) In octants III and IV, the critical displacements for Q were approximately the same as those observed for the angle-ply laminates, except for $\theta_2 = 45^{\circ}$, where the results were similar to the highest values obtained for the angle-ply laminates, which was for the 30° included angle.

Fracture tests were also conducted on a series of graphite/polyimide composites made with Thornel 300 fiber at included angles of 30°, 45°, 60°, and 90°, and with a

(0, ±45, 90°) quasi-isotropic lay-up. The resin was Hexcel F178. The individual test results are presented in Figs. 22 - 26 and the failure surfaces in Figs. 27 - 31.

In general, the test results are again quite reproducible. The results obtained for the critical displacement are quite similar quantitatively to those obtained for the 5208 epoxy resin. In the first quadrant, the values increase as the reinforcement included angle increases, except at $\theta_1 = 0$, i.e., pure shear, where the results are variable. The few results obtained for negative values of θ_1 were found to be independent of reinforcement angle at any given loading condition. Thus changing the resin matrix from the 5208 epoxy to the F178 polyimide had no significant effect on the fracture toughness of the graphite fiber composite at room temperature.

BOX BEAM STUDIES

Additional tests were conducted using a box beam to demonstrate the failure prediction capability developed on the in-plane loader. The technique was described in detail in the previous annual report [2]. Briefly, an aluminum box beam approximately 12 in. x 18 in. x 1.5 in deep (305 mm x 457 mm x 38 mm) is used. A notched composite test disk 4.5 in. (115 mm) in diameter is bolted over a circular cut-out in one face of the box beam. Two multi-holed loading plates were bolted to the ends of the box beam to permit the development of a range of complex loadings, consisting of combinations of tension, shear, and in-plane bending, using a single actuator testing machine. The point of failure initiation is determined by visual observation.

There are seven holes each in the top and bottom loading plates of the box beam and to graphically represent the combination for a particular test, the coordinates of the upper and lower loading holes were specified by the distance from the respective center holes. The x and y coordinates represent the upper and lower holes, respectively, and the vertical axis represents the load at the initiation of failure. For unsymmetric loading, it is necessary to make independent predictions of the failure load for both ends of the notch since the stress states were different. The results are presented in Table I and Figures 32 and 33. Tests 1-4 were reported in the previous annual report. For all of the tests conducted, the predicted load for failure initiation differed from the observed by an average of 11%. However, in every case, failure initiated at that end of the notch predicted. These results certainly verify

the validity of this method for predicting failure initiation under in-plane loads in composite structural components containing a notch.

REFERENCES

1. L. A. Beaubien, et al, "Design Optimization," in "High Performance Composites and Adhesives for V/STOL Aircraft" (W. D. Bascom and L. B. Lockhart, Jr, ed.), First Annual Report, NRL Memorandum Report 3433, p. 101 (December 1976).

2. L. A. Beaubien, et al, "Failure Criteria for Composite Structures," in "High Performance Composites and Adhesives for V/STOL Aircraft," (W. D. Bascom and L. B. Lockhart, Jr. ed.), Second Annual Report, NRL Memorandum Report 3721, p. 103 (February 1978).

TABLE I. LOAD AT FRACTURE INITIATION

EXPERIMENT	TYPE OF LOADING	LEFT END		RIGHT END		DIFFERENCE
		PREDICTED LB	OBSERVED LB	PREDICTED LB	OBSERVED LB	%
1	TENSION	9,015	10,600	9,015	10,600	15.0
2	TENSION BENDING	6,900	6,240	9,130	-	10.6
3	TENSION SHEAR	10,600	8,320	10,600	8,320	27.4
4	TENSION SHEAR BENDING	8,500	8,700	10,000	-	2.3
5	TENSION SHEAR BENDING	8,500	7,600	10,000	-	11.8
6	TENSION SHEAR	9,760	8,580	9,760	10,080	13.8 (L) 3.2 (R)
7	TENSION BENDING	8,400	8,270	9,280	-	1.6
8	TENSION SHEAR BENDING	9,440	-	7,520	8,000	6.0
9	TENSION SHEAR BENDING	9,600	-	8,800	10,870	19.0
10	TENSION SHEAR BENDING	9,040	8,370	10,240	-	8.0

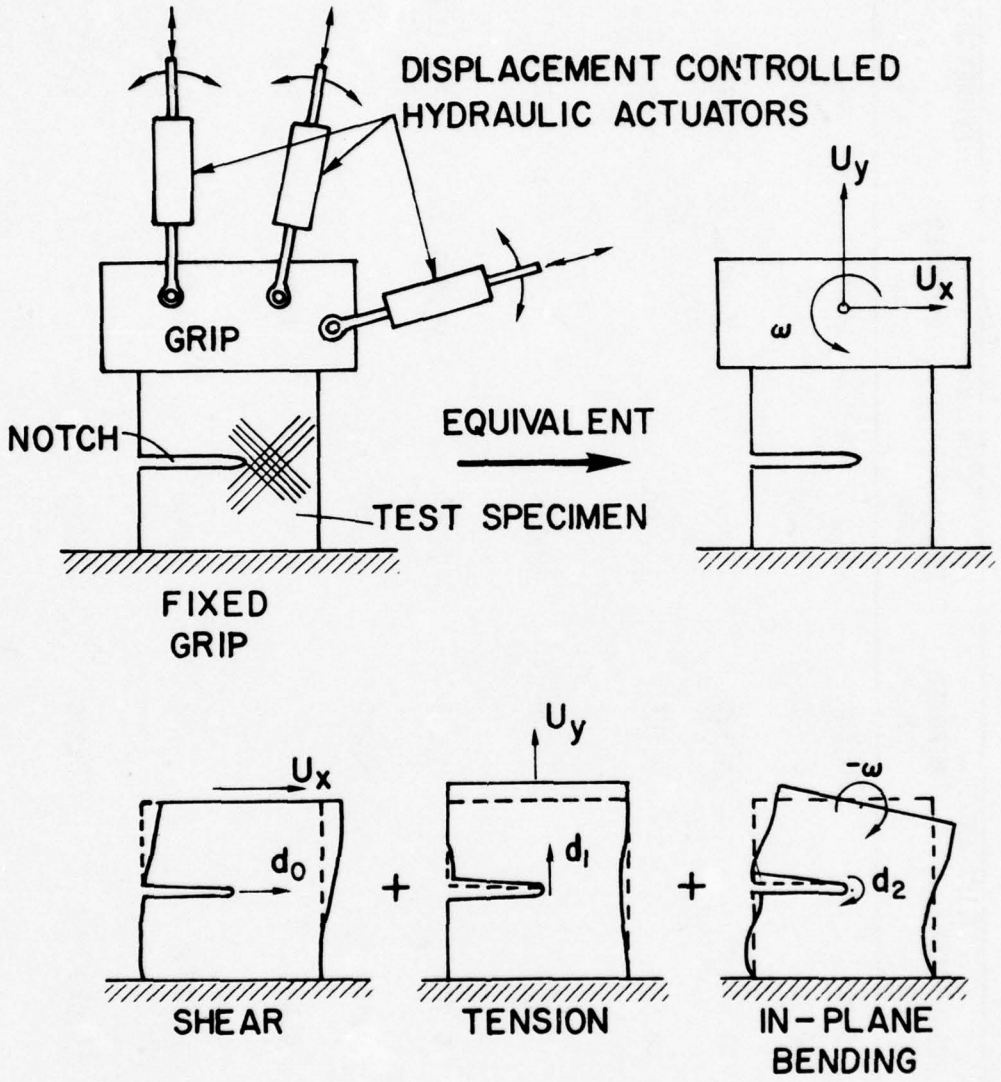

Fig. 1 - Displacements produced by in-plane loader

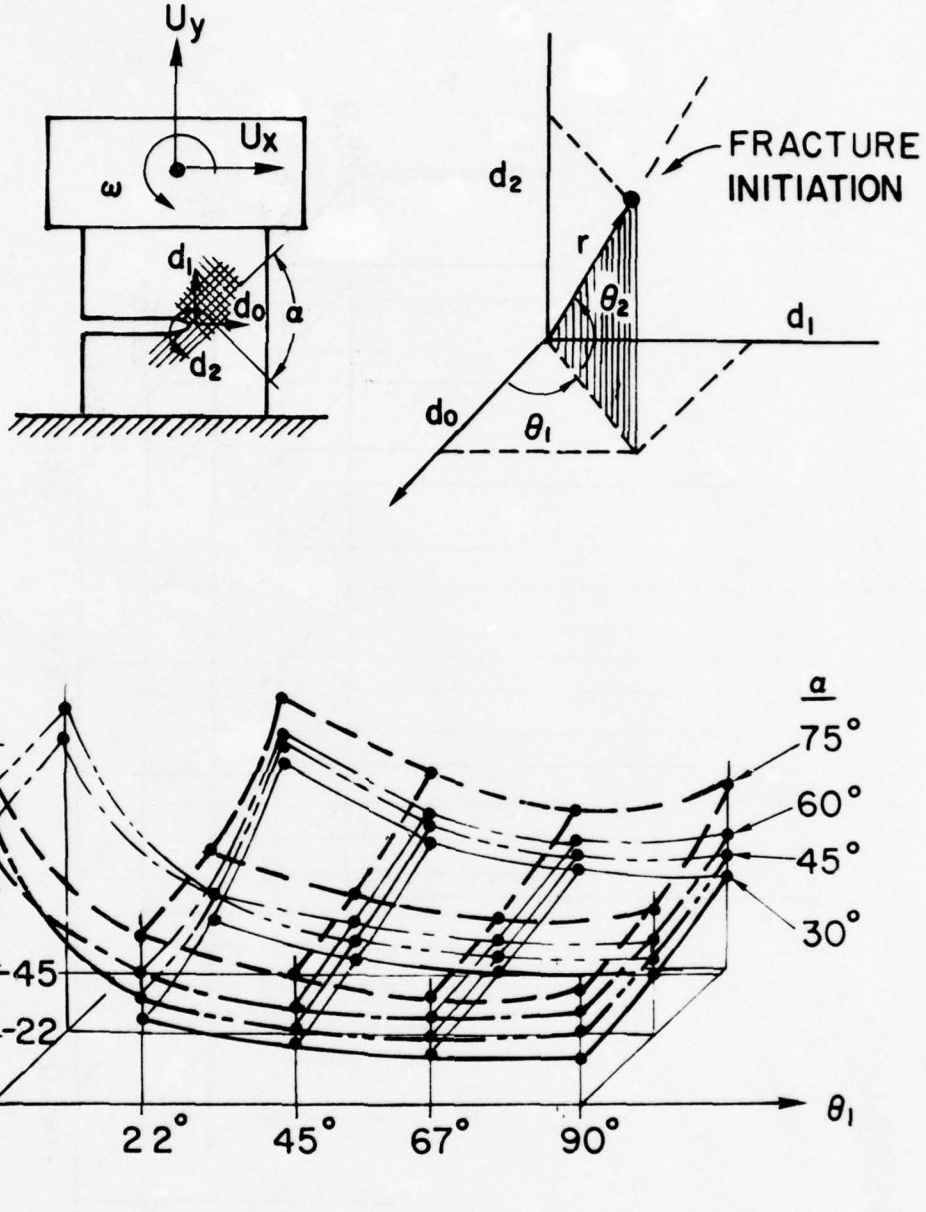

Fig. 2 - Failure surfaces for T300/5208 graphite/epoxy composites for different fiber orientations in one octant of load space

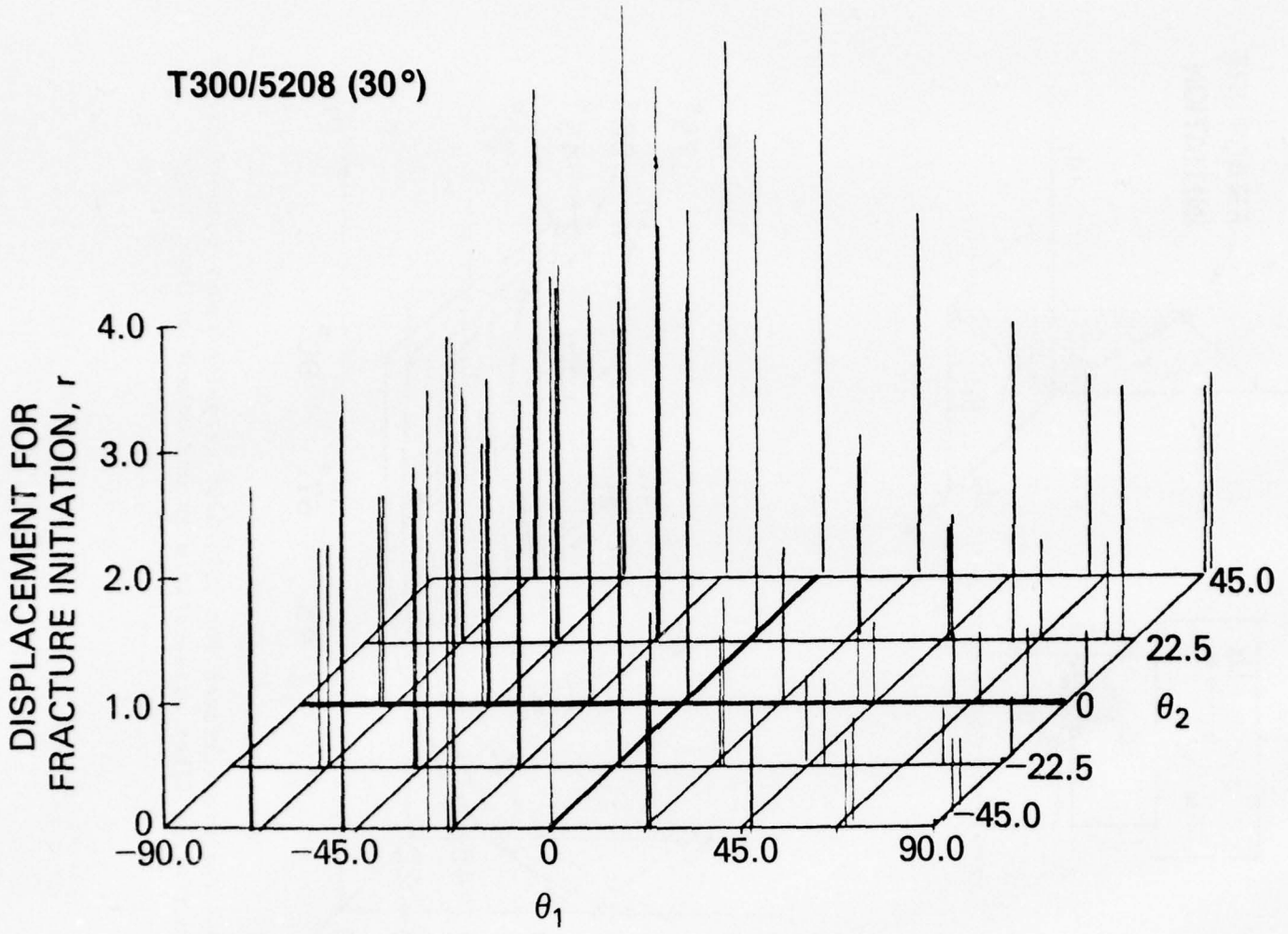

Fig. 3 - Failure data for T300/5208 graphite/epoxy composite for four octants of load space (Reinforcement included angle = 30^{o})

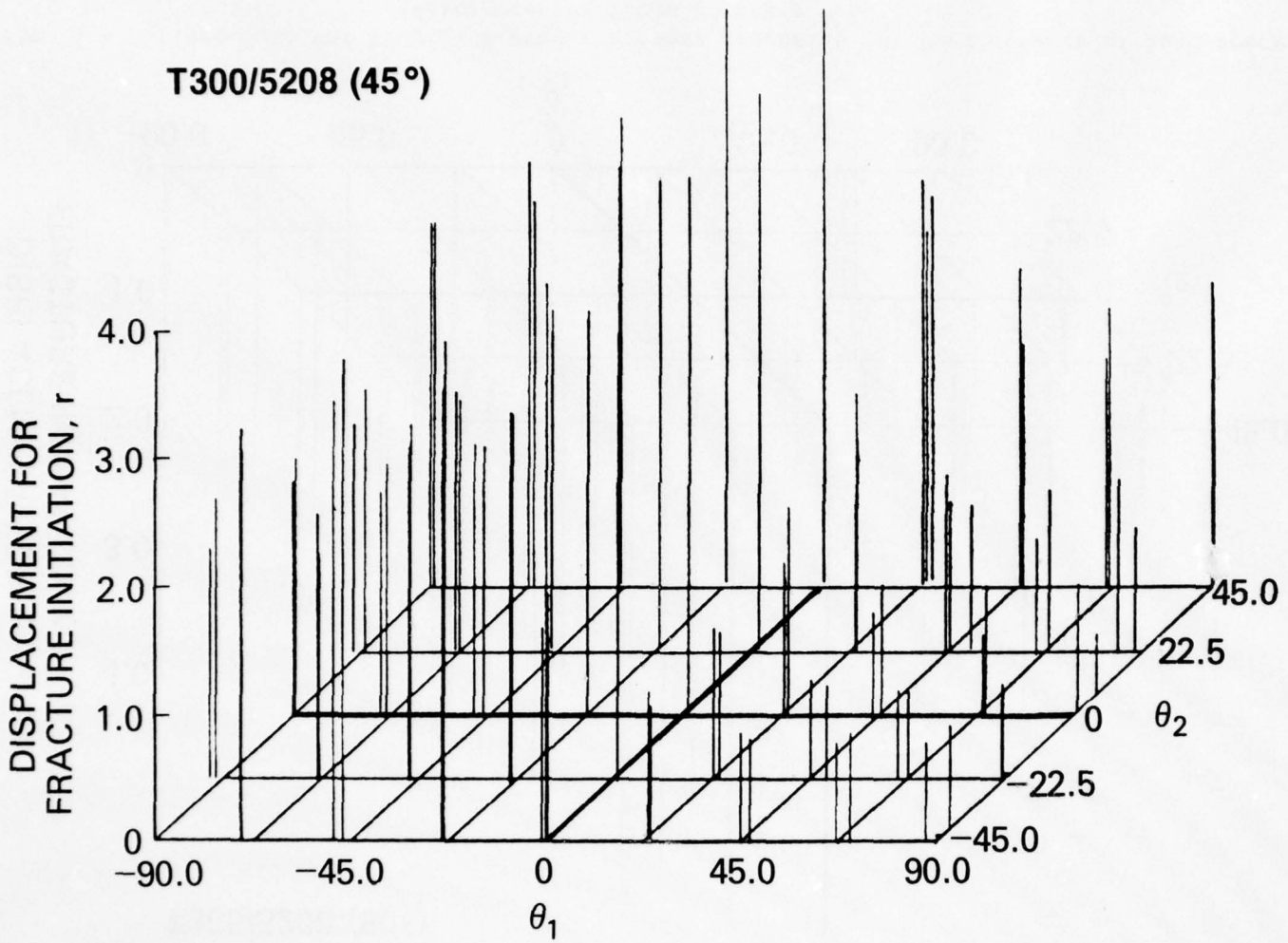

Fig. 4 - Failure data for T300/5208 graphite/epoxy composite for four octants of load space (Reinforcement included angle = 45°)

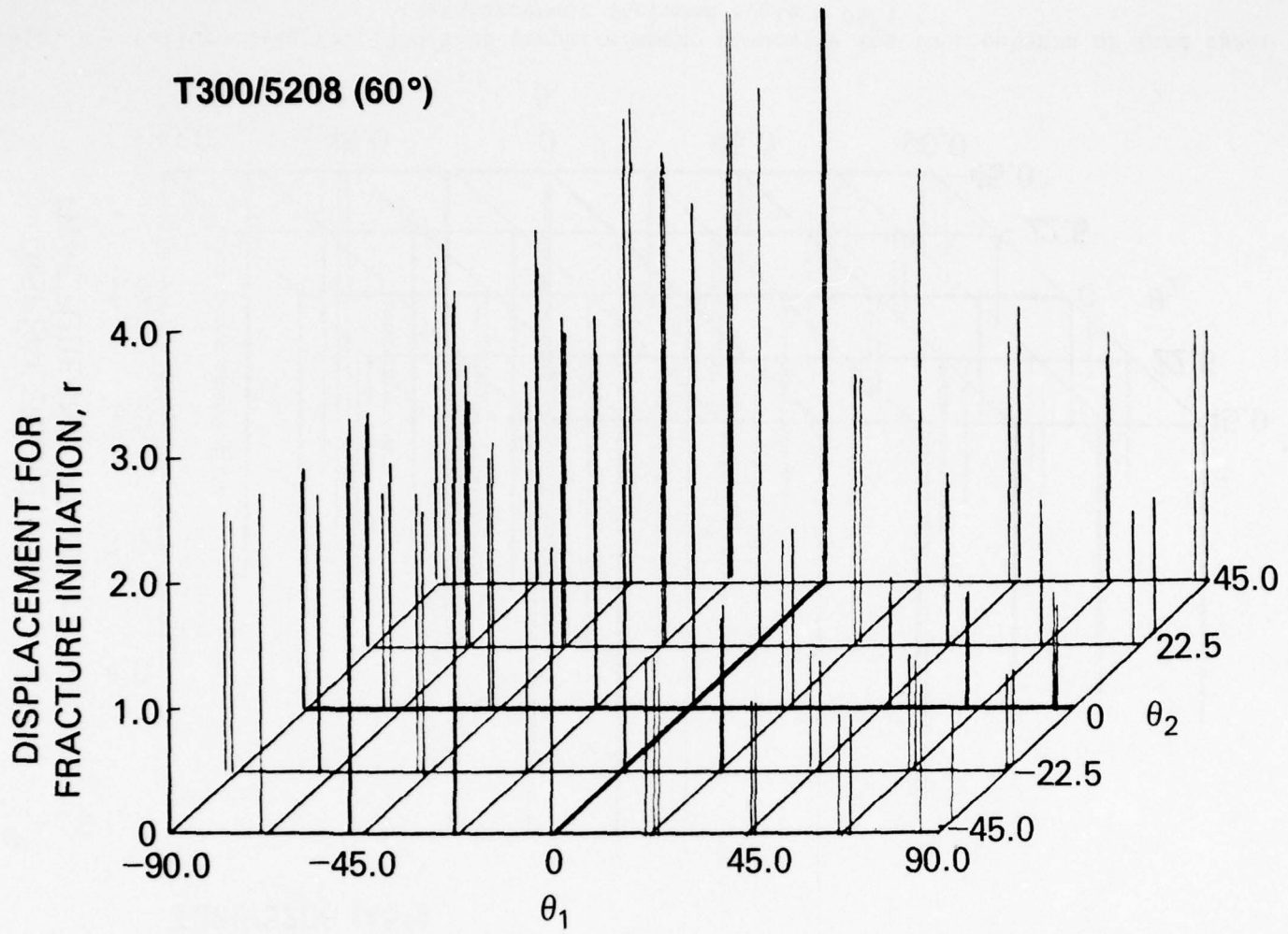

Fig. 5 - Failure data for T300/5208 graphite/epoxy composite for four octants of load space (Reinforcement included angle = 60^{o})

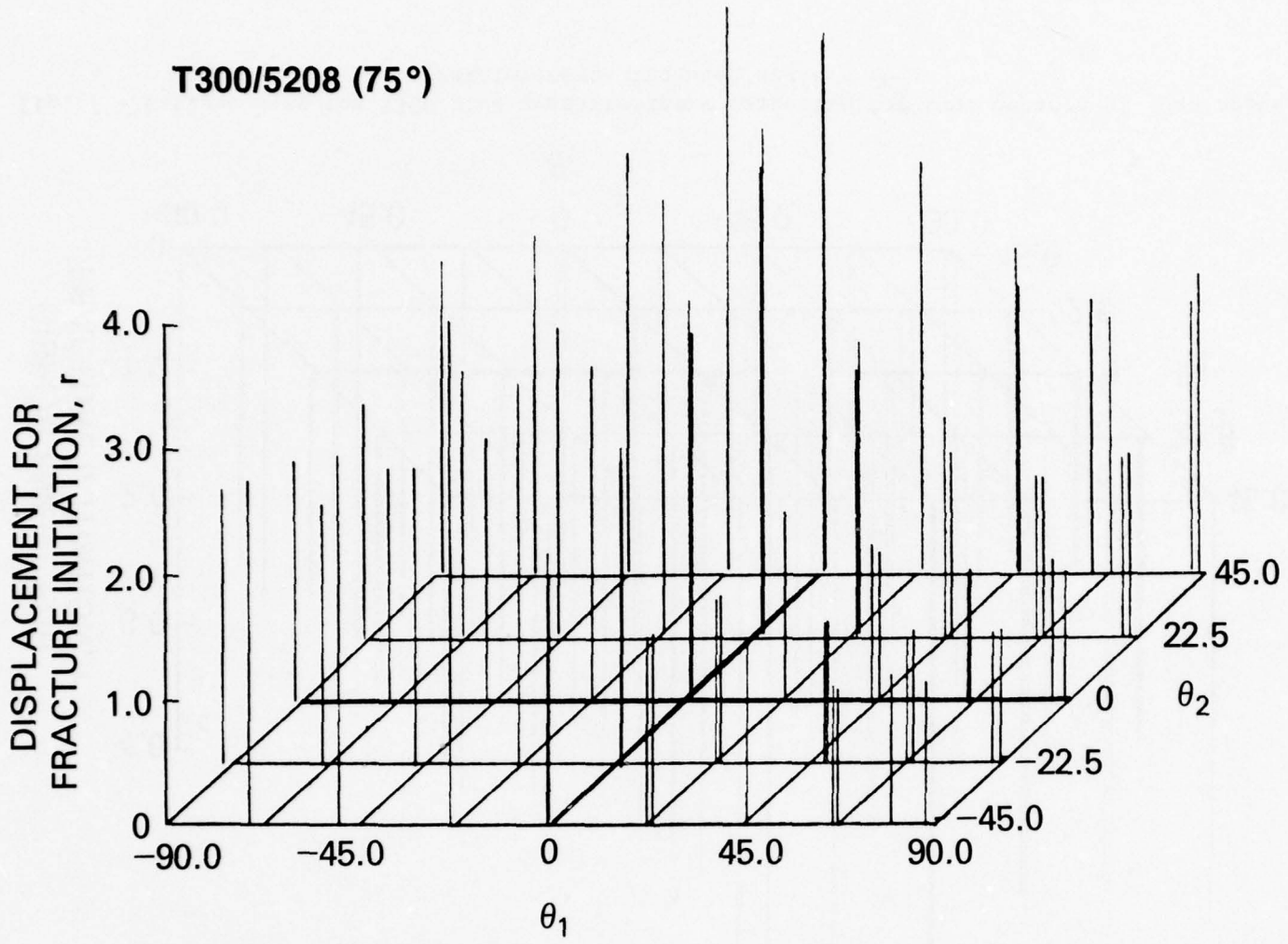

Fig. 6 - Failure data for T300/5208 graphite/epoxy composite for four octants of load space (Reinforcement included angle = 75°)

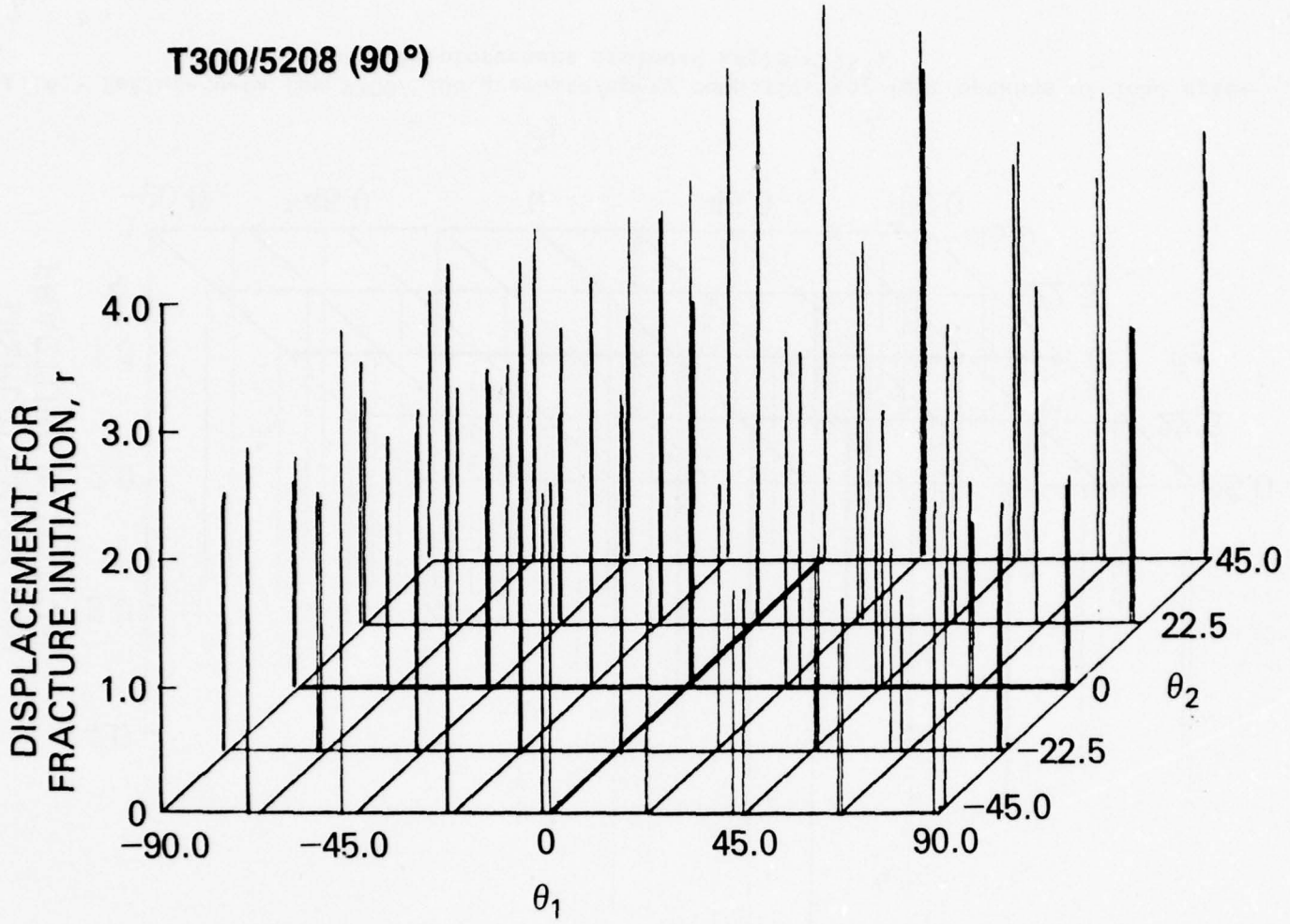

Fig. 7 - Failure data for T300/5208 graphite/epoxy composite for four octants of load space (Reinforcement included angle = 90^{o})

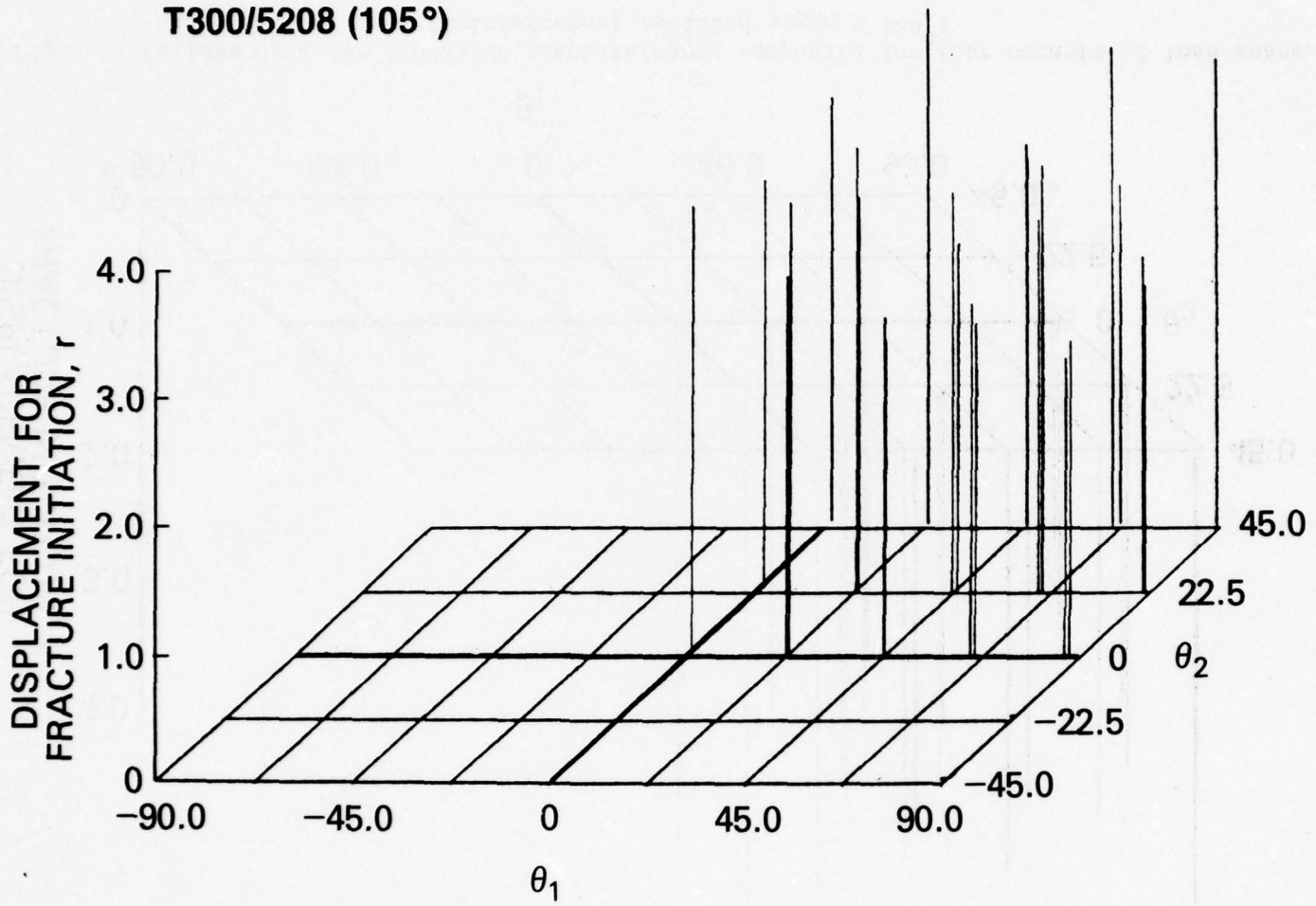

Fig. 8 - Failure data for T300/5208 graphite/epoxy composite for four octants of load space (Reinforcement included angle = 105°)

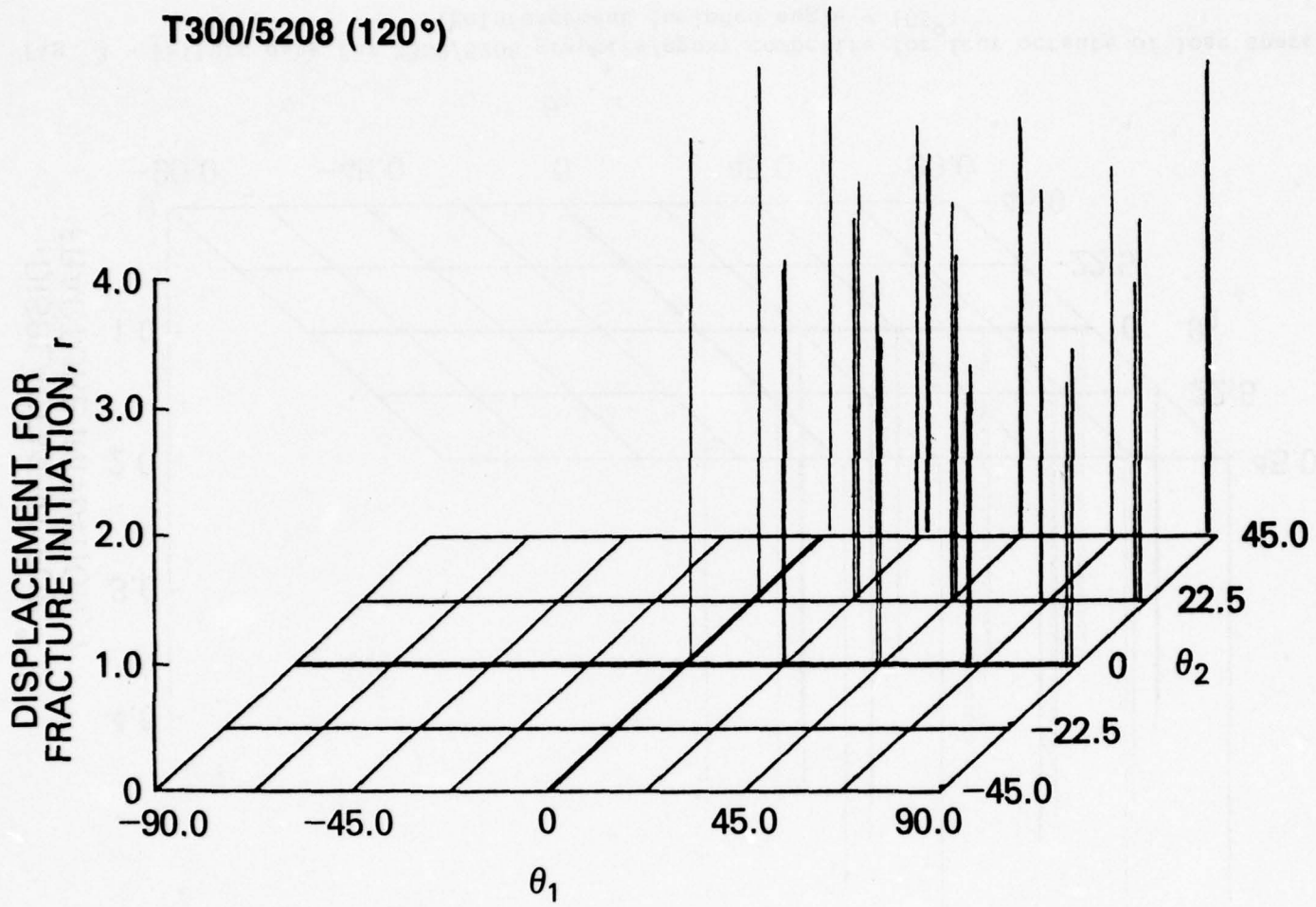

Fig. 9 - Failure data for T300/5208 graphite/epoxy composite for four octants of load space (Reinforcement included angle = 120°)

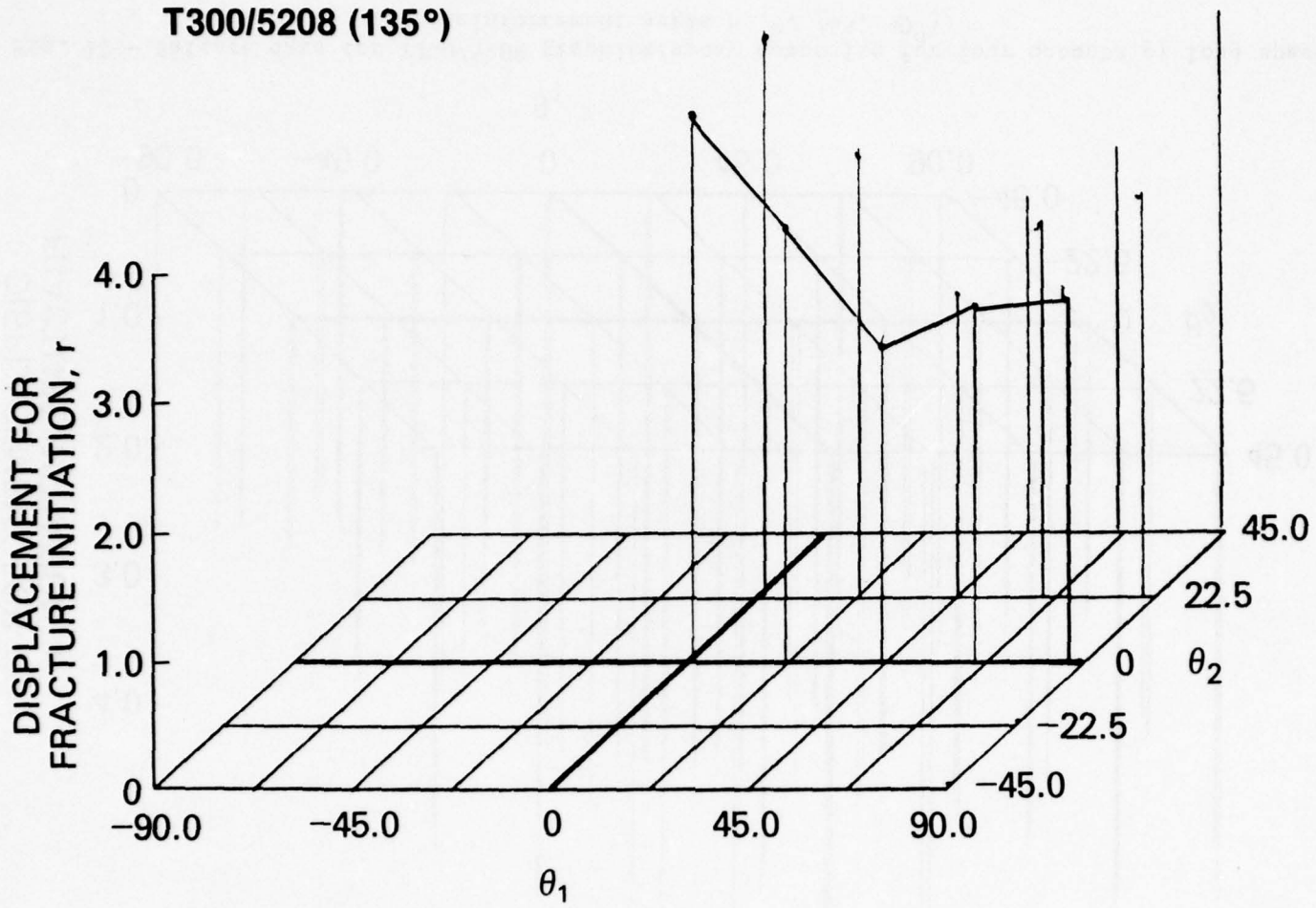

Fig. 10 - Failure data for T300/5208 graphite/epoxy composite for four octants of load space (Reinforcement included angle = 135°)

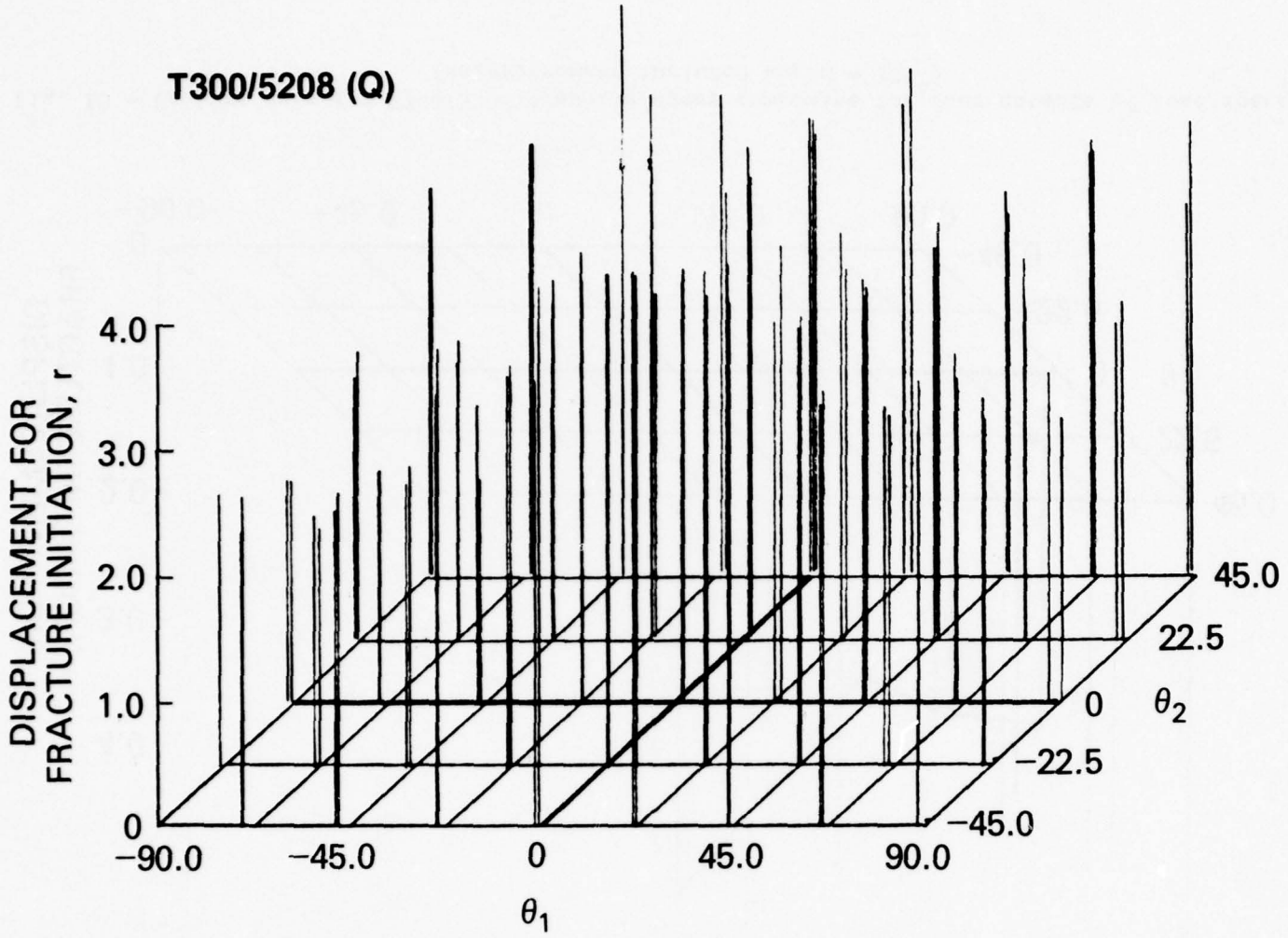

Fig. 11 - Failure data for T300/5208 graphite/epoxy composite for four octants of load space (Reinforcement angle = (0, ±45, 90°))

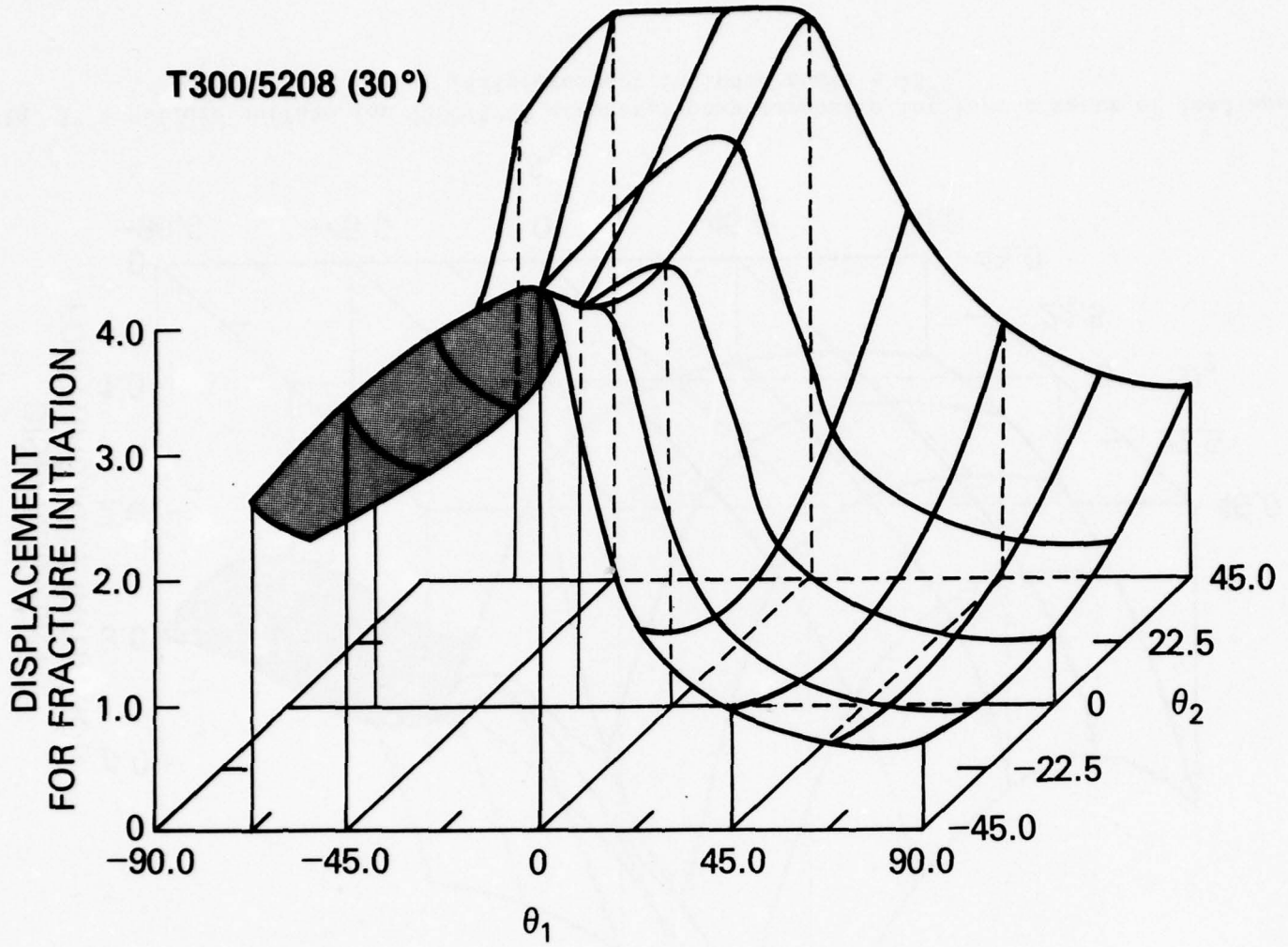

Fig. 12 - Failure surface for T300/5208 graphite/epoxy composite for four octants of load space (Reinforcement included angle = 30°)

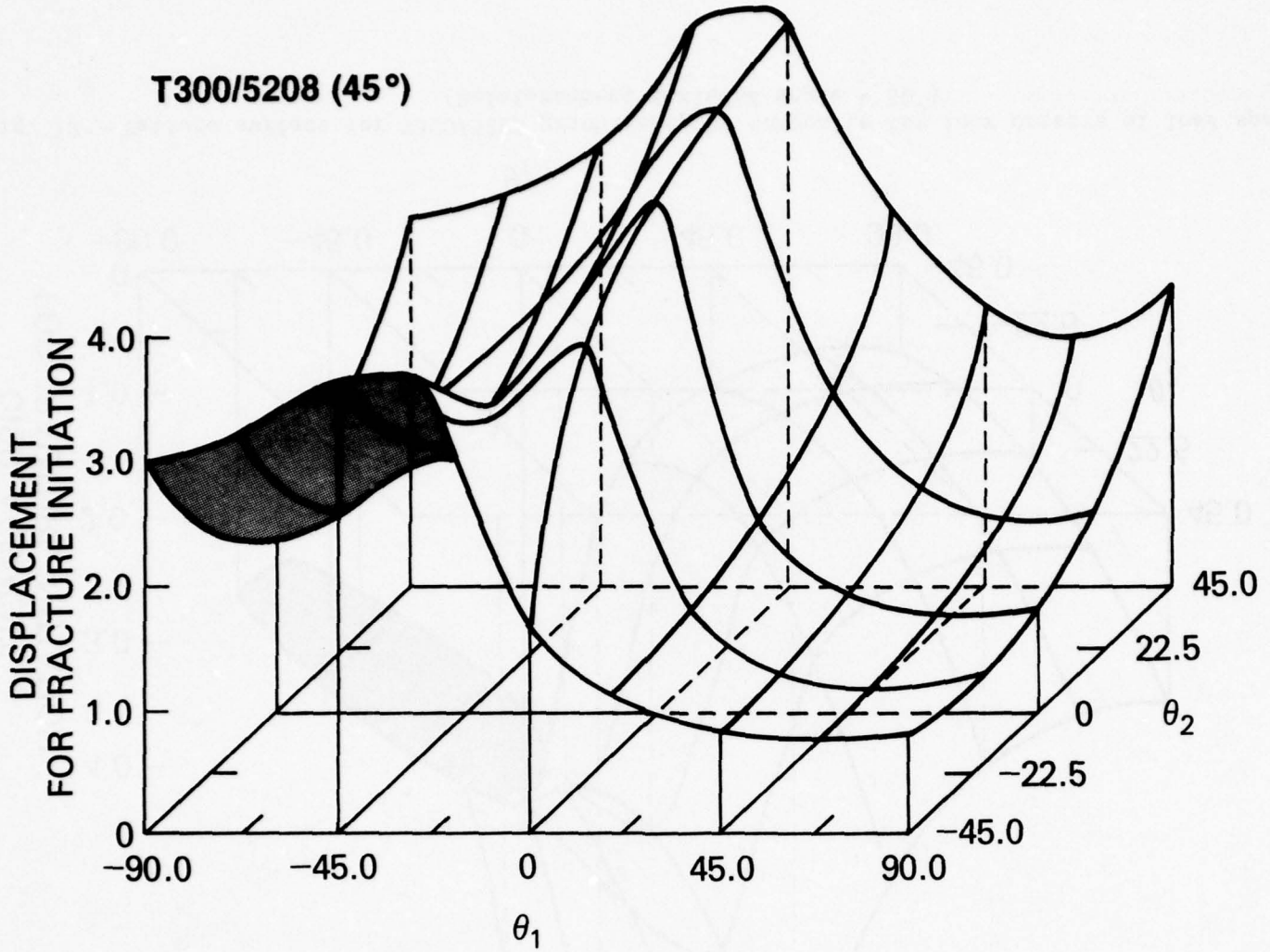

Fig. 13 - Failure surface for T300/5208 graphite/epoxy composite for four octants of load space (Reinforcement included angle = 45°)

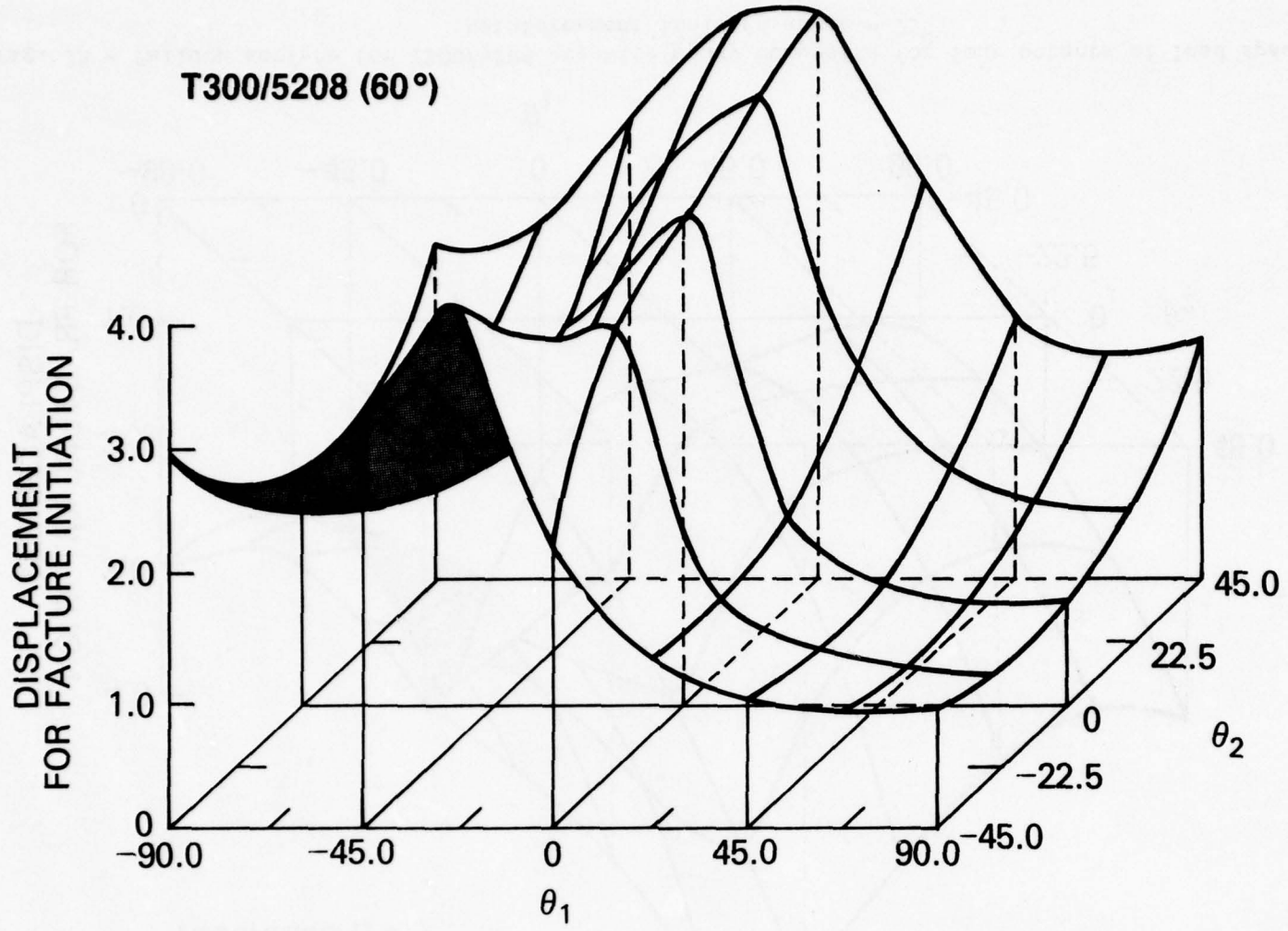

Fig. 14 - Failure surface for T300/5208 graphite/epoxy composite for four octants of load space (Reinforcement included angle = 60°)

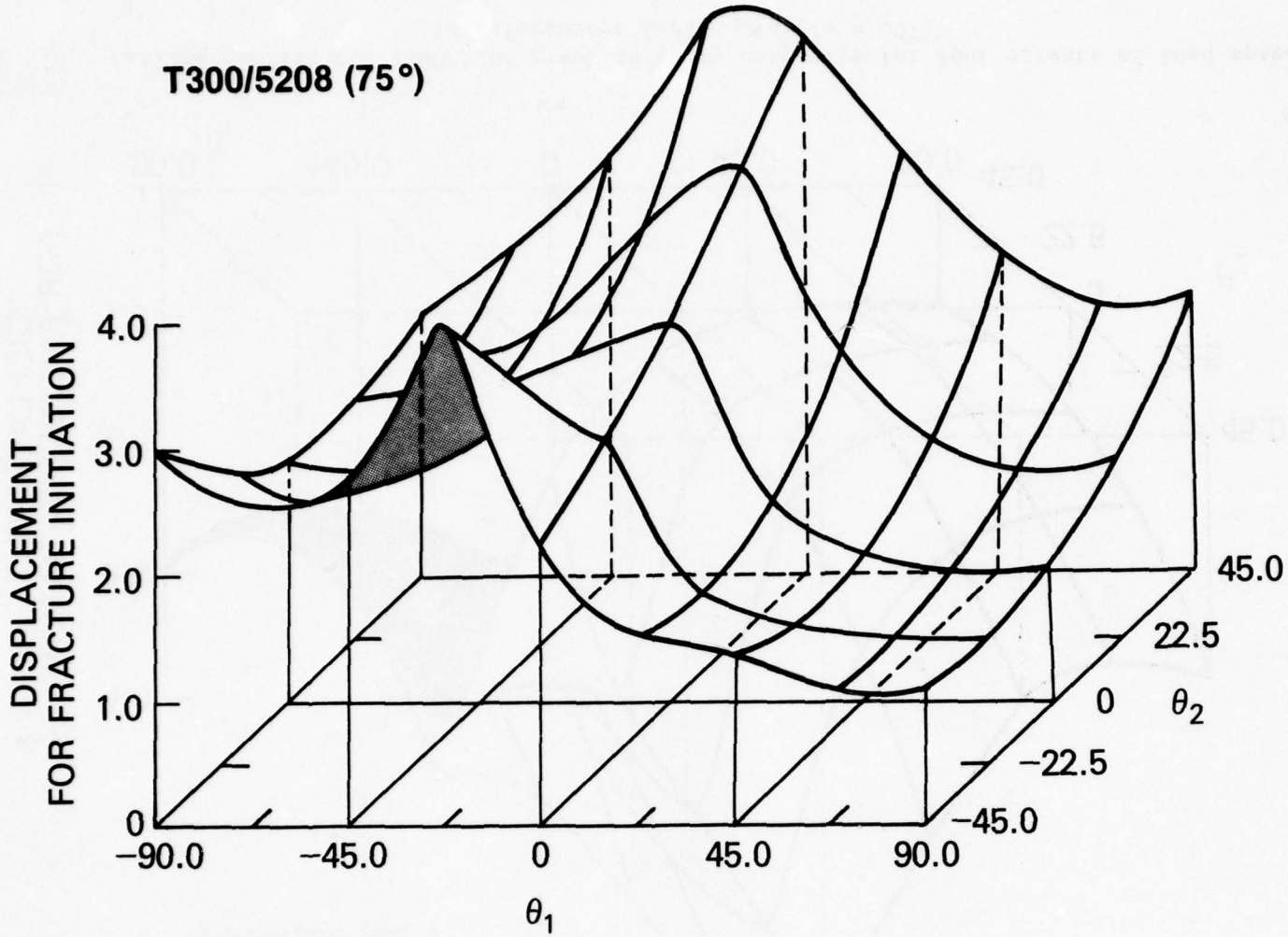

Fig. 15 - Failure surface for T300/5208 graphite/epoxy composite for four octants of load space (Reinforcement included angle = 75°)

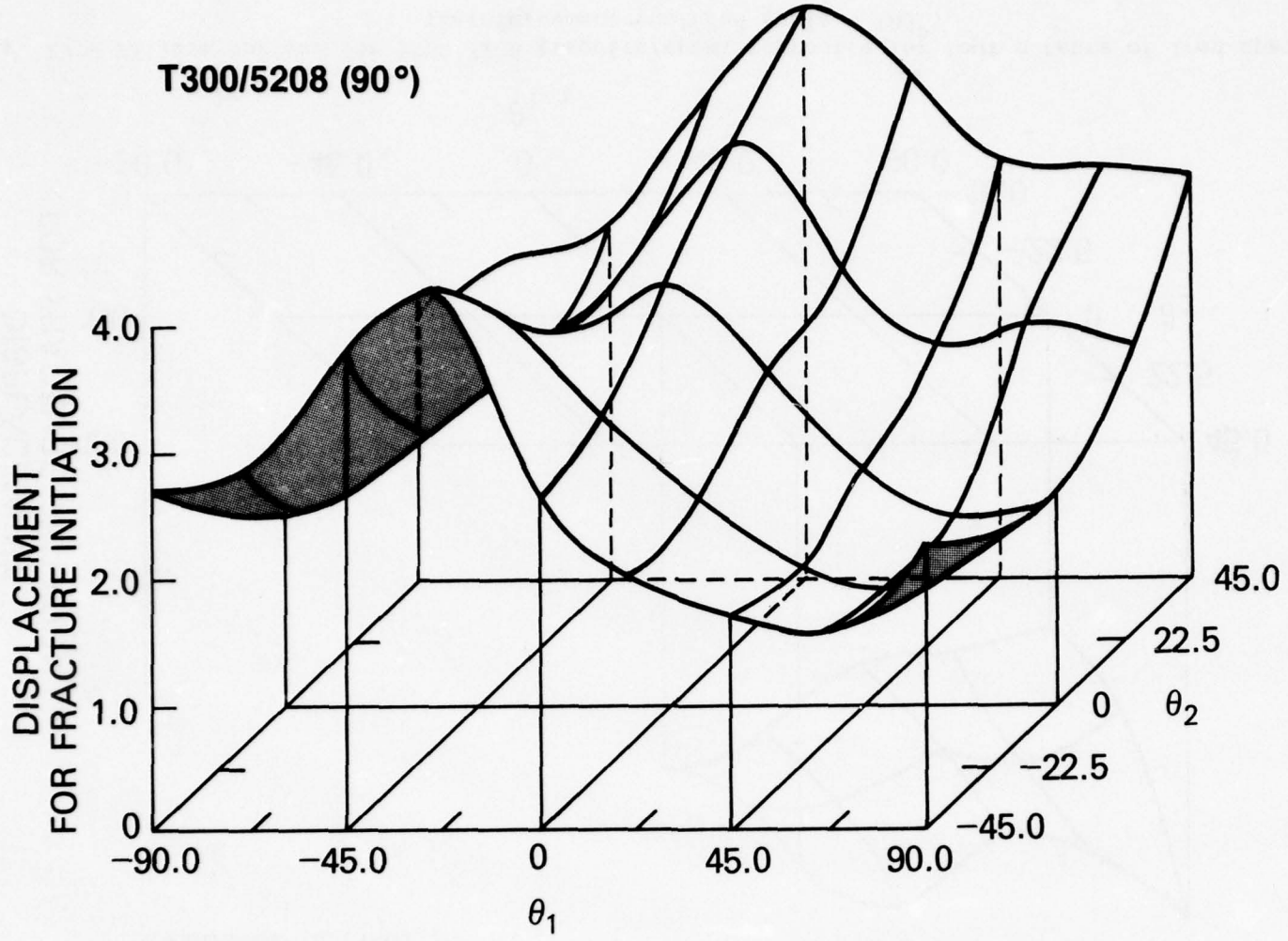

Fig. 16 - Failure surface for T300/5208 graphite/epoxy composite for four octants of load space (Reinforcement included angle = 90°)

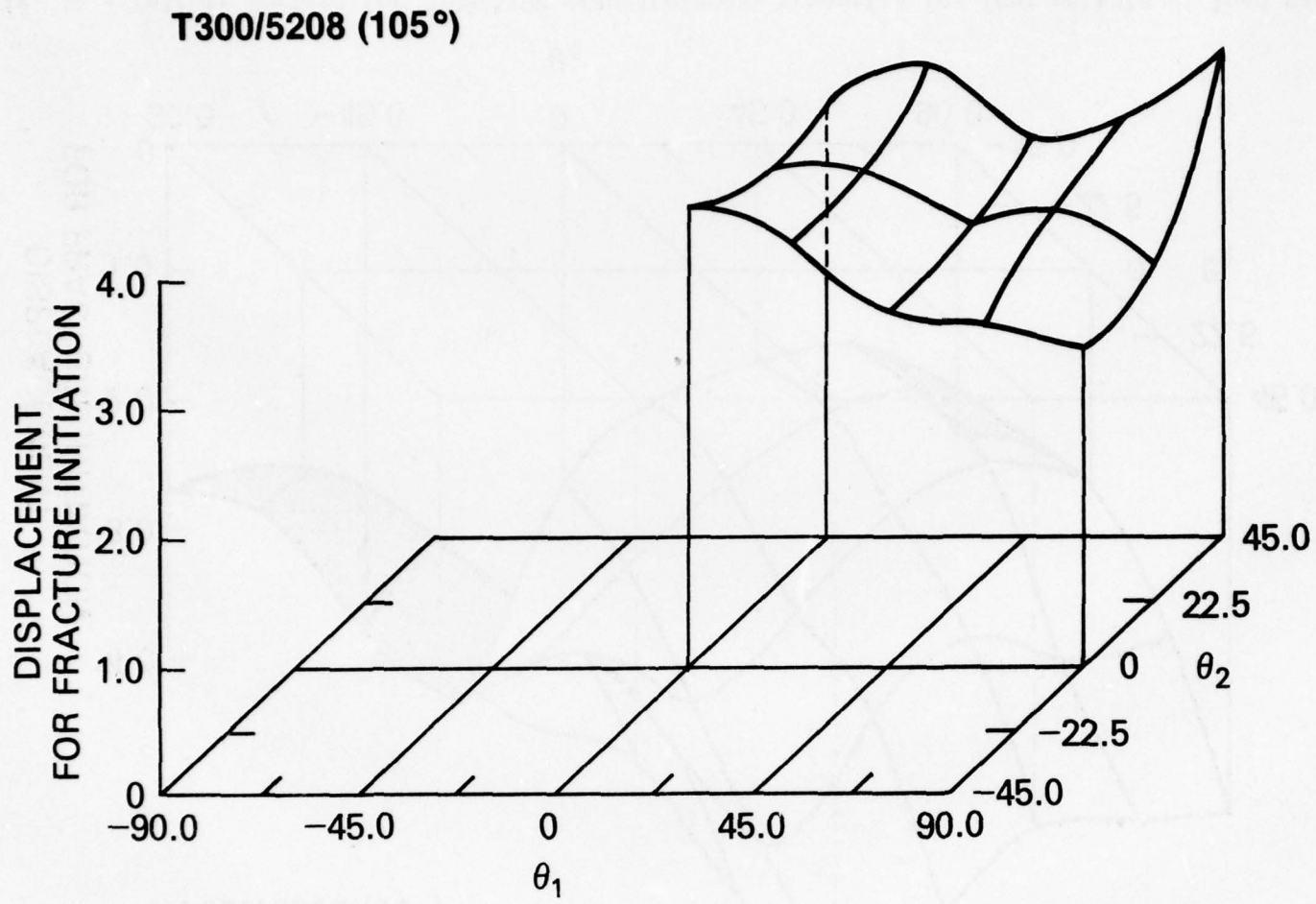

Fig. 17 - Failure surface for T300/5208 graphite/epoxy composite for four octants of load space (Reinforcement included angle = 105°)

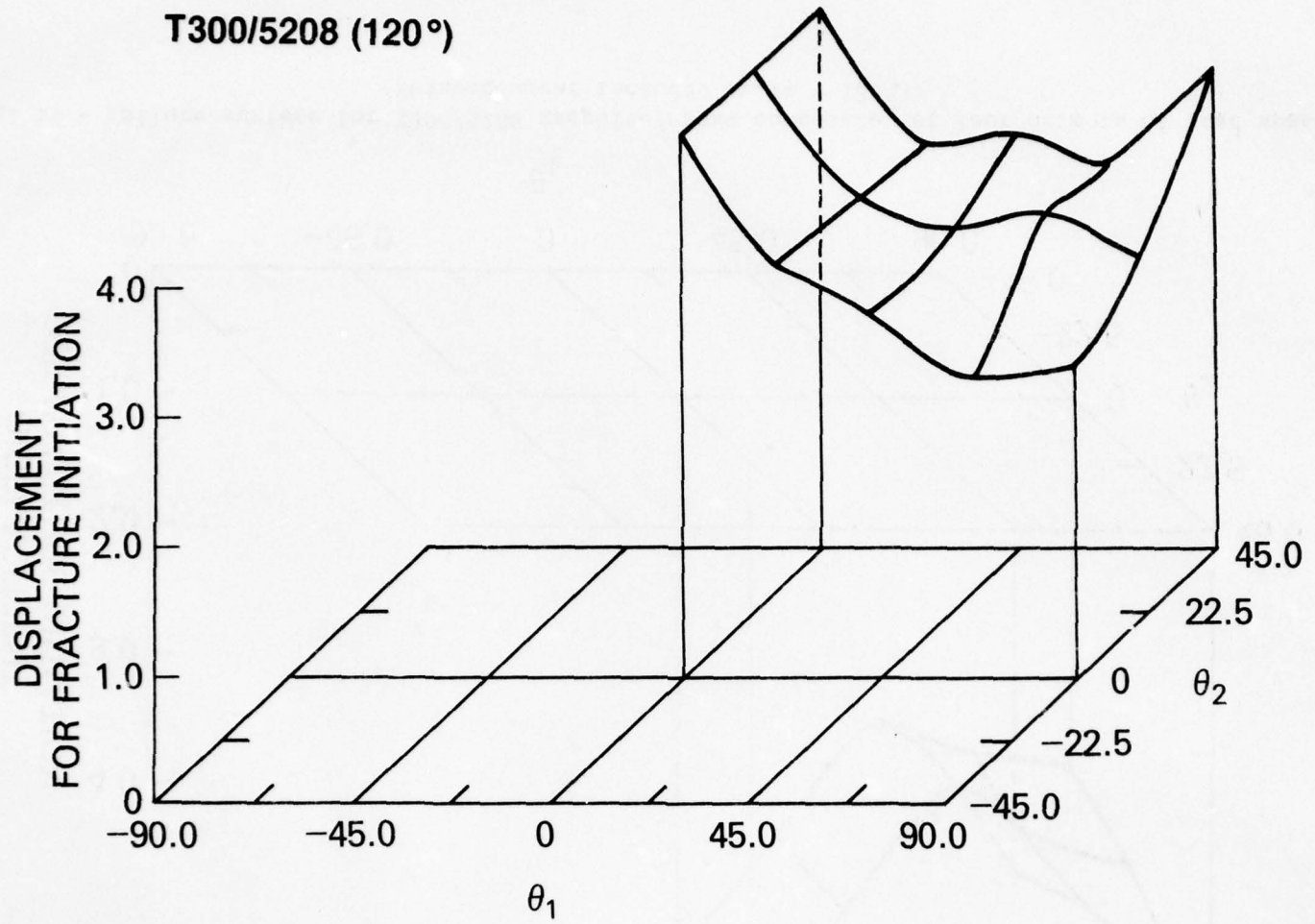

Fig. 18 - Failure surface for T300/5208 graphite/epoxy composite for four octants of load space (Reinforcement included angle = 120°)

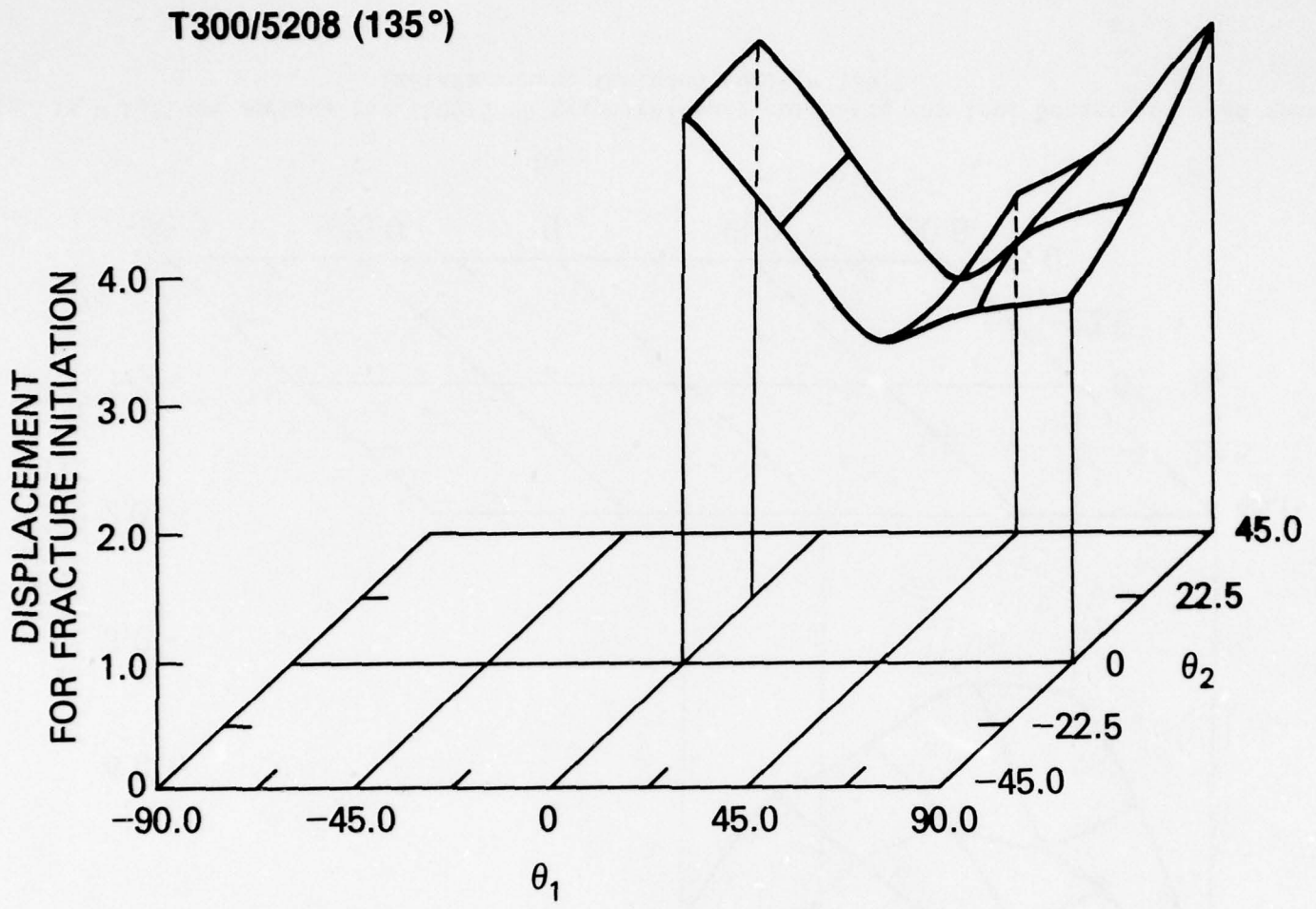

Fig. 19 - Failure surface for T300/5208 graphite/epoxy composite for four octants of load space (Reinforcement included angle = 135°)

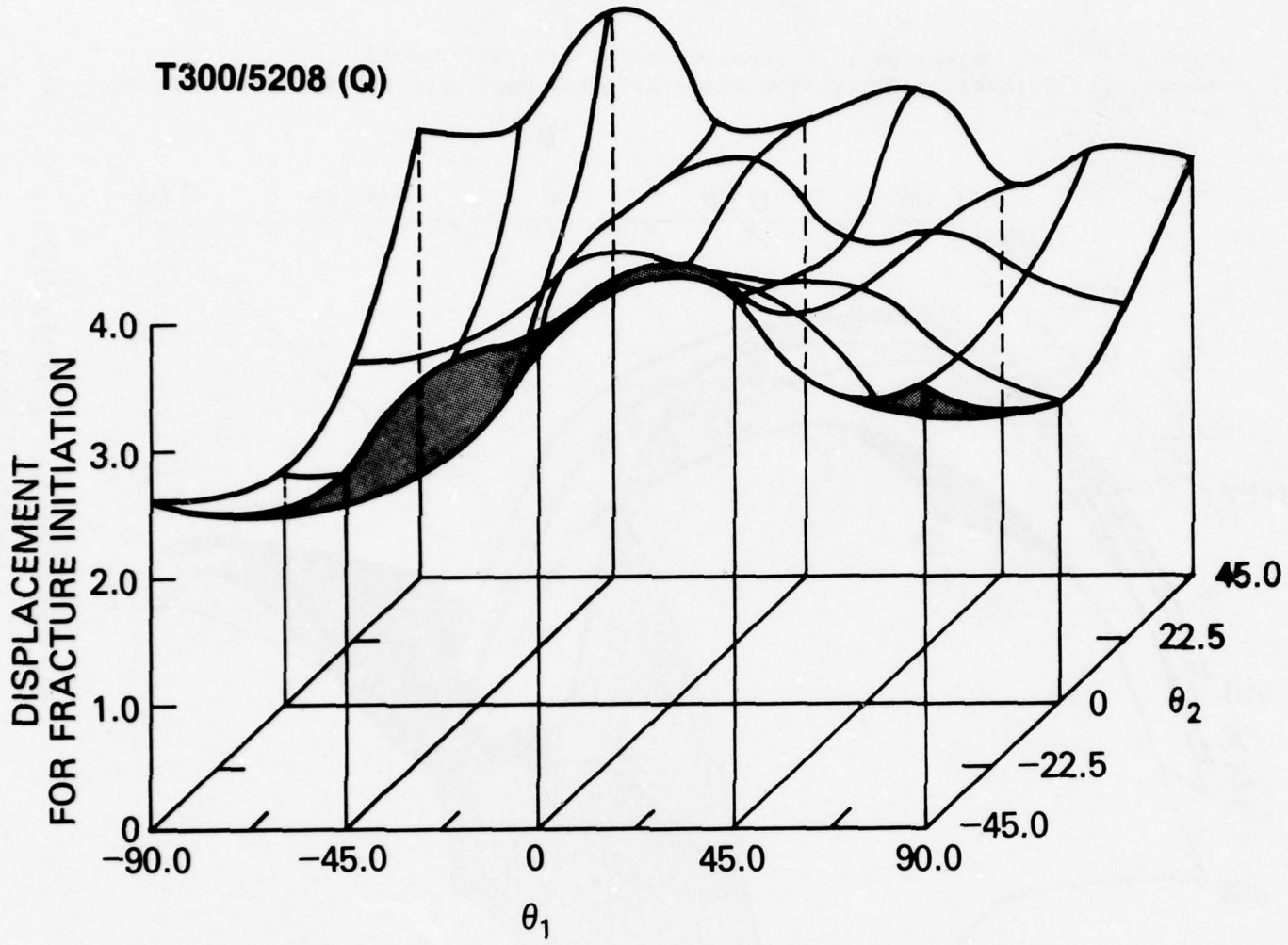

Fig. 20 - Failure surface for T300/5208 graphite/epoxy composite for four octants of load space (Reinforcement angle = $(0, \pm 45, 90^{o})$)

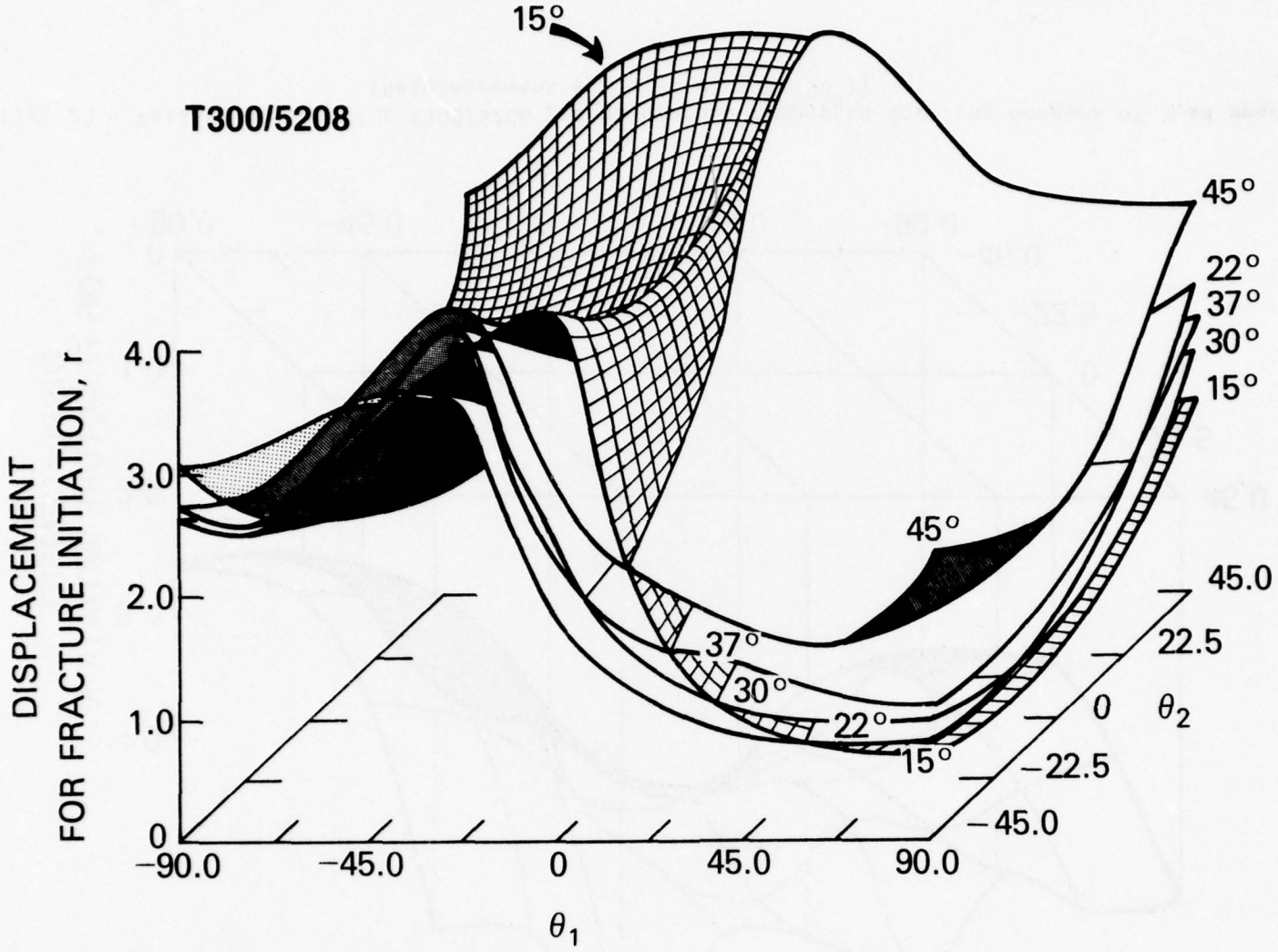

Fig. 21 - Failure surfaces for T300/5208 graphite/epoxy composites of varying reinforcement included angles for four octants of load space

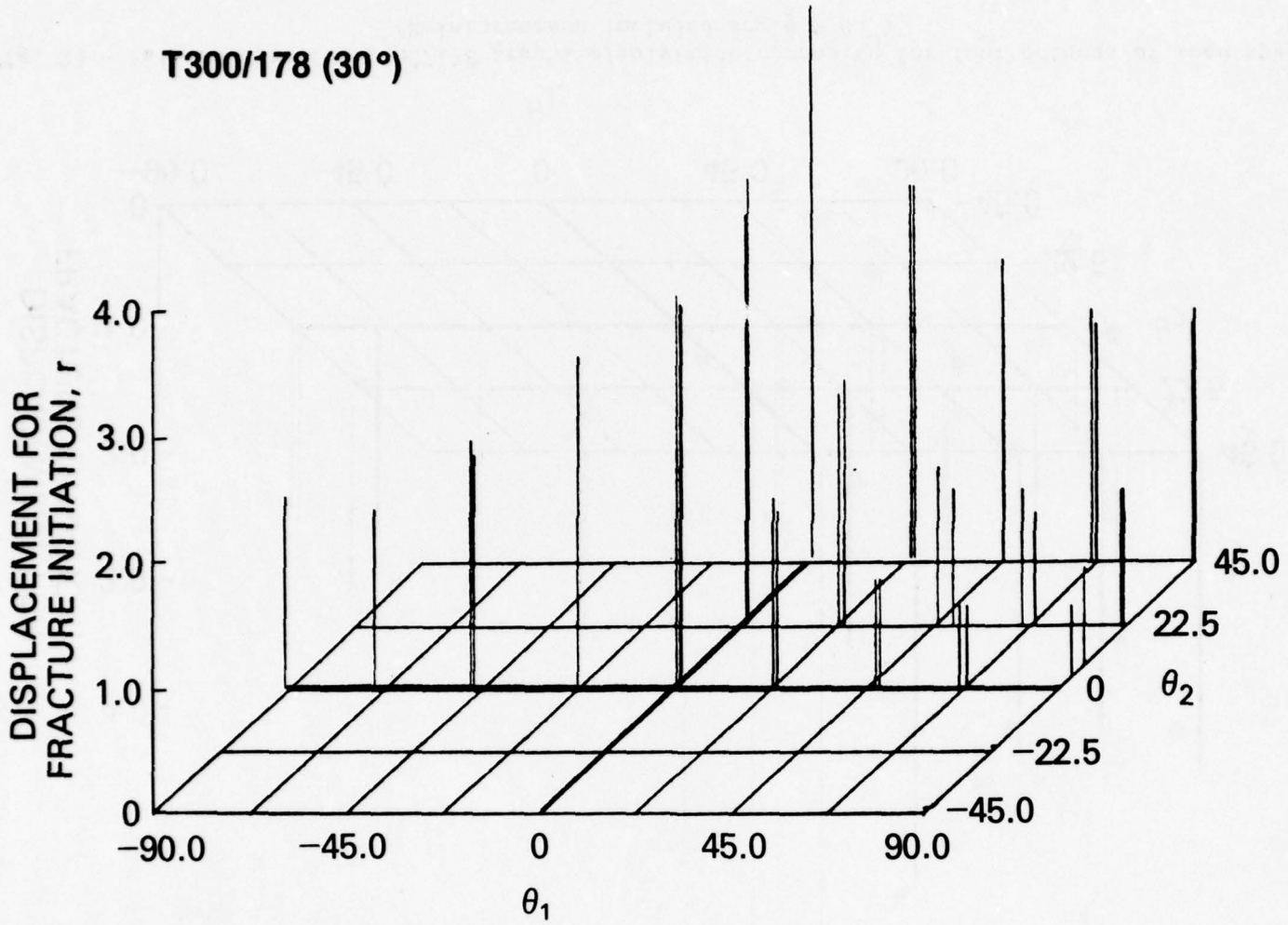

Fig. 22 - Failure data for T300/178 graphite/polyimide composite for four octants of load space (Reinforcement included angle = 30°)

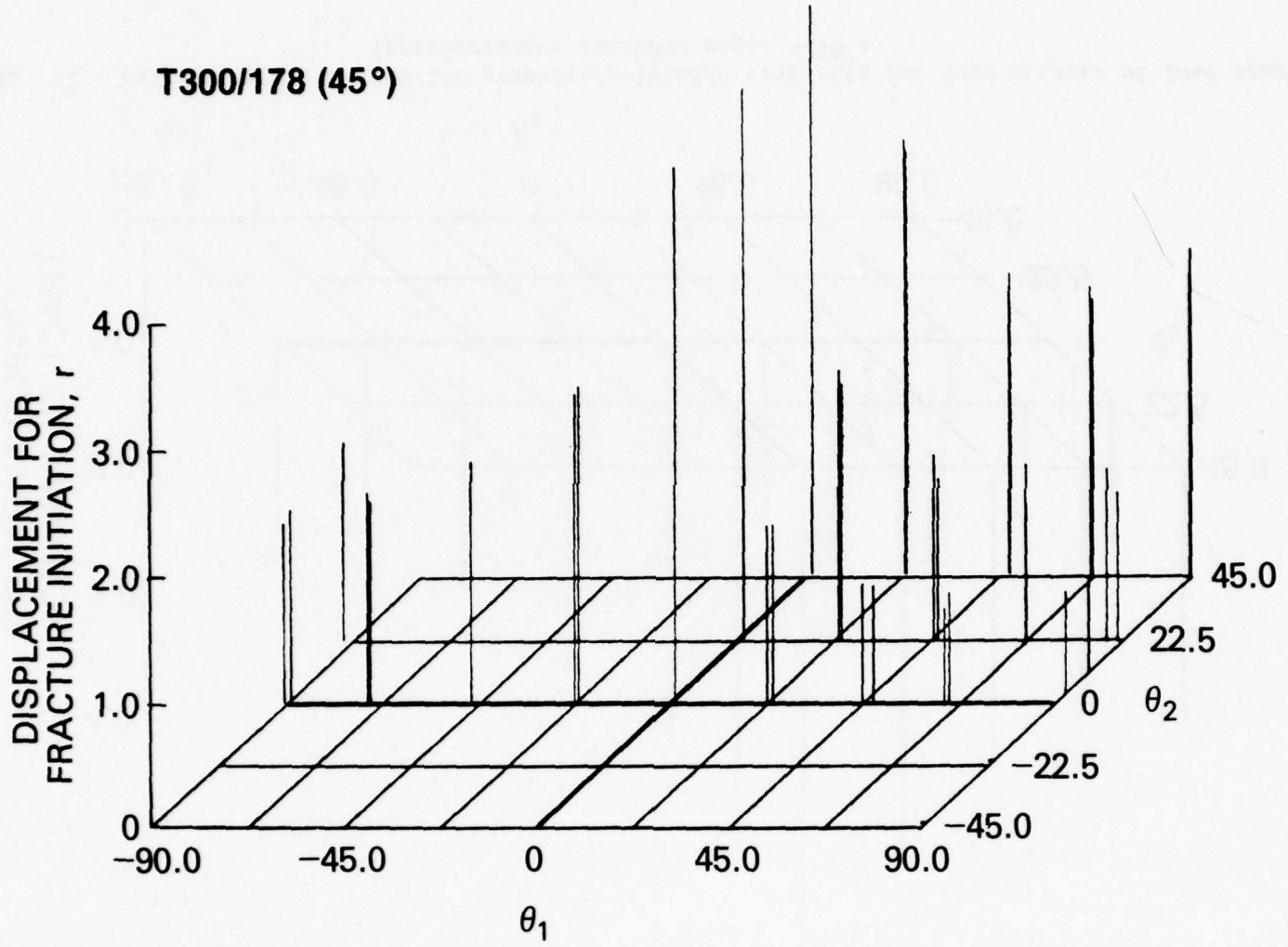

Fig. 23 - Failure data for T300/178 graphite/polyimide composite for four octants of load space (Reinforcement included angle = 45°)

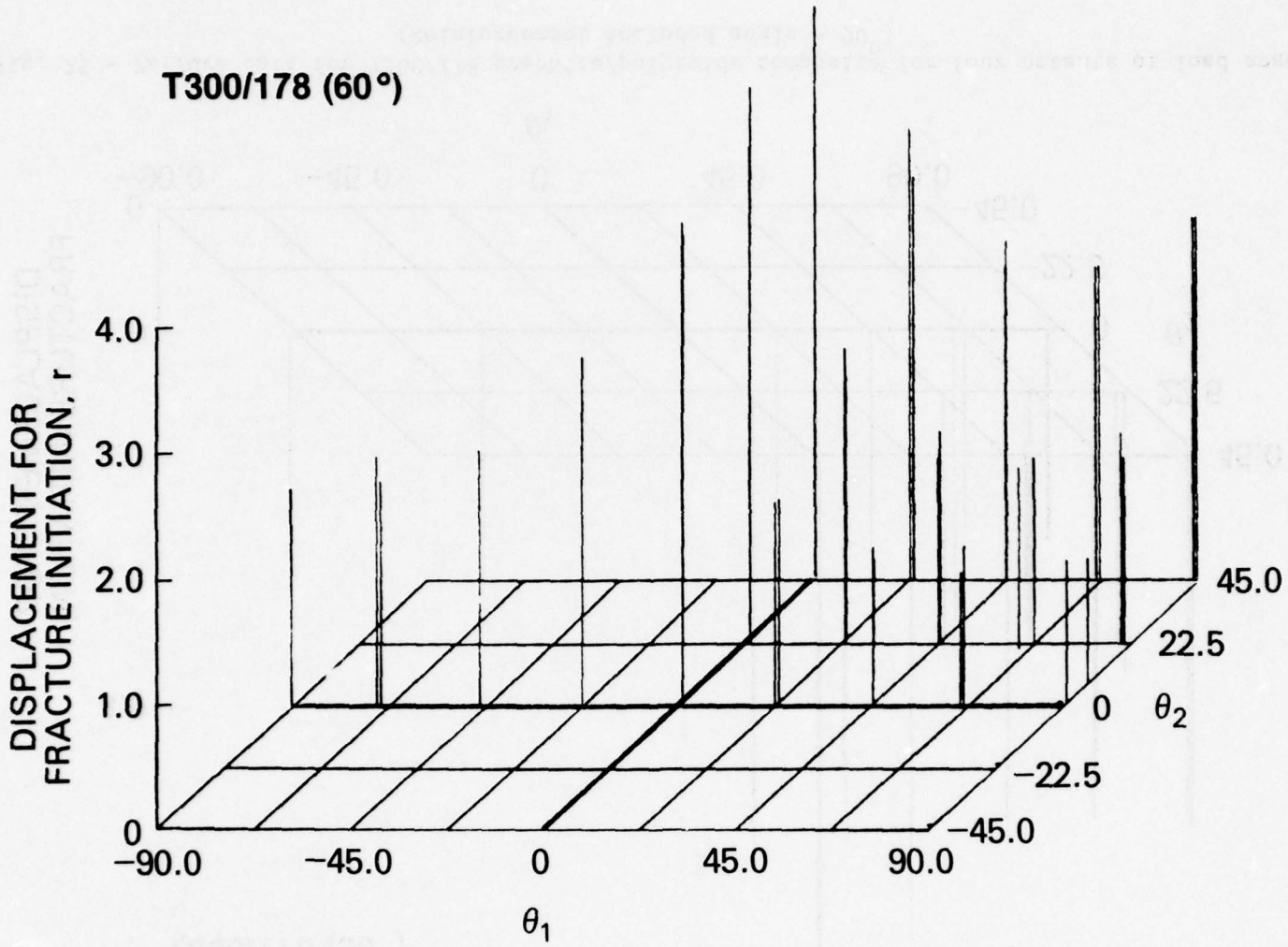

Fig. 24 - Failure data for T300/178 graphite/polyimide composite for four octants of load space (Reinforcement included angle = 60°)

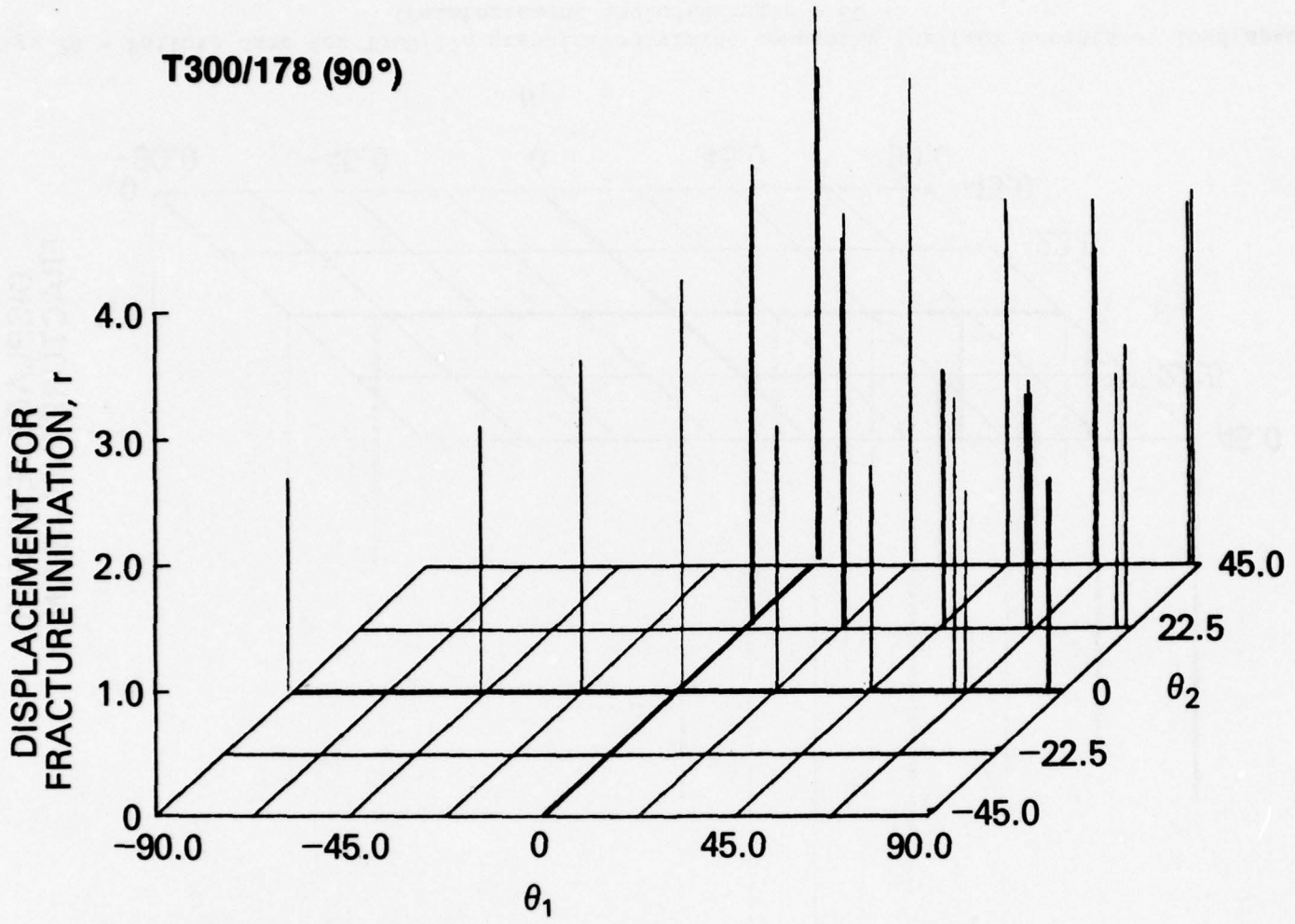

Fig. 25 - Failure data for T300/178 graphite/polyimide composite for four octants of load space (Reinforcement included angle = 90°)

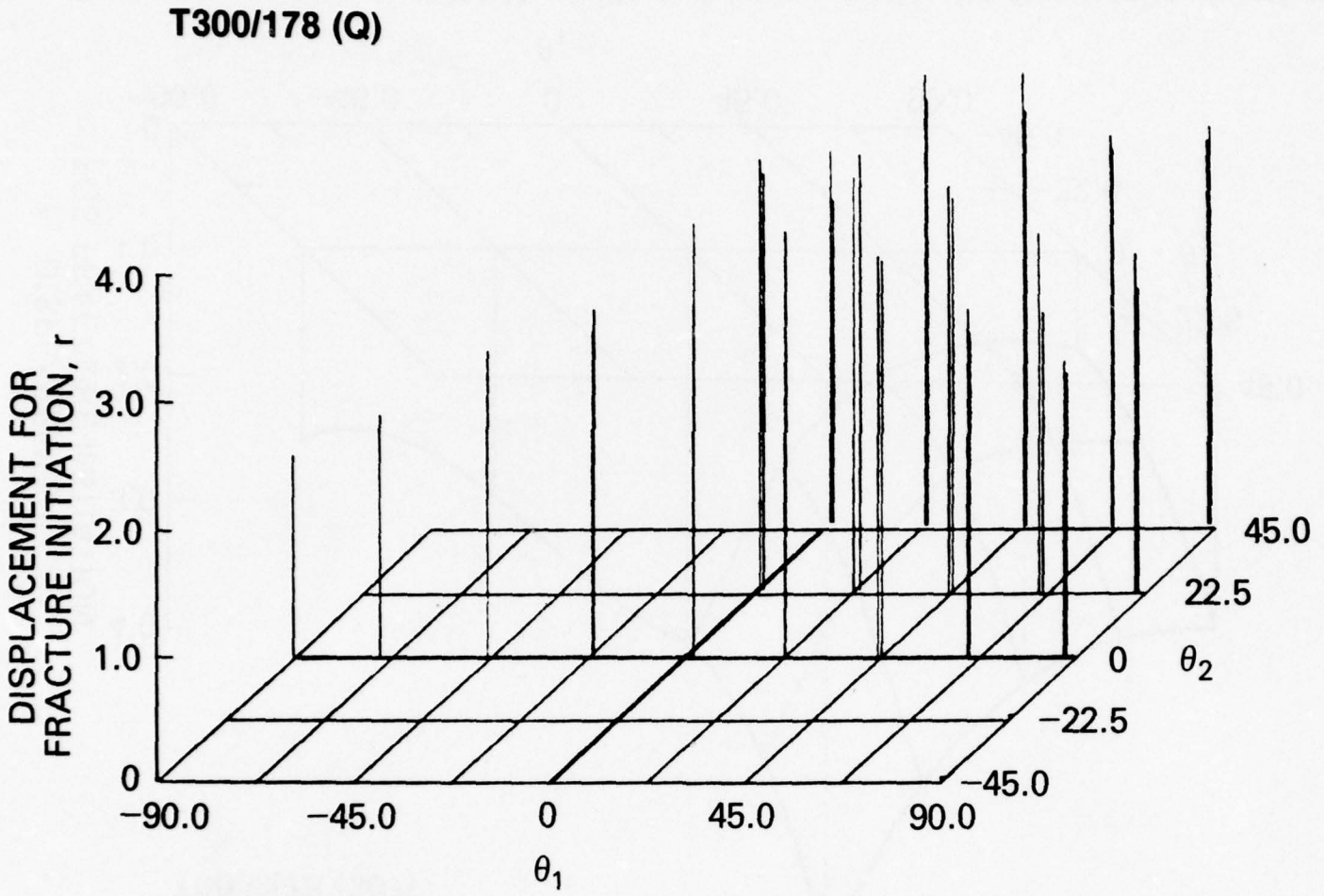

Fig. 26 - Failure data for T300/178 graphite/polyimide composite for four octants of load space (Reinforcement angle = (0, $\pm$45, 90^{o}))

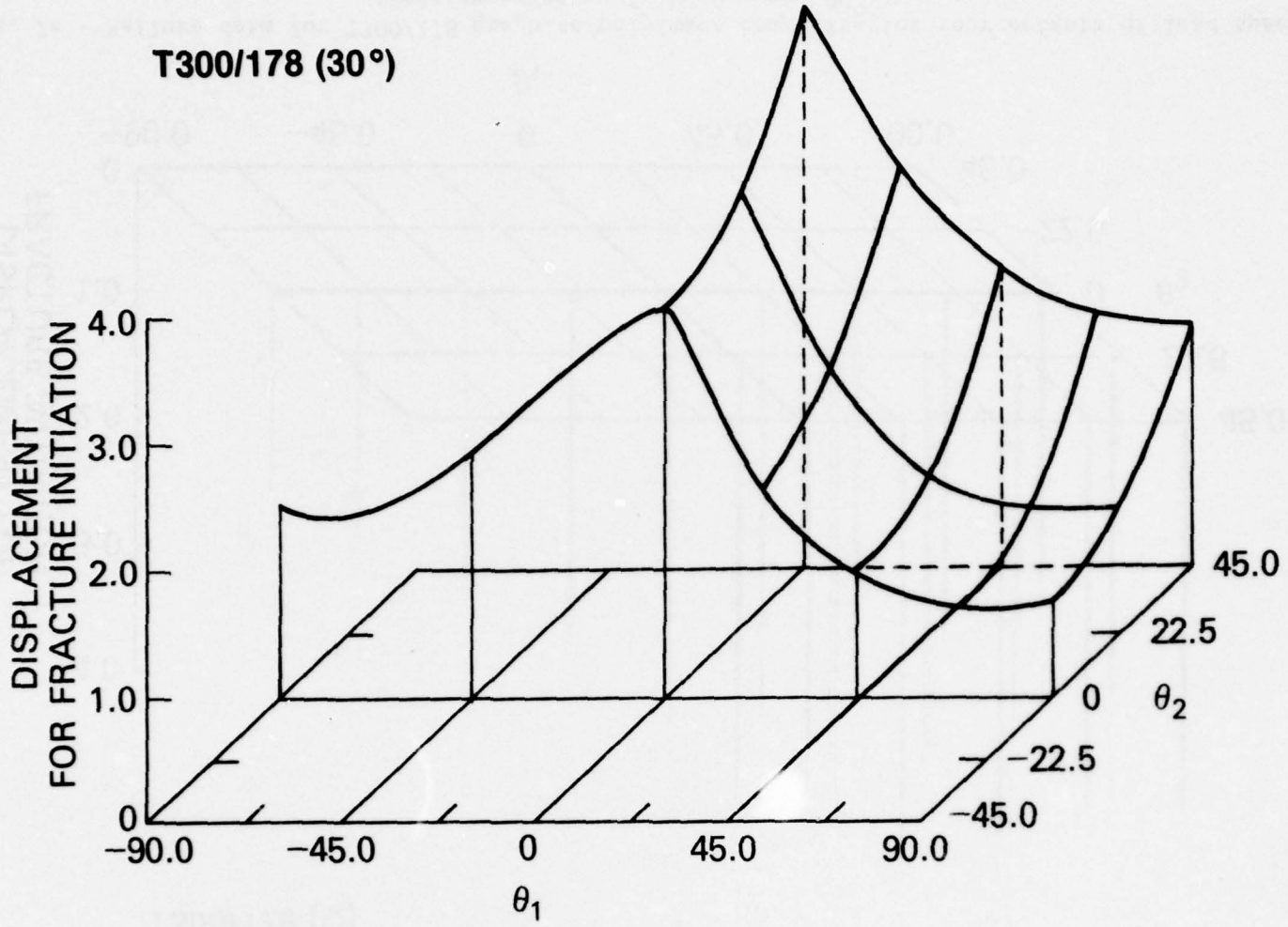

Fig. 27 - Failure surface for T300/178 graphite/polyimide composite for four octants of load space (Reinforcement included angle = 30°)

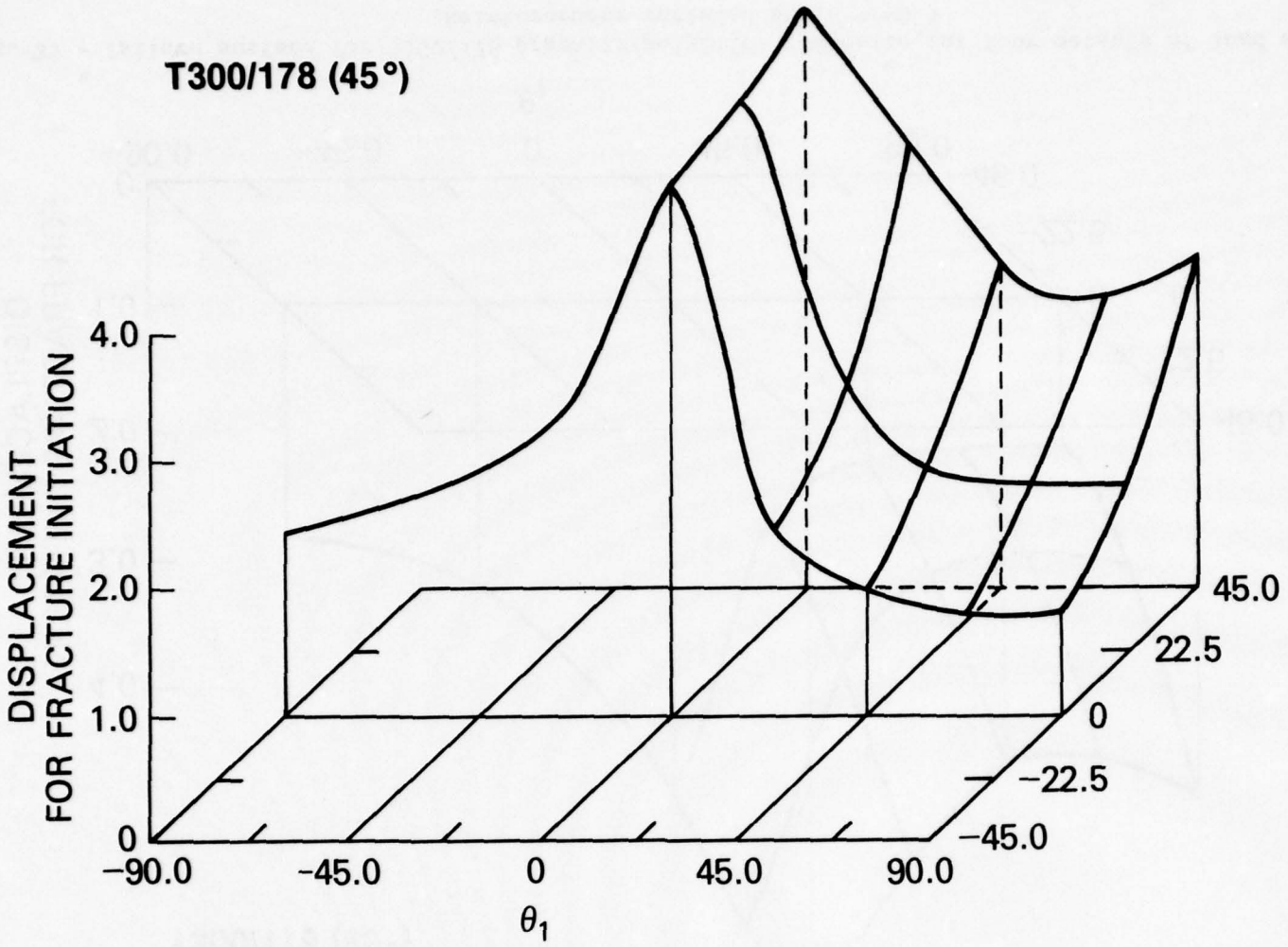

Fig. 28 - Failure surface for T300/178 graphite/polyimide composite for four octants of load space (Reinforcement included angle = 45°)

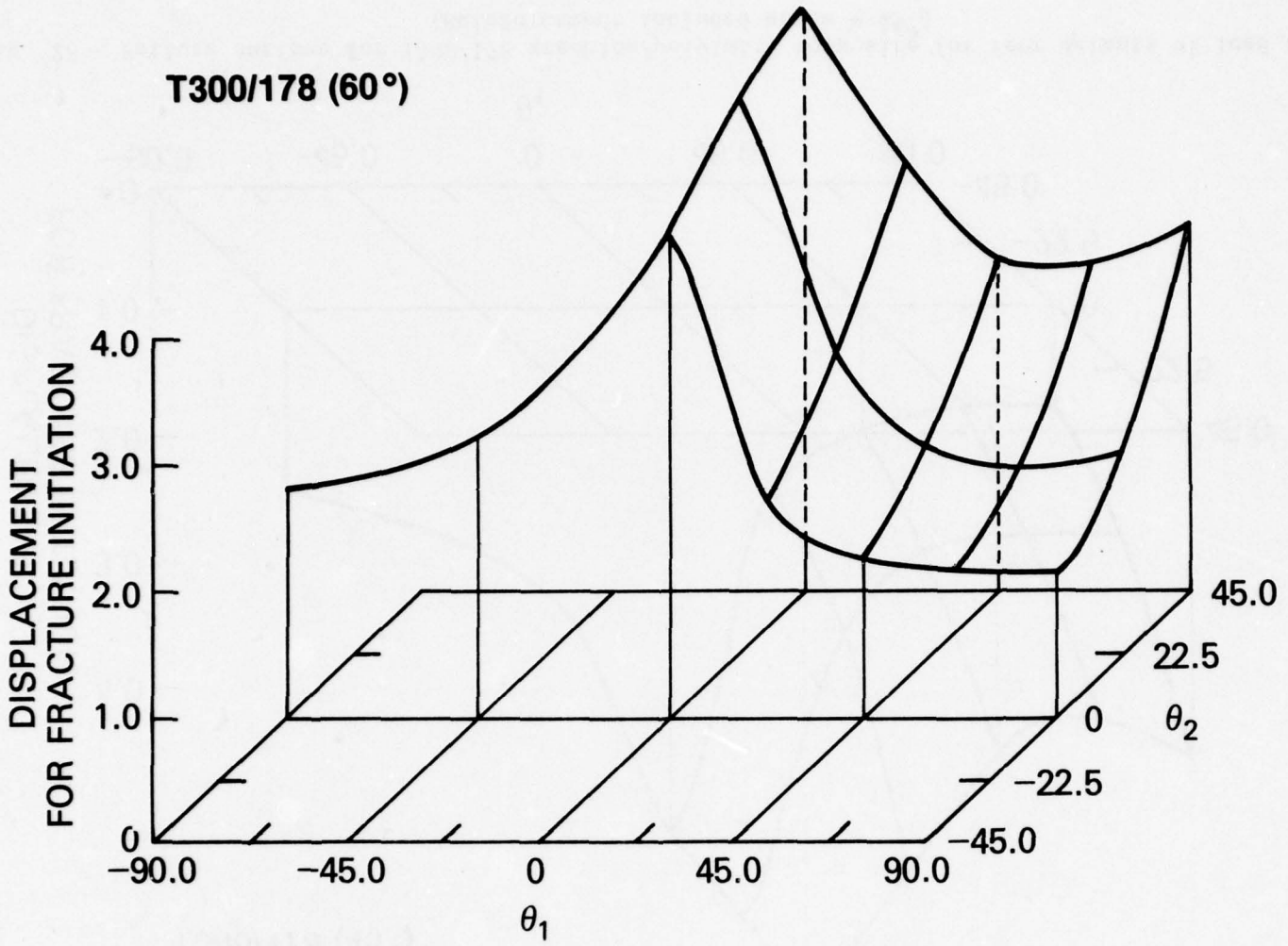

Fig. 29 - Failure surface for T300/178 graphite/polyimide composite for four octants of load space (Reinforcement included angle = 60°)

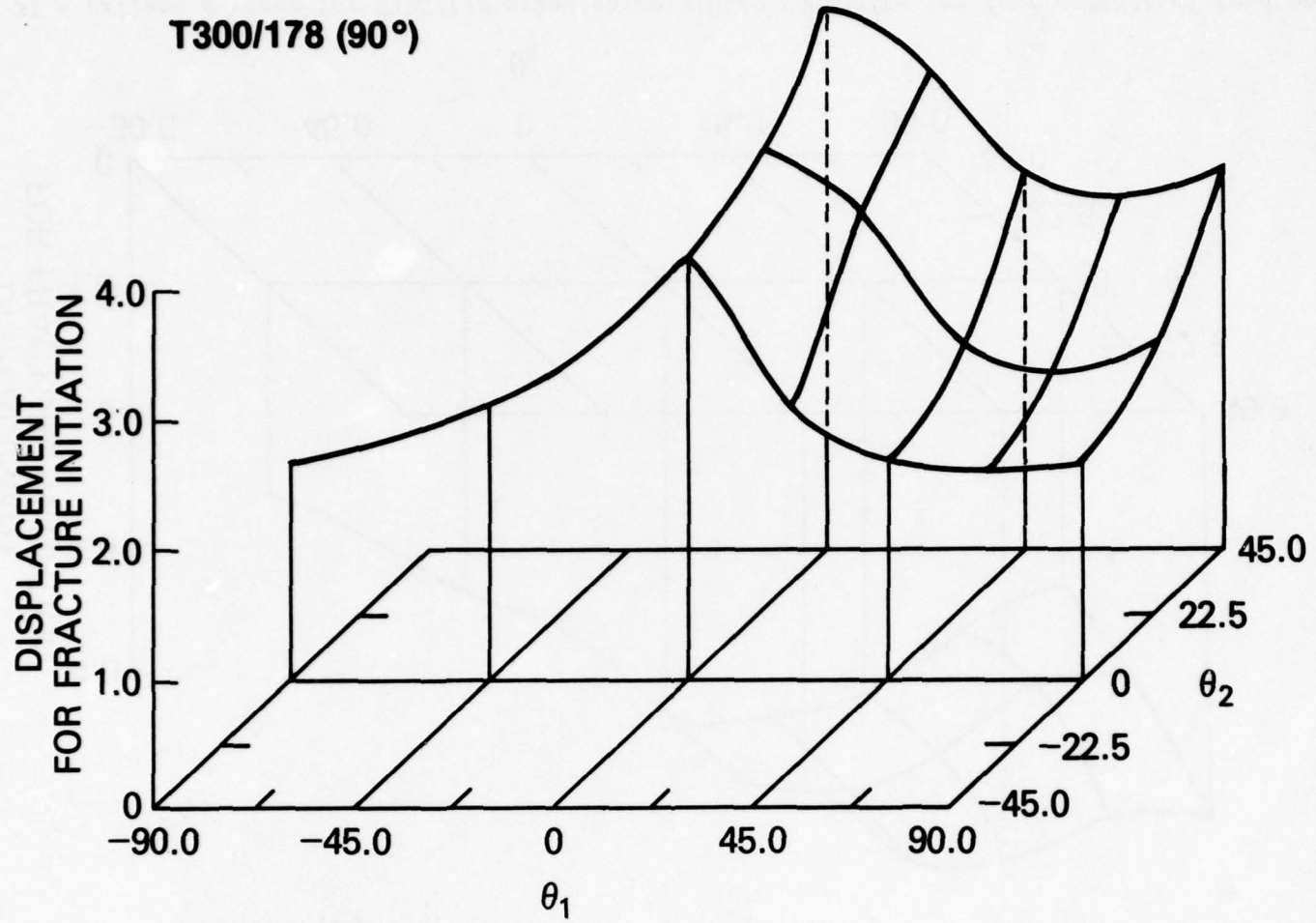

Fig. 30 - Failure surface for T300/178 graphite/polyimide composite for four octants of load space (Reinforcement included angle = 90°)

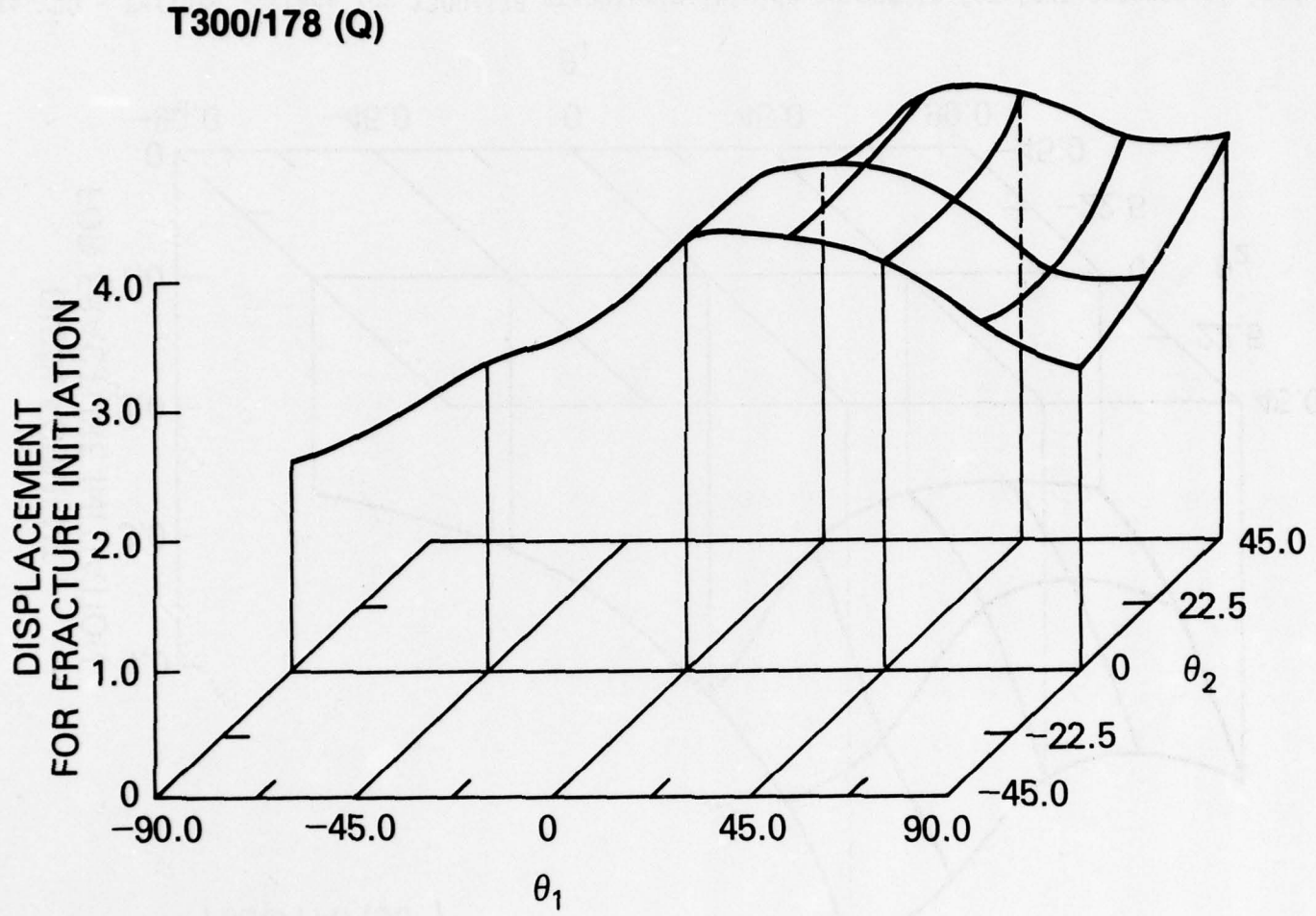

Fig. 31 - Failure surface for T300/178 graphite/polyimide composite for four octants of load space (Reinforcement angle = (0, $\pm$45, 90^{o})

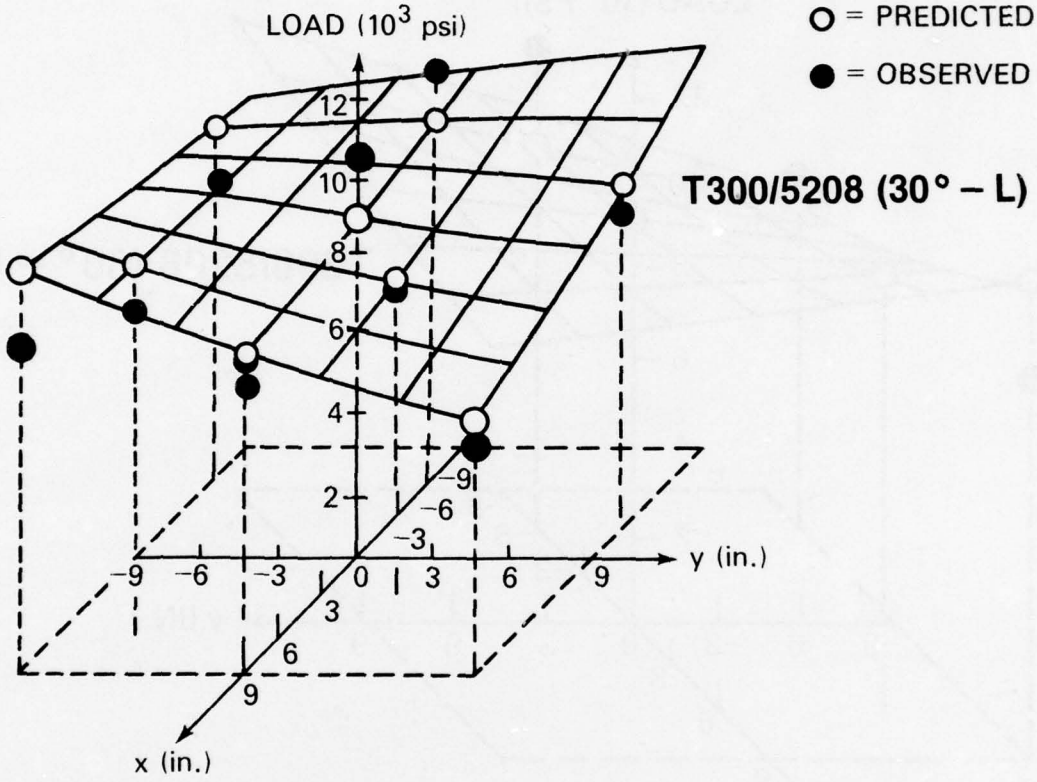

Fig. 32 - Box beam failure surface for left end of notch for T300/5208 graphite/epoxy composite with reinforcement included angle of 30°, showing predicted failure initiation load (on calculated failure surface) and observed loads for various loading conditions. x and y refer to location of top and bottom loading pins, respectively.

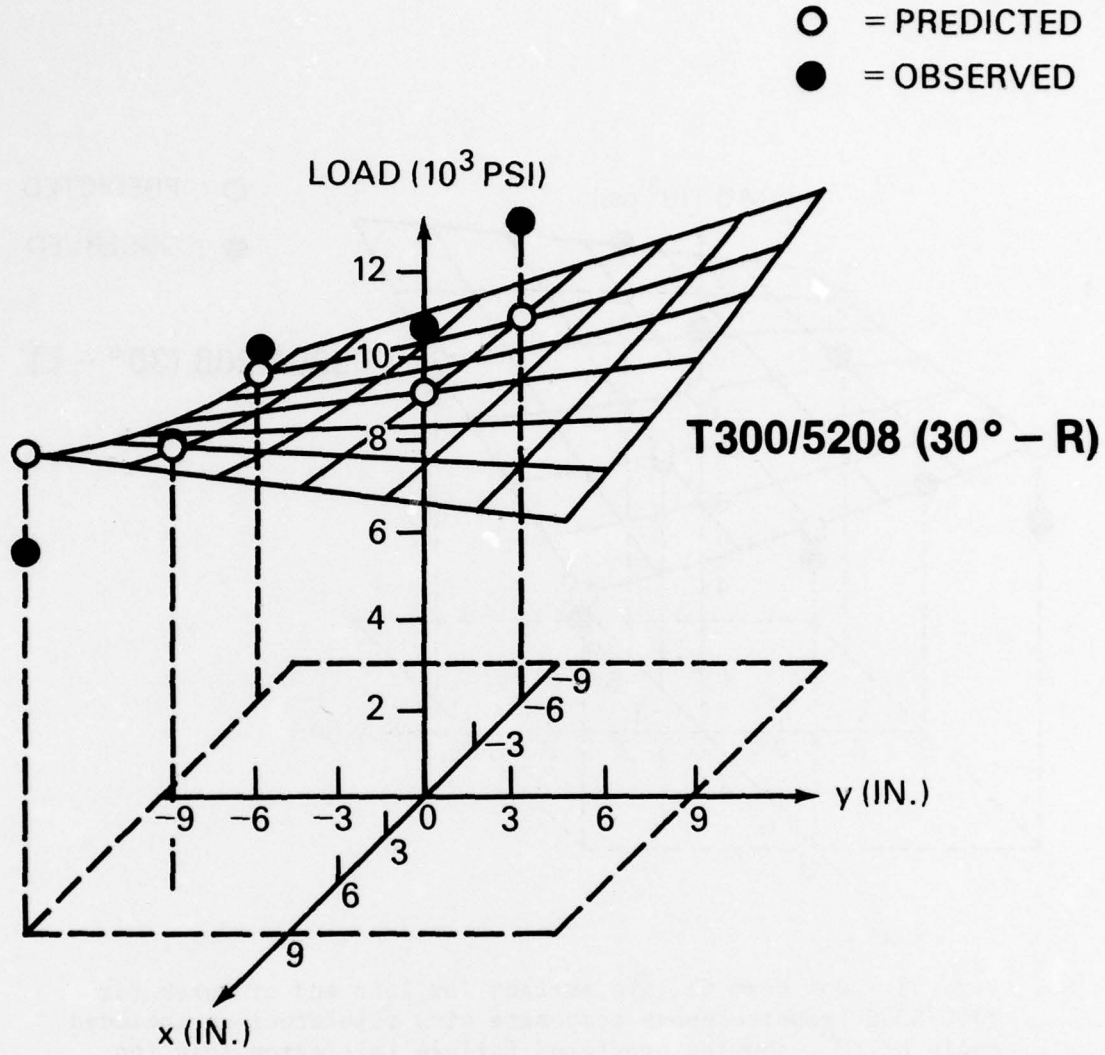

Fig. 33 - Box beam failure surface for right end of notch for T300/5208 graphite/epoxy composite with reinforcement included angle of 30°, showing predicted failure initiation load (on calculated failure surface) and observed loads for various loading conditions. x and y refer to location of top and bottom loading pins, respectively.

PART II. FAILURE CRITERIA FOR ADHESIVE JOINTS

INTRODUCTION

Most previous studies of failure in adhesive joints have considered relatively simple loading conditions, whereas in actual service bonded structures usually see a rather complex load environment. Consequently, it is desirable to extend the range of experimental failure studies to conditions which simulate service loading. This section describes an experimental study of failure in adhesive joints subjected to a wide range of applied loads typical of actual service conditions. Results of these studies were analyzed using fracture mechanics parameters as well as by representing the loci of failure initiation points as a failure surface. Transition between brittle and ductile behavior in both adhesive and bulk epoxy was observed depending on the type of loading applied to the specimens. Observations of the fracture surface of the specimen were also used to relate the mode of failure to the applied loading.

EXPERIMENTAL PROCEDURE

Materials

The particular adhesive chosen for this study was a commercial structural adhesive, FM-73M, supplied by American Cyanamid as a film adhesive with a random polyester mat. This adhesive was selected because it is the same adhesive chosen by the Air Force for evaluation in their Primary Adhesively Bonded Structure Technology (PABST) program.

Laboratory coupons fabricated for failure studies were single-edge-notch type specimens of the geometry shown in Figure 1. The specimen configuration consisted of two plates of aluminum bonded together with the film adhesive. Specimens were made using 25 mm x 18 mm (1" x 3/4") 6061-T6 aluminum bars, 178 mm (7") long, whose surfaces had been glass-peened and treated with an acid chromate etch.

Prior to bonding, one of the 25 mm x 178 mm (1" x 7") surfaces of each bar was treated with a primer, BR 127, also supplied by American Cyanamid. This primer coating was selected based on the durability studies conducted in the PABST program. The film adhesive was then placed between two of the bars along the primer-treated surfaces and cured for 60 minutes at 121°C (250°F) and 280 kN/m^2 (40 psi). The bonded bars were then removed from the heated press and specimens were machined in two thicknesses, 2.5 mm (0.1 in.) and 6.3 mm (0.25 in.). Finally, a notch was machined along the bond line as shown in Figure 1.

While other specimen geometries could have been used to develop different components of loading, such as scarf joints or lap-shear joints, the advantage of a single specimen geometry is that the same stress analysis can be used for all loading cases.

Loading System

Complex loading states were applied using a uniaxial loading system and the testing fixtures shown schematically in Figure 2. With the grips clamped to the edges of the specimens it was possible to apply a range of in-plane tension, shear and bending loads. While this range of loads is not as broad as that possible with the in-plane loading system described in the first annual report [1], it does permit the evaluation of adhesive joints over a wider range than simple tensile or shear loading.

DATA ANALYSIS

The point of failure initiation was determined by observing the point of deviation from linearity in the load-displacement curve as shown, for example, in Figure 3. Values of shear, tension and bending loading at this point were used as a failure criterion for this specific combined load state. Similar results were obtained for other loading states with the exception of those specimens which did not exhibit brittle behavior. For specimens which failed in a ductile manner, the point of non-linear deformation which exceeded that normally observed in the brittle specimen was used as a failure criterion. In addition to the point of failure initiation , the point of final failure was also observed, although in some cases considerable non-linear deformation occurred prior to this point. In general, tensile loading produced linear-elastic response and brittle behavior, whereas introduction of shear or bending produced non-linear response and ductile failure. Visual observations of the specimens during testing

provided a means of detecting crack growth. In most cases in which slow crack growth occurred in the adhesive, non-linearity was observed in the load-displacement curve.

Fracture initiation points are shown in Figure 4, where the tips of the arrows indicate the load components. It can be seen from these data that relatively high values of shear and tension required for failure initiation are reduced significantly when bending loading is applied to the specimen. High shear and low tensile loading correspond to the type of loading in lap-shear tests, and high bending and low shear correspond to peel tests although there is considerably less deformation in the adherends.

Fracture Mechanics Analysis

A fracture mechanics representation for failure initiation can be obtained using stress-intensity factors based on analytic formulation by Paris and Sih [2]. These methods are applicable only for linear elastic materials behavior and are restricted to self-similar crack growth. Consequently, the stress-intensity factor analysis can only be applied when these conditions are satisfied.

Based on results presented by Paris and Sih, the stress intensity factors for homogenous, isotropic edge-notched plates subjected to tension, T, shear, S, and in-plane bending, M, are

$$K_I = \frac{T}{2bt}(\pi a)^{1/2}\left(\frac{2b}{\pi a}\tan\frac{\pi a}{2b}\right)^{1/2} h\left(\frac{a}{b}\right) + \frac{6M}{t(2b-a)^{3/2}}\, g\left(\frac{a}{2b}\right)$$

and

$$K_{II} = \frac{S}{2bt}(\pi a)^{1/2}\left(\frac{2b}{\pi a}\tan\frac{\pi a}{2b}\right)^{1/2} h(a/b)$$

where a is the notch depth, 2b is the plate width, t is the thickness and h(a/b) and g(a/2b) are correction factors for finite width plates. The values of h(a/b) and g(a/2b) for this specimen geometry are 1.16 and 0.6 respectively. The various modes of loading applied to the specimen are shown schematically in Figure 5. In the following analysis an initial notch length of 5 mm (0.2 in.) and a specimen width of 25 mm (1.0 in.) were used in the computation for the values of K_I and K_{II}. Although other fracture parameters can be used to describe the data, they have not been implemented to date. Further studies will be conducted to explore other failure criteria.

RESULTS AND DISCUSSION

Using the formulation for the stress-intensity factors K_I and K_{II}, a failure surface showing their respective components is presented in Figure 6. Points along the K_I axis correspond to tension or tension plus bending loading. Other points above the K_I axis represent cases of combined tension, bending and shear loading. The inner ellipse represents the lower bound on fracture initiation values under combined loading. Points on this surface represent those which satisfy the restrictions imposed by the assumption of linear elastic fracture mechanics. The outer ellipse represents the K_I - K_{II} values which would correspond to materials response which was linear elastic up to the final failure point. However, for the open parts shown in Figure 6,materials response was non-linear and consequently the K_I and K_{II} values indicated are not valid from a linear elastic viewpoint, although they give some indication of the difference between initiation and final failure. All of the data shown in this figure was obtained at the same testing machine displacement rate; however, this does not produce the same K_I rate or K_{II} rate for each specimen. Consequently, it is not possible to distinguish rate effects which may be present in this adhesive material. This point is an important consideration in making comparisons of tension and shear behavior, since the K_I rates applied for tensile loading differ from the K_I rates in combined tension and shear.

Scanning electron microscope studies were conducted on failure surfaces of specimens subjected to combined tension and shear loading. A significant change in the fracture surface was observed as the shear component of loading was increased, as shown in Figure 7. In these cases pull out and peeling of fibers in the random polyester mat increased with increasing shear. It is not clear at this point what the contribution to total strength or to non-linearity is supplied by the supporting film.

CONCLUSIONS

Based on the results of this preliminary investigation, the fracture mechanics concepts presented can be used to describe initiation of failure in some loading cases, specifically tensile loading alone or with slight amounts of bending and shear loading. Other loading combinations of tension, shear and bending introduce non-linear response in the adhesive bonded specimen and as a result classical

fracture concepts may not be applicable. In summary, the following conclusions can be stated: 1) Over a range of complex loading states it may not be possible to use a single fracture parameter as a failure criterion. 2) The application of classical fracture mechanics, specifically stress intensity factors, to these adhesive joints is limited to tensile loading cases or tensile loading with small amounts of shear and/or bending, where the materials respond in a linear elastic manner to failure. 3) The basic mechanisms of failure of a film adhesive (FM-73M) involve considerable non-linear deformation for combined tension, shear and bending, but not for tension alone or for tension plus small amounts of shear and/or bending.

REFERENCES

1. L. A. Beaubien et al, "Design Optimization", in "High Performance Composites and Adhesives for V/STOL Aircraft (W. D. Bascom and L. B. Lockhart,Jr, ed.), First Annual Report, NRL Memorandum Report 3433, p. 101 (December 1976).

2. P. C. Paris and G. C. Sih, "Stress Analysis of Cracks," ASTM STP 381, 1964, American Society for Testing and Materials, Philadelphia, Pennsylvania.

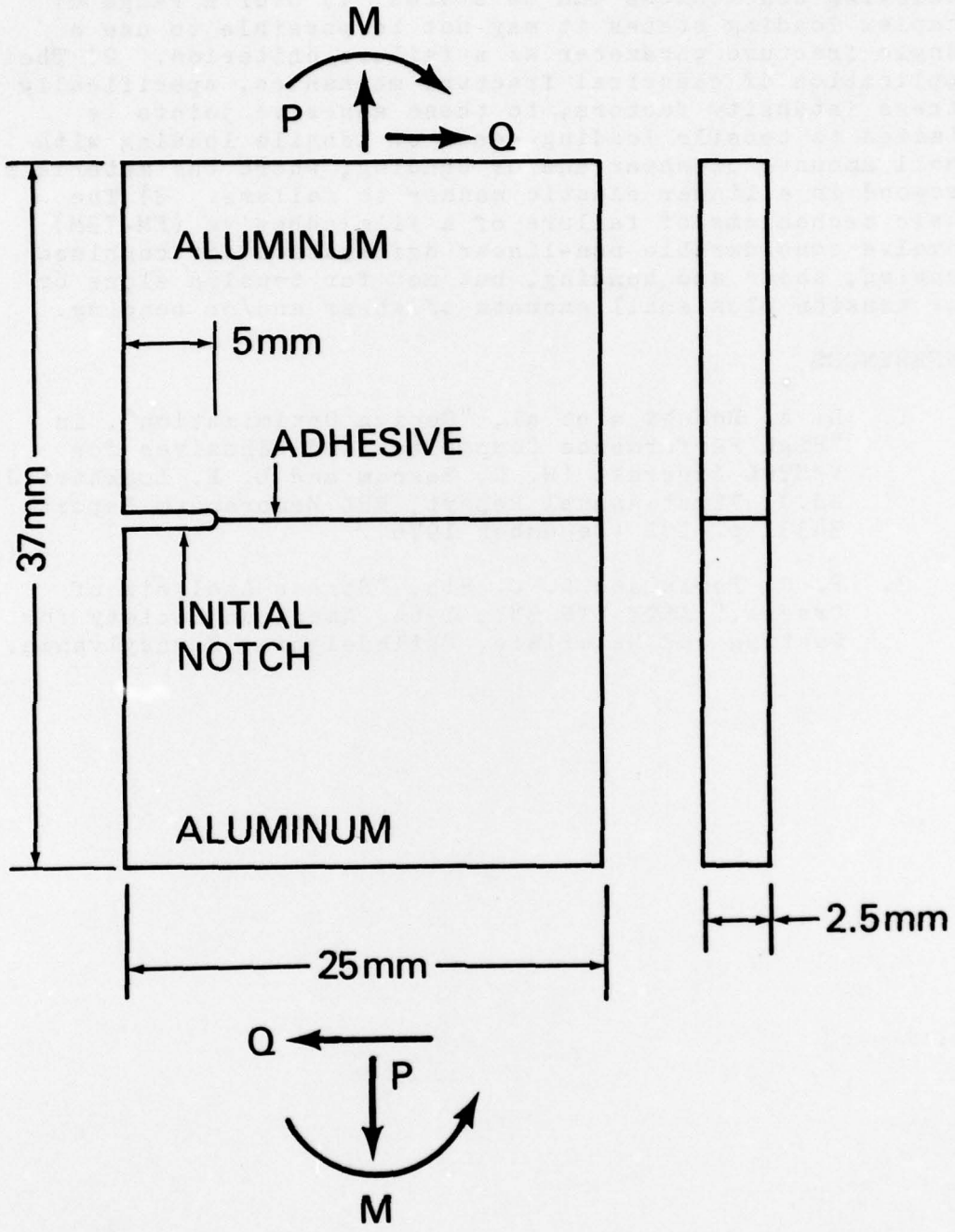

Fig. 1 - Single-edge-notch bonded specimen

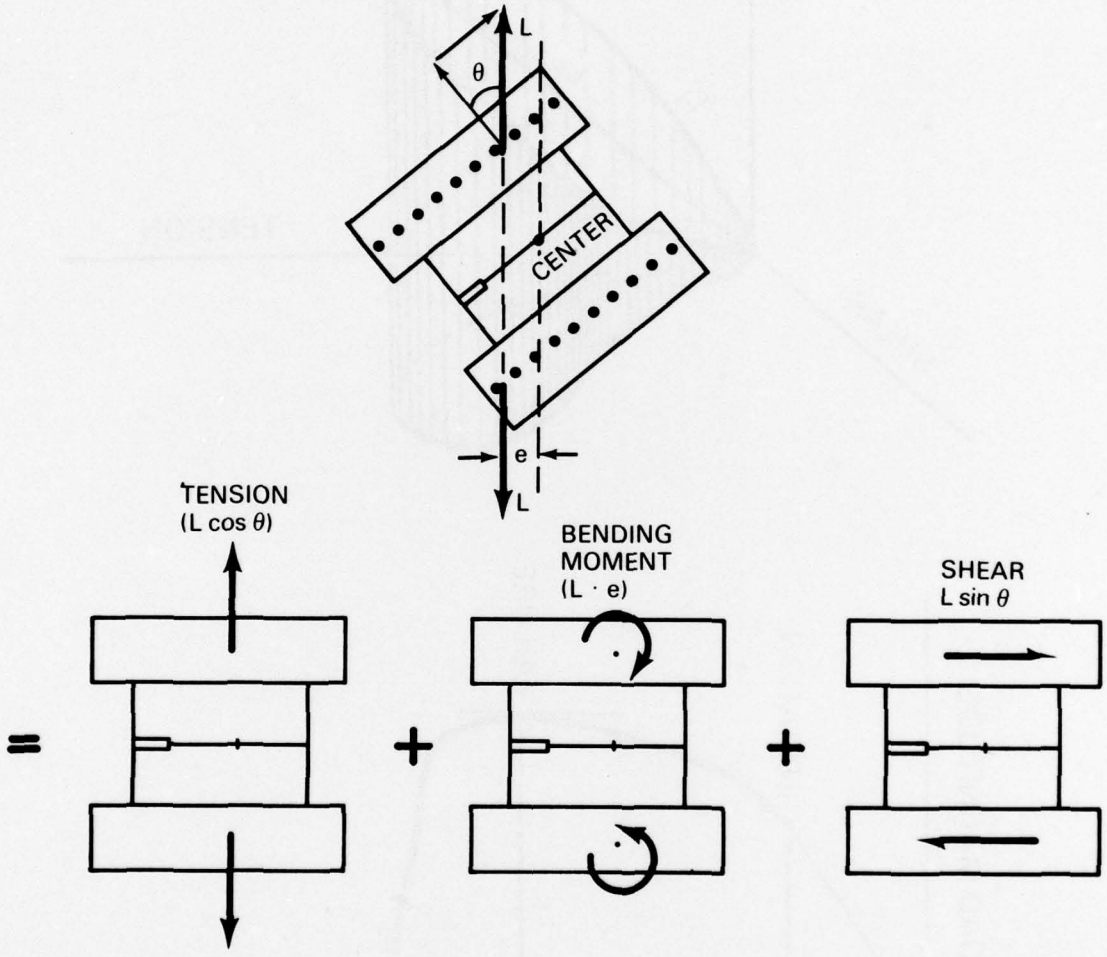

Fig. 2 - Single-edge-notch speciment subjected to tension, shear and bending by pin loading

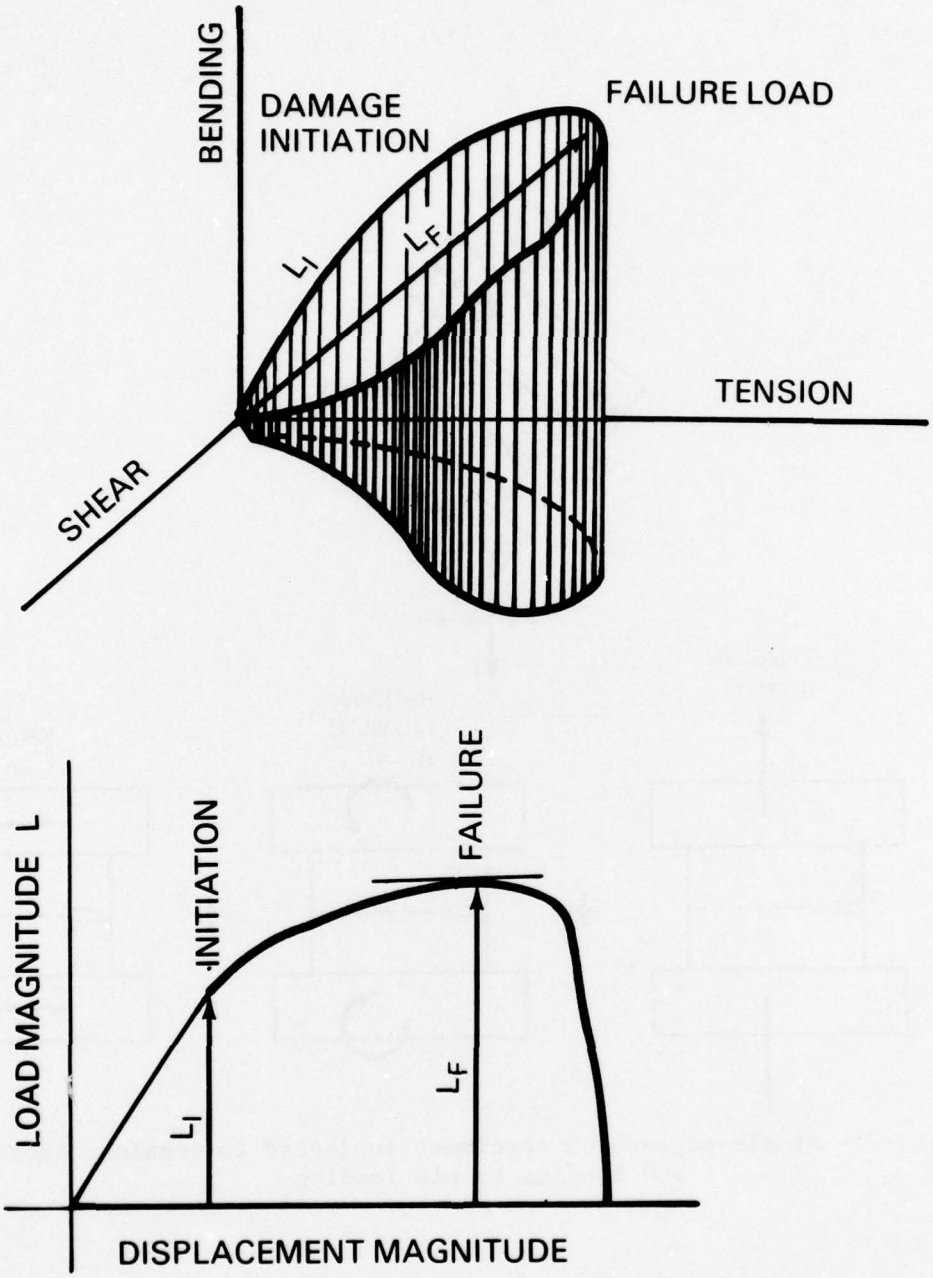

Fig. 3 - Typical load magnitude vs displacement magnitude response for bonded specimens

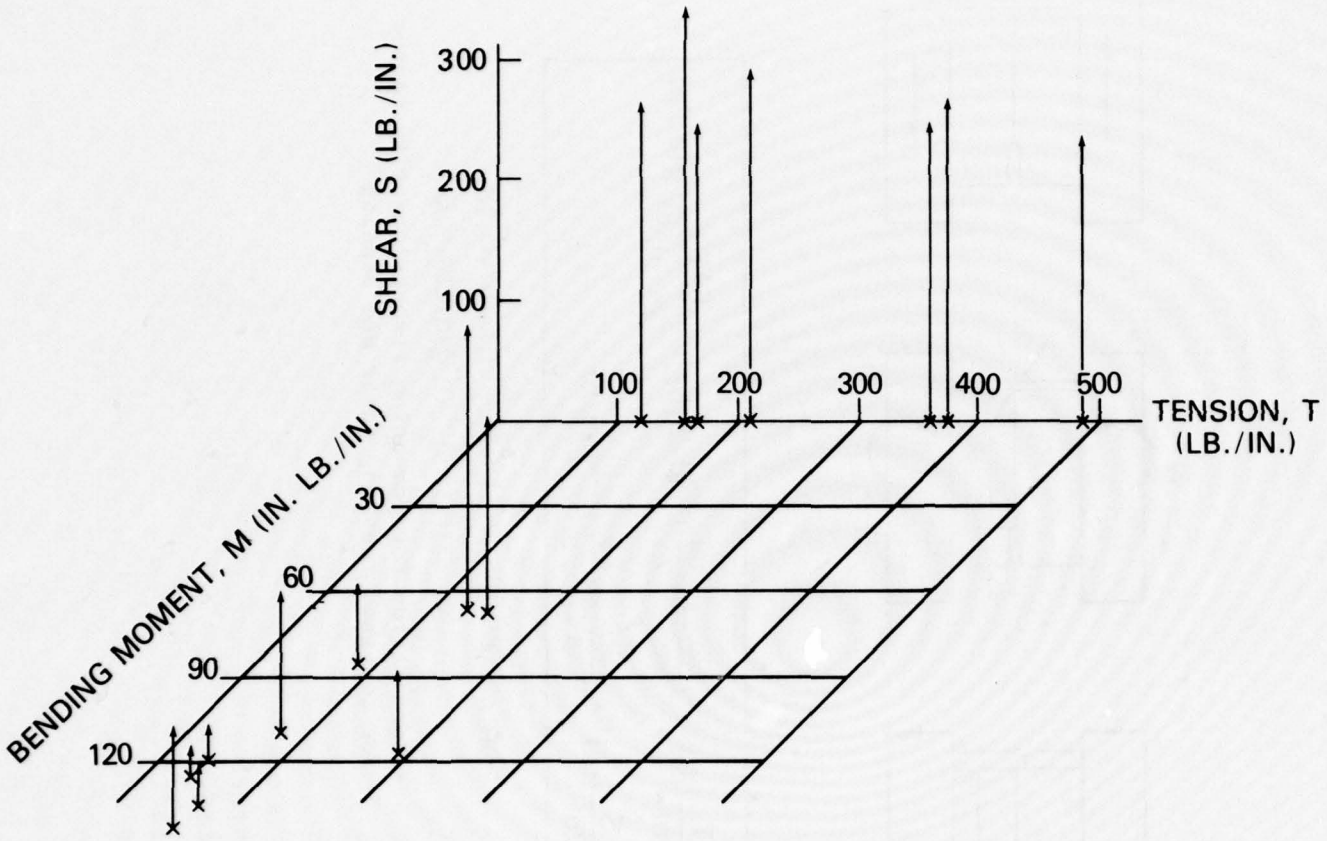

Fig. 4 - Fracture initiation points in the tension, shear and bending load space. Arrow tip indicates critical loading condition.

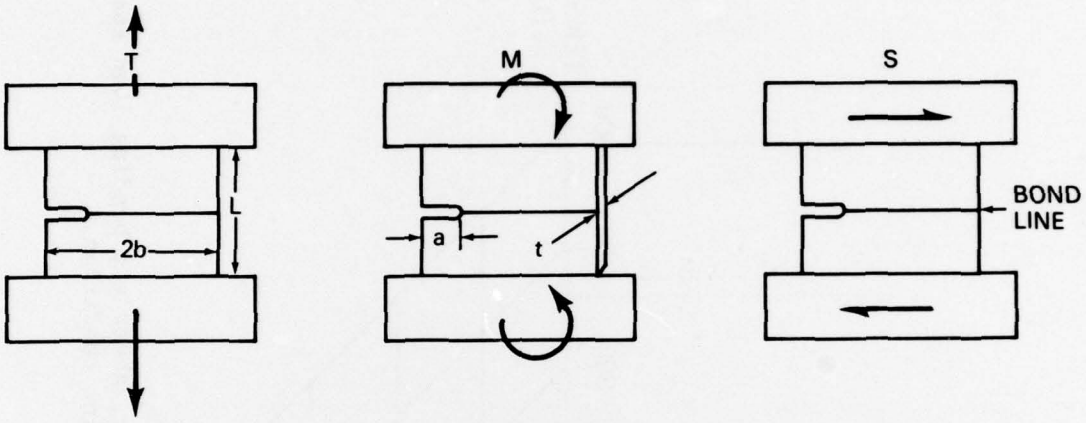

$$K_I = \frac{T}{2bt}(\pi a)^{1/2}\left(\frac{2b}{\pi a}\tan\frac{\pi a}{2b}\right)^{1/2} h(a/b) + \frac{6M/t}{(2b-a)^{3/2}}\, g(a/2b)$$

$$K_{II} = \frac{S}{2bt}(\pi a)^{1/2}\left(\frac{2b}{\pi a}\tan\frac{\pi a}{2b}\right)^{1/2} h(a/b)$$

FOR $a=.2''$ $b=.5''$ $L=b$ $\quad h(a/b)=1.16$

$g(a/2b)=.6$

Fig. 5 - Formulation for computing stress-intensity factor for combined tension, shear and bending

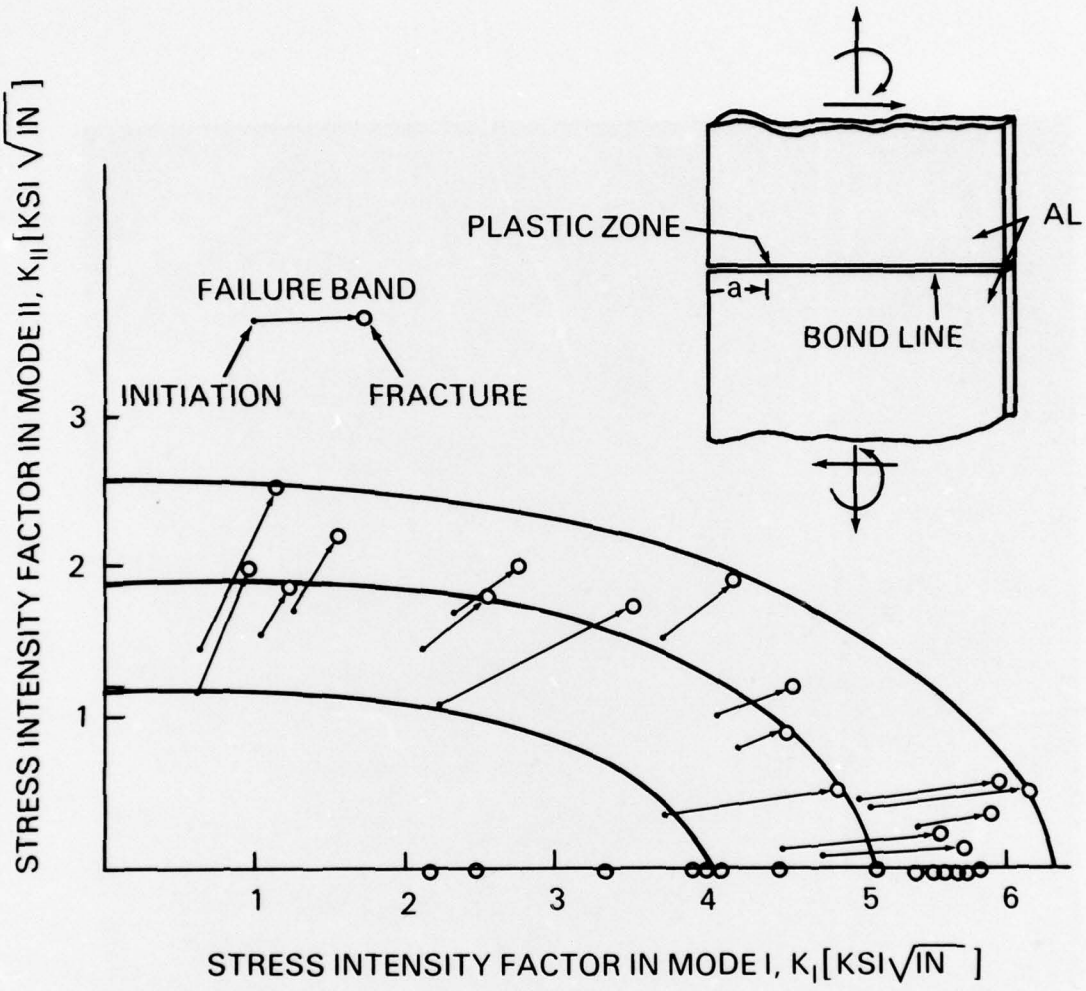

THE LENGTH, a, OF THE CRACK IS CORRECTED BY $a_{eff} = a + 1/4\pi\,(K_1^2/\sigma_y^2)$ WHERE K_I IS TAKEN AT INITIATION POINTS

Fig. 6 - Stress-intensity factors K_I and K_{II} for failure initiation and final fracture

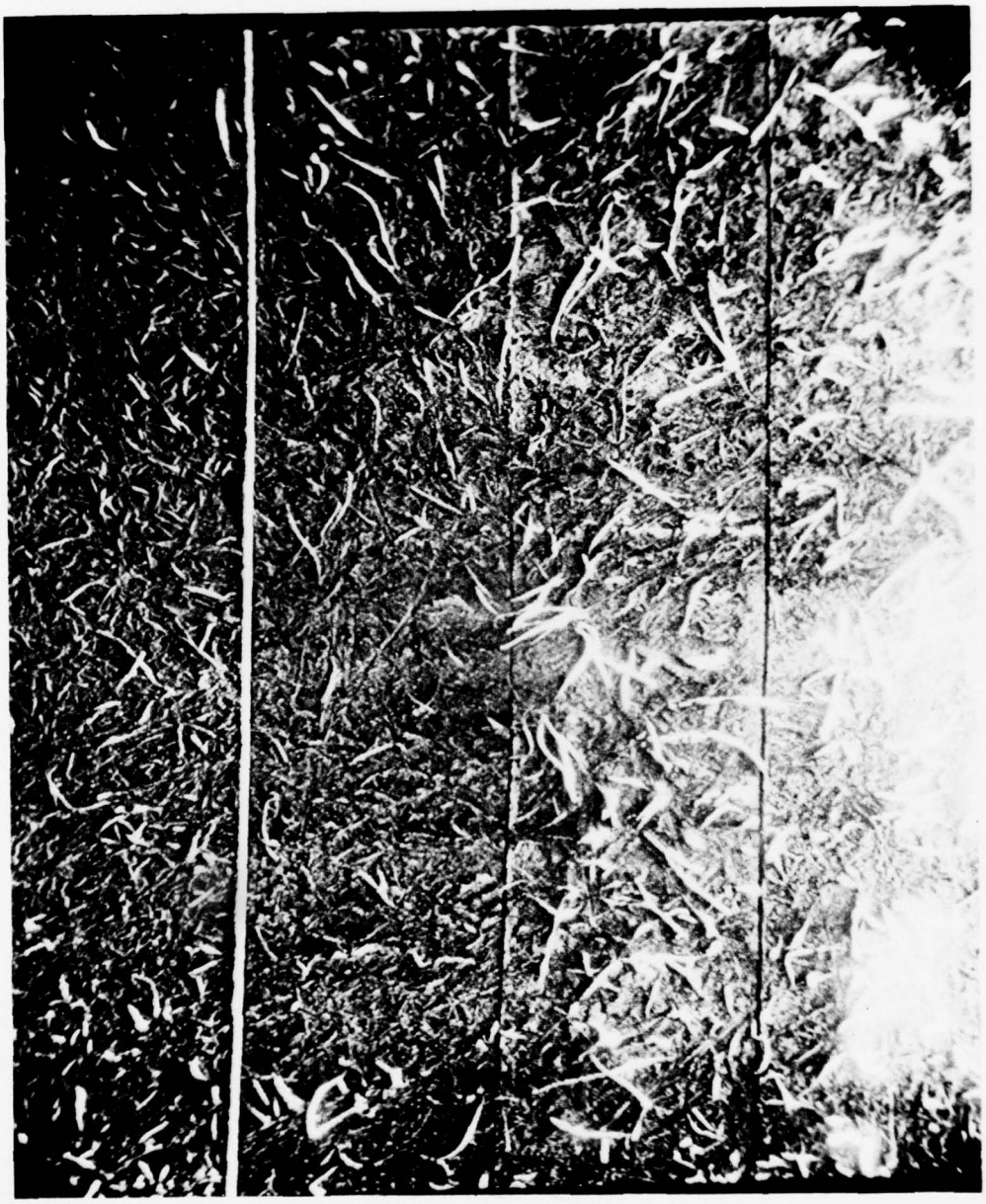

Fig. 7 - Photomicrographs of failed adhesive specimens with increasing amounts of shear vs. tension